ABSTRACT

Impact of MHD-E3 on Power System Equipment and Loads

Andrew K. Mattei, Ph.D.

Mentor: W. Mack Grady, Ph.D.

The detonation of a nuclear weapon in the Earth's upper atmosphere will cause a variety of electromagnetic disturbances at the Earth's surface. One of these disturbances – the magnetohydrodynamic late-time or MHD-E3 pulse – is characterized by a strong yet minute-long electric field that is capable of inducing quasi-direct currents in long conductors such as electric transmission lines. These quasi-direct currents, on the order of 1000 amps within the power grid, will cause transformer saturation that leads to abnormal power absorption and high levels of harmonics in the power system. Research herein explores the impact of these direct currents on transformers, the impact of elevated levels of harmonics on power system protective relays, and the impact of harmonic-rich voltages on information technology equipment. A benchtop transformer DC injection testing apparatus was designed and constructed, and these laboratory transformer test results are analyzed and compared with the results of DC injection tests performed on power system transformers at Idaho National Laboratories. Electromechanical, solid state, and microprocessor-based protective relays were subjected to harmonic currents and this performance is documented, analyzed, and recommendations for mitigating protection system mis-operations are provided. The response of a modern microprocessor-based transformer differential relay to harmonic current simulations, including a relay with a second harmonic waveshape recognition algorithm, is presented and analyzed. Finally, a testing system was constructed and the evaluation process, analysis, and results for the response of information technology equipment to harmonic voltage waveforms measured during the Defense Threat Reduction Agency DC-injection transformer testing at Idaho National Laboratories in 2012 are included.

Impact of MHD-E3 on Power System Equipment and Loads

by

Andrew K. Mattei, B.S., M.S.

A Dissertation

Approved by the Department of Electrical and Computer Engineering

Kwang Y. Lee, Ph.D., Chairperson

Submitted to the Graduate Faculty of
Baylor University in Partial Fulfillment of the
Requirements for the Degree
of
Doctor of Philosophy

Approved by the Dissertation Committee

W. Mack Grady, Ph.D., Chairperson

Scott Koziol, Ph.D.

Stephen T. McClain, Ph.D.

Dennis O'Neal, Ph.D.

Annette von Jouanne, Ph.D.

Accepted by the Graduate School
May 2021

J. Larry Lyon, Ph.D., Dean

Page bearing signatures is kept on file in the Graduate School.

TABLE OF CONTENTS

LIST OF FIGURES

LIST OF TABLES

ACKNOWLEDGMENTS

I would like to thank my advisor and friend, Dr. Mack Grady, for inviting me to join him with his research at Baylor University and all of the hard work, revelations, and fun we have had while learning more about the electric grid. We have worked on some great projects together, and I have enjoyed all of them.

A thank you to Mike Bollen for his valuable feedback during our time working together on the DoD-DTRA MHD-E3 project. Mike asks just the right questions and delivers great insights, and those are characteristics that I admire.

Thank you to my committee members - Dr. Dennis O'Neal, Dr. Scott Koziol, Dr. Annette von Jouanne, and Dr. Stephen McClain for helping me see this through to completion.

Thanks to Schweitzer Engineering Laboratories employees Derrick Haas and Jared Candeleria for co-authoring a technical paper with me, and to David Costello for equipping our Baylor research lab with SEL hardware and software so that we can test relays and keep our synchrophasor system running smoothly. We have appreciated SEL's support, and SEL has been a highly valued contributor to our research.

I would like to thank the leadership at the Defense Threat Reduction Agency for the opportunity to work on this project of exploring areas related to the impact of MHD-E3 on the electric grid. It is a fascinating topic and there is still more to learn.

Thanks to Dave Fromme of Scientific Applications Research Associates for working with us and inviting me to work with SARA to contribute to EMP research.

Finally, I thank my coworkers and management at Brazos Electric Power Cooperative for their flexibility and willingness to invest in my education.

DEDICATION

To my wife Carrie Lynn Mattei. You have sacrificed so many nights and weekends along the way. I appreciate and love you. You are awesome.

ATTRIBUTION

Chapter Five was co-authored by Dr. W. Mack Grady of Baylor University. Reference [1]. The paper was written by Andrew Mattei, and Dr. Grady checked for accuracy of the modeling portion and offered suggestions for clarity.

Chapter Six was co-authored with Derrick Haas and Jared Candelaria of Schweitzer Engineering Laboratories, and with Dr. W. Mack Grady of Baylor University. Reference [2]. Andrew Mattei created the ATP simulation model, ran several hundred ATP simulations, converted the results of those simulations to relay test COMTRADE files, programmed the protective relays with appropriate settings, performed relay testing, collected data files and logged results of all relay tests. Authorship of the paper was split in the following manner: Andrew Mattei wrote the sections on modeling, testing, and the first part of the test results summary. Derrick Haas wrote the paper introduction (not included in Chapter Six because of redundancy with Chapter Two), technical sections on relay operations including harmonic blocking and harmonic restraint, the conclusion, and provided overall editing and consolidation of the paper contents. Both Jared Candelaria and Derrick Haas wrote the analysis portion of the relay operations and performance regarding waveshape recognition versus blocking and restraint. Schweitzer Engineering Laboratories provided graphic design assistance for editing of figures and also provided grammar evaluation. A technical review by senior engineers at SEL provided valuable feedback and changes for accuracy. Dr. Grady provided suggestions for clarity within the paper. This paper was presented at the 2020 Western Protective Relay Conference and is presently available on the Schweitzer Engineering Laboratories web site.

CHAPTER ONE

Introduction

The power grid infrastructure is perhaps the most extensive and essential man-made system in the United States. A large scale, extended-period power outage would cause significant hardship across a large part of the country [3]. While astoundingly resilient, there exist several scenarios wherein the power grid infrastructure may be subjected to stresses that overwhelm the stability and integrity of the system.

One of the ways that the power grid may be destabilized is by the introduction of low frequency non-sinusoidal currents into the system. A frequently discussed example of this type of signal is the induction of quasi-direct currents (DC) via the interaction between charged solar particles and the Earth's geomagnetic field, commonly called geomagnetically induced currents (GIC) [4, 5, 6]. Solar GIC incidents may persist for hours but will have considerable variations in current magnitudes. A similar but potentially far more destructive phenomenon occurs when a nuclear weapon is detonated above the Earth's atmosphere (High-altitude Electromagnetic Pulse – HEMP). The interaction between the radiation, ionization, and thermal characteristics of a nuclear detonation and the Earth's geomagnetic field can cause substantial quasi-DC geomagnetically induced currents in the electric power grid of over a thousand amps for a period of up to several minutes [7, 8].

This research explores some of the significant impact areas for the high levels of quasi-DC currents experienced during the magnetohydrodynamic (MHD) period of a HEMP event, with a particular emphasis on protective relaying and its required inputs. The areas of interest are the impact on power transformers, the impact on protective relays and transformer protection, and the impact of significant harmonic voltage distortion on information technology and communications devices.

Because the research spans three subject areas, chapters herein are dedicated to each area. The research areas do have overlap and dependencies: transformer saturation testing leads to modeling that provides a simulation environment for testing protective relays, while transformer test data also provides sample voltage waveforms for testing common off-the-shelf information technology (COTS-IT) equipment.

Research Areas Explored

Transformer Response to DC Injection

The question: What are the magnetic circuit saturation characteristics of transformers, and do benchtop transformer test results scale to utility grade transformers under similar test conditions?

The expectation: Low voltage benchtop transformers during DC injection periods will exhibit similar saturation characteristics to larger utility grade transformers. These characteristics include current harmonics, power absorption, and secondary voltage distortion. Chapter Four contains test results and comparisons between benchtop transformers utility grade transformers.

Protective Relay Performance During High-harmonic Current Events

The question: Is the performance of protective relays degraded during a period of high harmonic currents?

The first expectation: Electromechanical relays without harmonic filtering are negatively impacted by harmonic-rich currents and exhibit unpredictable trip characteristics. Relays that incorporate harmonic filtering such as solid state and microprocessor-based relays will not exhibit this behavior. Chapter Five describes the three harmonic-rich test current waveforms and the results of relay testing based on these currents.

The second expectation: Transformer differential relays are desensitized to internal faults by the traditional harmonic blocking and harmonic restraint elements.

Chapter Six describes the software modeling, testing, and discusses the response of a pair of modern microprocessor-based transformer differential relays.

COTS-IT Equipment Response to Harmonic-rich Voltage Waveforms

The question: How does COTS-IT equipment react when exposed to harmonic-rich voltage waveforms similar to those found during DC injection testing at Idaho National Laboratories?

The expectation: COTS-IT equipment will fail to continue to operate correctly. Failure may include a self-reset, require a manual intervention to reset, or permanent damage to the device. Chapter Seven includes a description of the method and waveforms used to test COTS-IT equipment against harmonic-rich voltage waveforms.

Relationship of the Study Areas

The relationship between the areas of study is based on the DC response of transformers. The quasi-DC signals will polarize the orientation the magnetic dipoles within transformer steel and likely result in saturation of the magnetic material. In a power transformer, DC saturation causes substantial harmonics in the current and a significant increase in power absorption by the transformer [9]. Power system protective relays may operate unpredictably to these harmonics, which leads to an increase in the chance that protection systems may operate incorrectly [10]. End load devices may be damaged by the resulting downstream voltage harmonics [11].

This work was funded and supported by the United States Department of Defense / Defense Threat Reduction Agency (DTRA). During the course of research, direction was provided for an exploration of the sensitivity of protective relays and grid-connected devices (e.g. transformers and loads).

CHAPTER TWO

MHD-E3 and the Grid

Characteristics of the MHD-E3 Phenomenon

When a nuclear weapon detonation occurs above 30 km altitude, the effect is different than that of a ground or atmospheric burst. For ground level or detonation within the atmosphere, damage is primarily caused by the atmospheric pressure wave and thermal radiation, with a short EMP burst that is high in magnitude but limited in distance from the center of the blast [12]. When high altitude detonation occurs, the damage is nearly all electromagnetic, with the resulting electromagnetic disturbance exhibiting three distinct time periods [7, 13, 14, 15, 16].

The HEMP event is well described in the literature and has evolved over the years as more information has been disseminated by government research publications. The government-published research literature from the early 1960s through the mid-1970s made no mention of the magnetohydrodynamic characteristics of the HEMP event [17, 18]. It was not until the late 1970s that concerns about the MHD-EMP period began appearing in the literature [19]. The phenomenon was initially referred to as MHD-EMP, but eventually the literature began addressing the event as separate time period components. There are three distinct periods to a nuclear EMP event: E1, the "Early Time" period; E2, the "Intermediate Time" period; and E3, the "Late Time" period. Figure 2.1 [16] is a graphical representation of the relative induced electric field over time. The initial strong impulse phase occurs very quickly (nanosecond rise time with very short duration), the middle phase has a duration and magnitude characteristic similar to lightning, and while the magnitude of the Late Time section is lower, the duration of the E3B phase is of serious concern for power systems.

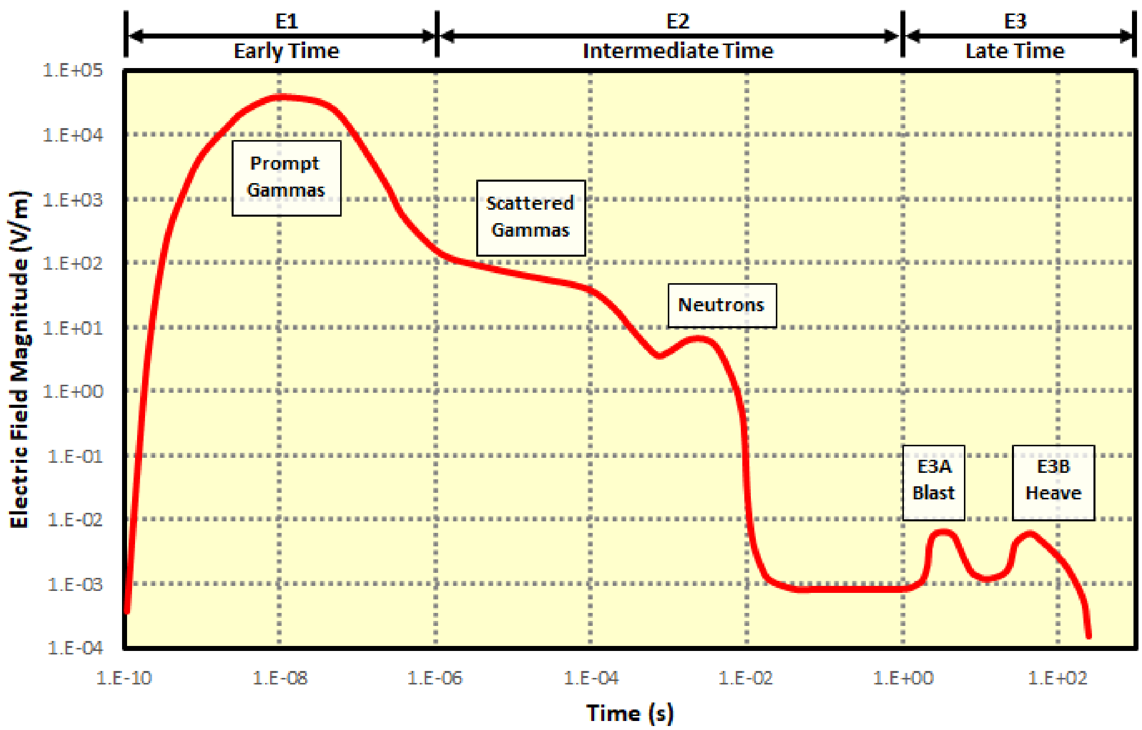

Figure 2.1. Example Timescales for High-altitude Electromagnetic Pulse [16]

Period 1: Prompt Gamma Rays (E1 – "Early Time")

Immediately after detonation, a fast rise time (<10 ns to peak) high energy (>6MeV) [20] burst of gamma rays spreads radially from the center of the blast. The gamma rays that travel toward the Earth as high-energy photons collide with upper atmospheric particles and forces the expulsion of free electrons via Compton scattering [20]. These free electrons interact with the Earth's magnetic field to generate a strong electromagnetic field that appears at the Earth's surface as the initial electromagnetic pulse. This pulse is extremely short in duration, reaching its peak in less than 10 ns and dropping significantly in magnitude by 100 ns. The affected surface area on the Earth is line-of-sight and is directly related to the altitude of the detonation. For example, at a 400km burst altitude that is centrally located over Kansas, an E1 event would nearly stretch coast-to-coast and would impact a significant portion of the United States.

The E1 EMP is considered extremely dangerous because of the susceptibility of semiconductor-based electronics to the high voltages induced by the pulse. Nearly any length of wire or circuit board trace becomes an antenna for an E1 impulse. E1 EMP hardening involves shielding sensitive cables and devices and well-designed grounding systems [21, 8].

Period 2: Neutron Gamma Rays (E2 – "Intermediate Time")

The E2 Intermediate Time EMP represents the period between the Early Time E1 collapse and the Late Time E3 rise. The E2 period begins about 1 µsec after detonation and ends approximately 1 second after detonation. It is the result of scattered gammas and the inelastic scattering of high-energy neutrons. The magnitude of the field generated during the E2 period is slightly lower than the E1 period, yet above the levels of E3. Protection for systems during the E2 period would resemble the protection required during the E1 period because of its relatively short duration [14, 22].

Period 3: Magnetohydrodynamic (MHD-E3 – "Late Time")

The E3 Late-Time period begins approximately one second after detonation and persists up to several hundred seconds. This period encompasses two distinct phases: the E3A "Blast" and the E3B "Heave" [7]. Note that Figure 2.1 is reflecting the magnitude (absolute value) of the electric field. The field changes direction between the Blast and Heave periods and one peak is positive polarity while the other peak is negative polarity [23].

The E3A Blast period begins about 1 second after detonation and ends approximately 10 seconds after detonation. It is the result of the expanding fireball and associated magnetic bubble. This magnetic bubble causes a distortion in the Earth's geomagnetic field lines and results in a slow-moving yet strong electromagnetic wave that is capable of inducing quasi-DC currents on power systems [7].

The E3B Heave period begins about 10 seconds after detonation and extends up to 100 seconds in duration. The Heave period is characterized by the heating and ionization of the Earth's atmosphere and the resultant buoyant rising of the heated air. This ionization and air movement also interacts with the Earth's geomagnetic field to produce a varying electric field that results in quasi-DC currents on power systems. The Defense Threat Reduction Agency uses the EMREP (Electromagnetic Reliability and Effects Predictions) computer program to simulate the effects of electromagnetic pulses on the Earth's geomagnetic field. Figure 2.2 shows an unclassified version of an EMREP-calculated MHD-E3 electric field response to a high altitude blast over Joint Base San Antonio (JBSA) [24]. The high-magnitude response areas are focused over San Antonio, but the affected area is widespread across Texas.

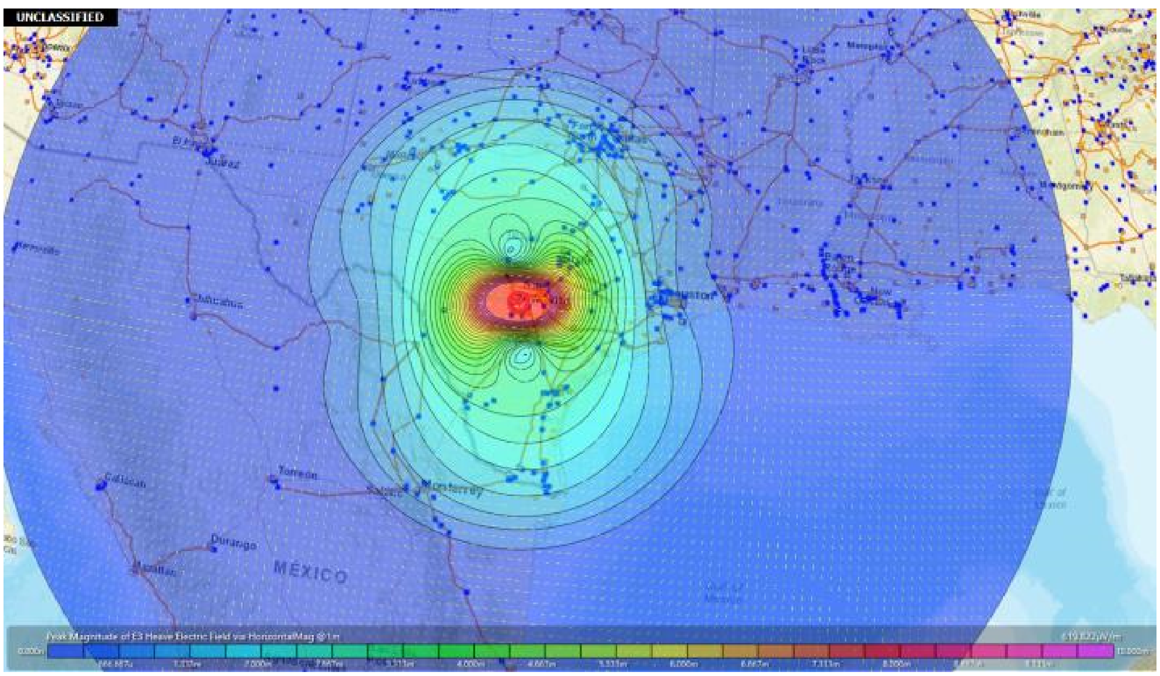

Figure 2.2. Distribution of Electric Field for E3B Heave over JBSA [24]

The Influence of MHD-E3 on the Power Grid

There is variation in the literature over standard electric field magnitudes during the E3 time period. The wide, slow-moving electric field established by a high-altitude nuclear detonation is capable of inducing at least 10 V/km [15], over 50 V/km [7], or even 85 V/km based on analysis of unclassified data from Soviet-era nuclear tests [25]. For comparison, the North American Electric Reliability Corporation's (NERC) solar geomagnetic disturbance planning standard TPL-007-1 has established 8 V/km as its baseline case field voltage, 12 V/km as a supplemental case field voltage, and a scaling factor that reduces field magnitude when calculating for southern latitudes [26].

For the EMP-E3 event, the electric field magnitude varies by the weapon's geomagnetic latitude and burst height. Opposite to solar GIC, the closer to the geomagnetic equator, the greater the field strength. By simulating HEMP at different locations based on extrapolation from the Soviet nuclear tests, the EMP Commission [25] estimated peaks of over 100 V/km at 22 degrees North (approximate geomagnetic latitude of Hawaii) and 85 V/km at 35 degrees North (approximate geomagnetic latitude of south Texas). As the weapon yield increases, peak values may eventually saturate but burst height will expand coverage of the impacted area.

While the effect of electric field induction of quasi-DC currents within the grid is functionally similar to solar GIC, the MHD-E3 event can have a more significant impact on power system equipment reliability and system stability. The impact of both magnitude and duration is necessary for study and analysis [22]. The MHD-E3 period will not be a long duration event like solar GIC, but harmonic voltage and current distortion will likely be orders of magnitude greater than solar GIC events.

The majority of the current literature regarding E3 and/or solar geomagnetic disturbances centers around the impact of the quasi-DC signal on a transformer. The magnetic core of a transformer is highly susceptible to saturation upon introduction of a DC component to the system. Sufficient quasi-DC current in an AC transformer results in very high levels of harmonics, excess power and VAR consumption, hot spots and/or overheating, and high levels of mechanical vibration at harmonics of the fundamental frequency [27]. Simulations have attempted to model the phenomenon on a grid-wide scale, with results ranging from very few problems found [15, 28] to predictions with dire results [29, 25]. While the limited duration of the E3 event may not lead to overheating of some transformers, there exist various scenarios for power system collapse or component damage.

The reference event for quasi-DC induction on a power system is the March 1989 solar geomagnetically induced current (GIC) event involving the northern United States and southern Canada. NERC has published a report based on this event [30], and an analysis of this report reveals that the stability of the power system was compromised by the removal of numerous capacitor banks from the grid by protective devices. Kundur [31] states that for a power grid in general, "the main factor causing instability is the inability of the power system to meet the demand for reactive power." In the 1989 event, with the loss of VAR control via disabled capacitor banks, voltage collapse became imminent. Capacitor bank protection systems activated because of excessive harmonics-related voltages and currents that were the result of transformer saturation. During this event, there were a few transformer protection systems that activated, some generator protection systems activations, but the majority of operations were related to capacitor banks. Exacerbating the voltage collapse problem is the common practice for capacitor banks that once de-energized, they may not be re-energized until a five-minute timer has expired so that the stored energy may discharge to zero and not cause an energization surge or voltage spike upon re-energization. Because of the similarities drawn between the quasi-DC injection for a solar geomagnetic storm and an MHD-E3 event, analyzing and describing the power consumption of a transformer core under DC saturation is essential to understanding the possible impacts that MHD-E3 may have on the power system.

Transformers

Within the electric grid, transformers exist in varying configurations and sizes. Winding configuration, ground connection, and core design all impact a transformer's susceptibility to MHD-E3 GIC [32]. There are several commercial solutions offering strategies for transformer protection during GIC events [33, 28]. These include:

- Neutral blocking devices that use DC-blocking capacitors and a bypass mechanism, coupled with DC and harmonic detection systems [34]
- Series compensation capacitors in transmission lines
- GIC reduction devices such as DC motors, semiconductor switching, or neutral resistors.

DTRA performed testing on a neutral-connected DC-blocking capacitor system during the transformer testing at Idaho National Laboratories [34] and found that while it did operate as expected, DC measurements at remote stations indicated widespread DC in the affected area. This highlights one of the common problems for local transformer protection during a GIC event: that the local transformer with GIC mitigation will be protected, but transformers in the surrounding area may be forced to absorb the distributed DC injection.

As an alternative to neutral connection, microprocessor-based protective relays may offer some relatively inexpensive alternatives to an electric utility for GIC mitigation. Bernabeau [35] has performed RTDS-based simulations of solar GIC and performed hardware-in-the-loop testing with protective relays, and others [36] have provided information related to their experiments with transformer protection and quasi-DC signals, but no experimental data has yet been found based on MHD-E3 levels of perturbation. Software simulations [9, 37, 38] typically focus on simulated VAR consumption and the potential for transformer damage based on overheating. Little to no actual data is publicly available related to saturation, thermal, or mechanical stress response to MHD-E3 signals.

Protective Relays

The 1989 Hydro Quebec event [30] drew industry attention to the susceptibility of protective relays to the influence of geomagnetically induced currents due to solar activity. At the time, relays were predominantly electromechanical and solid state in design, with microprocessor based relays just beginning to make inroads into grid protection systems. There were significant design variations within the electromechanical relay spectrum, with some protective devices having built-in harmonic filtering and some relays operating on the full RMS spectrum of the input signal [39]. In 1993, an IEEE Transmission & Distribution Committee Working Group produced a report [40] that described problems experienced with solid state relays that operate on peak values rather than the "effective value" measured by electromechanical relays, but did not provide sufficient detail to be of great benefit to protective relay engineers.

In 1996, the Power System Relaying Committee Working Group K-11 produced a report dedicated to summarizing and describing the effects of GIC on protective relays [10]. This summary included capacitor bank unbalance and overcurrent protection, transformer differential, sudden pressure, and neutral current protection, and generator protection. There was not a detailed study provided for protection schemes, but a thorough review of possible scenarios was described.

Other investigations have been performed into the current transformer (CT) instruments that are used as inputs to protective relays. A comprehensive study involving both simulations and testing [41] found that in general, CTs are not highly susceptible to saturation by GIC. One cautionary point is the case from the K-11 report [10] where a neutral CT on a capacitor bank exceeded its rating factor due to excessive harmonic currents and subsequently experienced a thermal failure.

Load Response to Harmonic-Rich Grids

Savage, Radasky, and Madrid [11] performed testing of "wall warts" - small commonly available DC power supplies. This research used harmonic injection with generalized distorted voltage waveforms that were rich in either second or third harmonics. The focus of their testing was stated as waveforms similar to MHD-E3 related voltage distortion. The process recorded time, temperature, and rate of failure. Device testing included switched mode power supplies, which survived the testing, and rectifier style, which failed the testing. They did not evaluate the stability of the power supply output nor offer waveform-level detail, and suggested testing to this level as possible future work.

Conclusion

There is disagreement in the literature on the overall impact of an MHD-E3 event to power system transformers. An Electric Power Research Institute (EPRI) study released in 2019 [28] indicates that there may be fewer than two dozen power transformers in the continental United States at risk for damage during an MHD-E3 event. The biggest risk cited in the EPRI study is regional voltage collapse resulting in a multi-state blackout. The EMP Commission report [25] states that its report, by "utilizing unclassified data from Soviet-era nuclear tests, establishes that recent estimates by the Electric Power Research Institute (EPRI) and others that the low-frequency component of nuclear high-altitude EMP (E3 HEMP) are too low by at least a factor of 3." Having these two well-regarded organizations at odds over the impact of MHD-E3 underscores the importance of additional research on power system transformers. In 2011-2012, DTRA performed power grid-level testing of transformers and found that real power absorption and secondary voltage harmonics were a significant problem [42], but this research came at a cost of millions of dollars at Idaho National Labs [43]. There was a need for research to determine if the economical laboratory testing of DC injection upon small transformers may be used as a reasonable comparison for the impact found with grid-level transformers.

The first line of defense for power system equipment such as transformers is the protective relay system. Protective relays must operate in a predictable and consistent manner for a faulted condition within their zone of protection, but should not operate for non-fault conditions. For inverse time-overcurrent relays, the literature mentions but does not quantify the mis-operation characteristics apparent during a GIC event. Of greater importance, though, is quantifying the response of a transformer differential relay to the harmonic-rich currents present during a geomagnetic disturbance. Harmonic restraint and harmonic blocking will desensitize transformer protection during periods of elevated GIC due to the increase in second harmonic currents. Research evaluating relay sensitivity to in-zone faults is needed to determine if they will operate correctly for faults during high levels of current harmonics. Likewise, the susceptibility to out-of-zone faults on modern transformer protective relays is needed to determine whether transformer protection systems may cause large power transformers to be erroneously removed from the grid during a high harmonic current MHD-E3 event.

There has been a considerable amount of DTRA testing related to the response of common, off-the-shelf IT (COTS-IT) equipment to the high energy Early Time E1 impulse, but there has been no DTRA testing and only one article found in the literature related to the response of COTS-IT equipment to E3-related voltage harmonics [11]. The testing performed in [11] was based on simple calculated harmonic waveforms using limited test and data acquisition equipment. Research using actual DTRA DC-injection distorted voltage waveform data along with high performance data acquisition equipment is needed to perform an improved evaluation of the COTS-IT equipment response to MHD-E3.

CHAPTER THREE

Transformer Test Bench Theory, Design, and Modeling

Transformer DC Injection Test Bench

In 2012, the Defense Threat Reduction Agency funded DC-injection tests on electric grid-scale equipment at Idaho National Laboratories (INL) [44]. These tests included wye-connected transformers with a bank of batteries between the primary winding neutral connections. Varying levels of DC and load were applied to the transformers, with the test results highlighting the increase in harmonics and power absorption [42].

Theory of Operation

The electrical performance behind the transformer test is dependent upon the saturation characteristics of the magnetic core steel in the transformer. As DC current is introduced into an AC transformer, the DC bias of the current will introduce a DC offset in the voltage and push the magnetic response of the material well beyond the knee point of the V-I magnetization curve and will extend the current response into the saturation region. In the saturation region of a transformer, the permeability of the core decreases while the current increases [45].

Characteristics of Magnetic Saturation

When the magnetic material of a transformer core is exposed to a time-varying magnetic field from the current flowing through the transformer windings, a flux is induced in the core. The response of the core to this increasing magnetic field is nonlinear; at the saturation point of the core material, the magnetic field (H) must increase substantially for a small increase in the magnetic flux (B).

Magnetic fields are proportional to the magnetizing current in the transformer's windings, while the flux density is proportional to the voltage. Recall the units for the magnetic field H within a transformer winding:

$$H = \frac{Ampere \cdot turn}{meter} \tag{3.1}$$

Likewise, the units for flux density B within the transformer core:

$$B = \frac{Weber}{meter^2} = \frac{Volt \cdot second}{meter^2} \tag{3.2}$$

Examining the units for both magnetic field intensity and flux density, it may be observed that other than amperes and volts, the remaining parameters are constants. The benefit of basing an evaluation on voltage and current while considering the rest of the system as constant is the ability to observe the B and H characteristics of the transformer without knowing specifics of the core dimensions or winding parameters. A method for observing the B and H characteristics based on current and voltage sampled values is introduced in Chapter Four.

The relationship between B and H is commonly referenced as a hysteresis curve, where the relationship is expressed as the equation:

$$B = \mu H \tag{3.3}$$

While this equation appears linear, in magnetic materials the field intensity vs. flux density relationship is not linear because the magnetic material exhibits the property of residual magnetism. Because of residual magnetism, there may be current flowing with no voltage applied, and likewise voltage apparent with no current flow. When placed on a graph, the hysteresis curve is formed.

In the previous equation, the scalar μ represents the magnetic permeability of the material in question. In free space (air and other non-magnetic materials), μ is often expressed as μ_0.

$$\mu_0 = 4\pi \cdot 10^{-7} H/m \tag{3.4}$$

In magnetic materials, the scalar μ represents a relationship between the material's relative magnetic permeability characteristic μ_r and that of free air.

$$\mu = \mu_r \cdot \mu_0 \tag{3.5}$$

Magnetic steel manufacturers often provide the material relative permeability at a specific magnetic field density. This value is not constant, however, as the permeability of a magnetic material initially increases, reaches a peak, and then decreases to approach $\mu_r = 1$ as deep magnetic saturation occurs.

V-I Excitation Curve

The relationship between transformer voltage, current, and core saturation may also be demonstrated through an excitation curve. The V-I excitation curve features a nearly linear region where voltage increases rapidly while current slowly increases, a nonlinear transition portion of the curve, and then another linear portion where voltage slowly increases but current rapidly increases. A V-I curve may be measured during transformer testing, and most power class transformer factory test reports contain a minimum of three test points at 90%, 100%, and 110% voltage input. A simulated V-I excitation was created in Matlab based on laboratory transformer measurements, and this curve is shown in Figure 3.1. In the case of the simulated transformer response in Figure 3.1, test points would be applied at 198V, 220V, and 242V to determine the approximate knee point characteristics of the V-I curve. When considering MHD-E3 performance with the V-I curve, the important area is the saturation region beyond 110% voltage input, where the current is increasing substantially for small increases in voltage. This region exists for both polarities of the voltage cycle, and DC polarity plays a role in the transformer primary current waveshape during saturation. The DC polarity will determine if the saturation occurs on the positive half-cycle or the negative half-cycle.

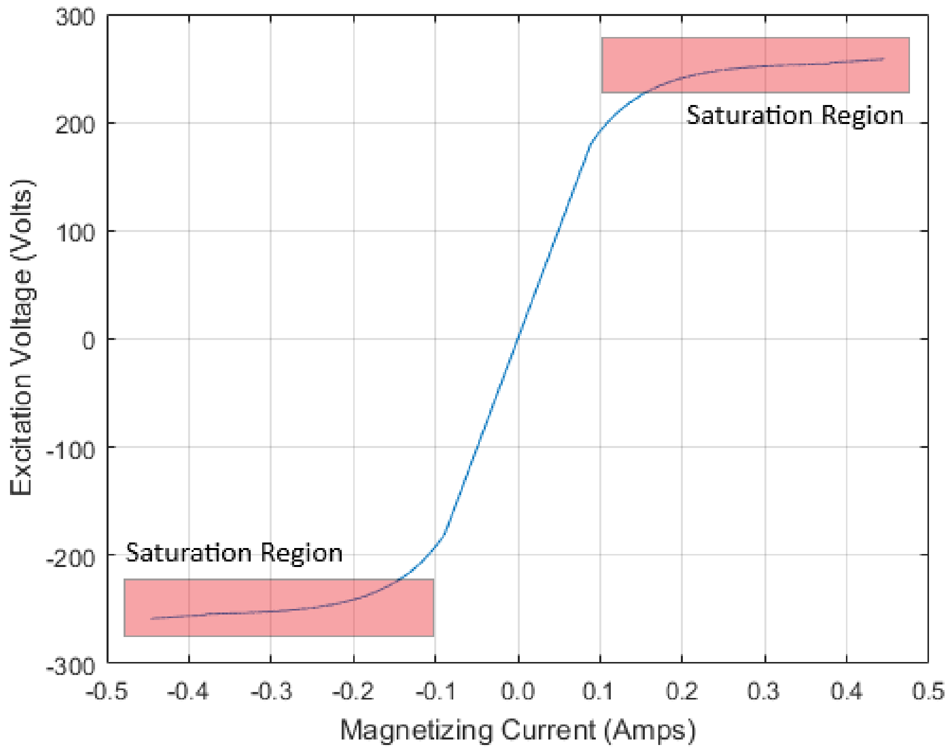

Figure 3.1. Simulated V-I Excitation Curve

As voltage increases beyond the knee-point of the V-I excitation curve (above 110%, or 242V on this graph), the transformer enters the saturation region. Magnetizing current is inductive and is a characteristic independent of load current, so the phase of the magnetizing current is 90 degrees offset from resistive current. The V-I curve in Figure 3.1 is used as the basis for the calculated currents shown in Figures 3.2 and 3.3.

Figure 3.2 shows three simulated current waveforms related to the primary winding of a transformer - the sinusoidal load current, the distorted triangle-waveshape of the magnetizing current phase-shifted by 90 degrees, and the distorted sum of the two currents. The sum of the currents would be observed when sampling or measuring the current directly. The waveforms in Figure 3.2 would be typical waveforms for a small transformer. In this simulation, the ideal load current is sinusoidal and flowing into the transformer while the magnetizing current is based on the V-I curve response to the applied voltage. The sum of the two would be the overall transformer primary winding current and exhibits a slight distortion at the peak of the magnetizing current.

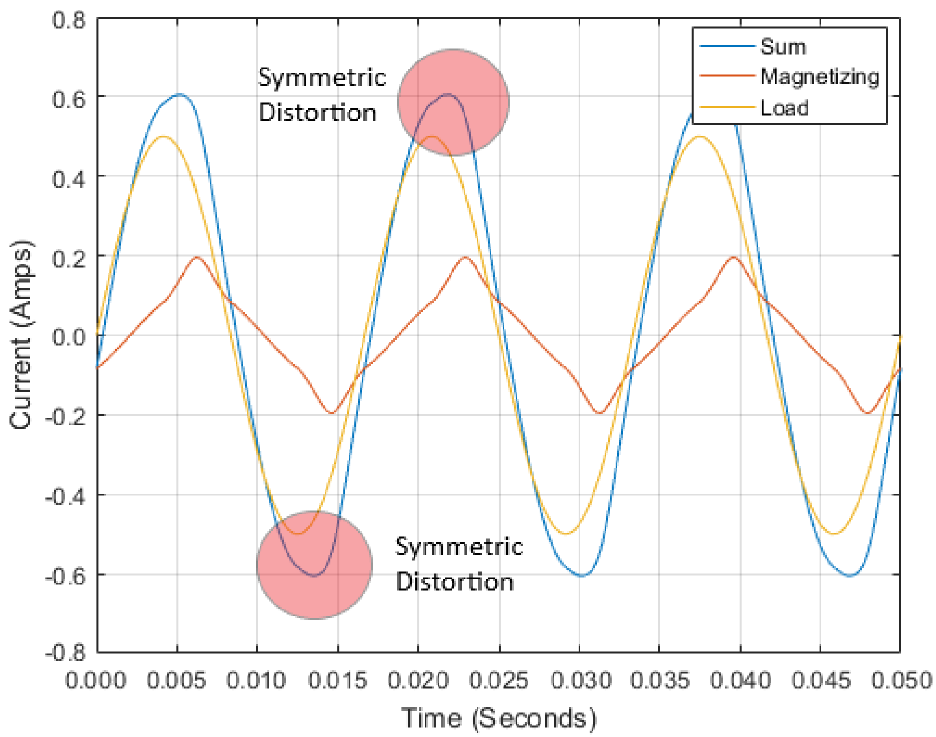

Figure 3.2. Typical Magnetizing, Load, and Sum (Source) Currents

When DC is introduced into a transformer, the neutral point of the AC voltage moves in the direction of the DC bias. This shift in voltage will push the peak of the magnetizing current further into the saturation region of the V-I excitation curve. Figure 3.3 shows the effect of a positive DC bias on the simulated transformer.

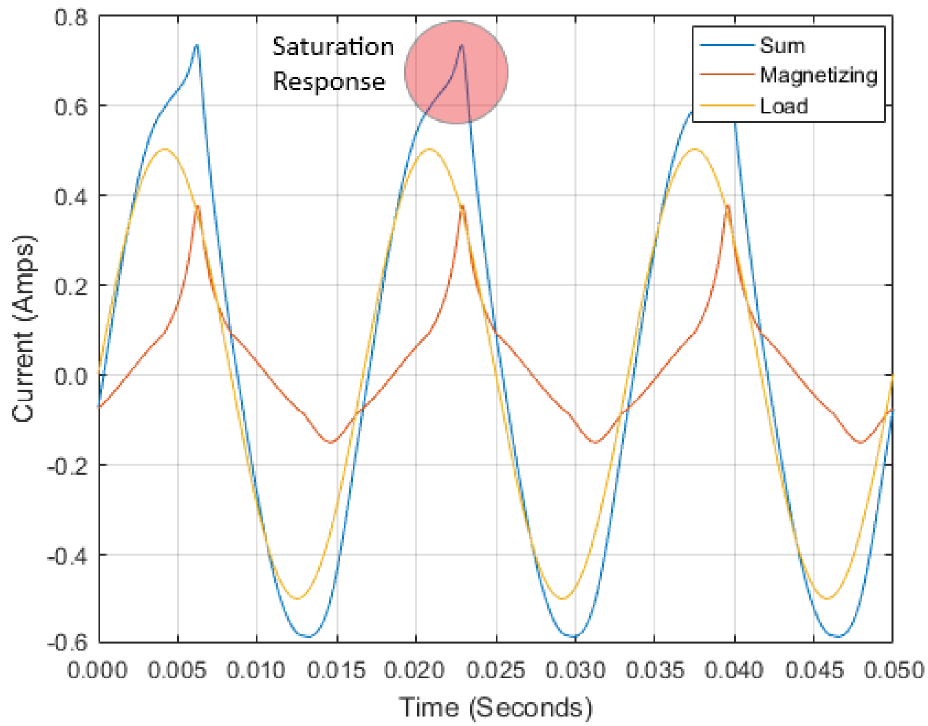

Figure 3.3. Typical Magnetizing, Load, and Sum (Source) Currents During Saturation

The magnetizing current has been shifted by the DC offset such that the positive half-cycle peak has entered the saturation region of the V-I curve. The increased peak of the magnetizing current and the related distortion is the sum of the magnetizing and load currents. This distortion 'bump' increases as DC increases and represents a second harmonic component that is the primary characteristic of a transformer undergoing DC related saturation. Chapter Four contains a section demonstrating the use of current and voltage measurements to obtain the magnetizing current (also considered as 'loss' current) and using that as a B-H curve analogy.

Transformer Core Magnetic Flux Performance

Transformer core design plays a significant role in the susceptibility to DC saturation. Two core designs were available for testing: shell-form single phase transformers, and three-phase three-limb core form transformers.

Several transformer core models were created in Finite Element Method Magnetics software (FEMM) [46], and the resulting magnetic flux density (B) fields are shown to demonstrate core flux density due to DC-only injection (no AC applied) based on transformer design. The modeling for the following transformers is based on the dimensions of one of the benchtop test transformers: 200mm height, 40mm windows, 40mm limbs, and 74mm depth using 0.5mm laminations at 0.987 fill. Core design of large power class transformers is much more complicated, with a focus on transformer efficiency and minimizing losses while accounting for structural components that may or may not offer paths for stray magnetic flux. In the examples to follow, these simple designs are used to show the response of the different common transformer core styles.

In the upcoming figures, the color gradient for the B-field scaling is not the same for each figure. This is done to highlight the intensity zones within the transformer core and to emphasize that some of the field loops are maintained through the air outside the core. For example, in the first figure (Figure 3.4), the B-field peak is over 1.3 Tesla because the core is saturating due to the current input. In the subsequent figure (Figure 3.5), the B-field peak is around 0.0016 Tesla because the DC that has been introduced into each winding forms opposing fields in the core.

For single phase shell-form transformers, the center limb is energized while the outer two limbs offer parallel return paths for the flux. When the transformer is subjected to DC-only, some of the center limb magnetic domains enter a fixed orientation, with the highest flux density apparent within the three limbs. An example of this phenomenon is shown in Figure 3.4. For single phase transformers, the outer two limbs are designed as half the width of the center limb. This transformer was designed as 200mm x 200mm x 74mm in size, 40mm x 80mm window, and a 14 AWG copper winding around the center limb (represented by the boxes on either side of the center limb), though the emphasis of this graphic is the response of this single phase shell-form (winding inside a shell of core steel laminations) transformer design.

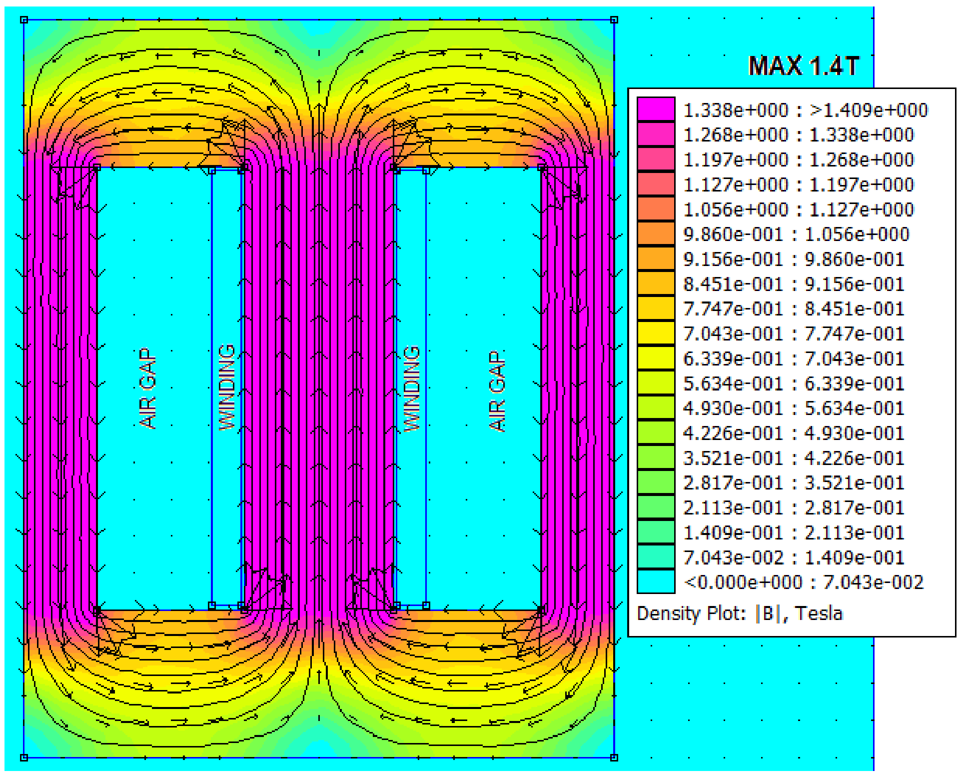

Figure 3.4. Flux Density Path in Single Phase Shell-Form Transformer, DC-only

The design of the single-phase transformer core provides a low-reluctance path for the magnetic flux, making it more susceptible to core saturation under quasi-DC conditions. In Figure 3.4, note the vector orientation and flux density characteristics. Under DC, this vector and density would be the "neutral point" for the AC oscillations in the flux density. The transformer then becomes susceptible to overexcitation and saturation because the flux density in the center and outer limbs is closer to saturation than under normal conditions.

For three-phase three-limb core-form transformers when the transformer connection includes a grounded-wye, the core design offers a much higher reluctance to quasi-DC conditions. In this transformer design, the core plus winding configuration provides a magnetic polarity that opposes DC flux in the core of the transformer, making the transformer design less susceptible to saturation. Figure 3.5 demonstrates the flux density performance of a grounded-wye three-phase three-limb transformer under the influence of a DC source that is supplying the same current magnitude and polarity through all three phases.

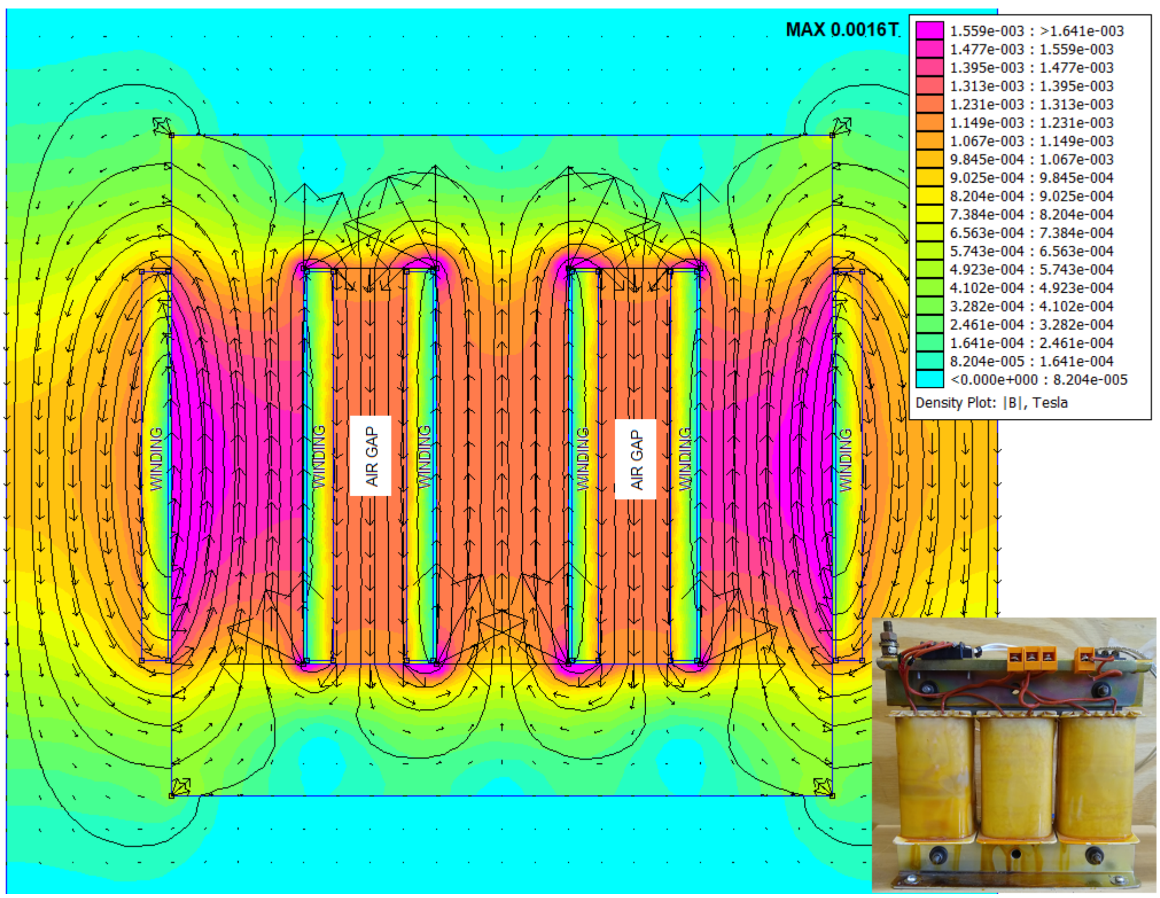

Figure 3.5. Flux Density Path in Three-Phase Core Form Transformer, DC-only

Again, the scaling for the magnitude of the B-field in Figure 3.5 is not the same as for Figure 3.4. Note that in the case of the three-phase three limb core-form transformer, the B-field that results from the DC source is near zero because of the opposing flux regions and the high reluctance of the return paths through the air both beyond the outer two limbs and within the center winding windows. If the assumption is made that DC is equal among the three phases, in theory, the magnetic dipoles in the core would only respond to the AC component of the winding current.

If there is a slight imbalance in DC between the three phases, a corresponding increase in DC flux appears on the limb with the elevated DC. An imbalance in the DC may result from a resistance difference in the transmission network or within the transformer winding resistance. Figure 3.6 displays the flux density and paths for the same transformer from Figure 3.5 but with 10% more DC on an outer limb winding.

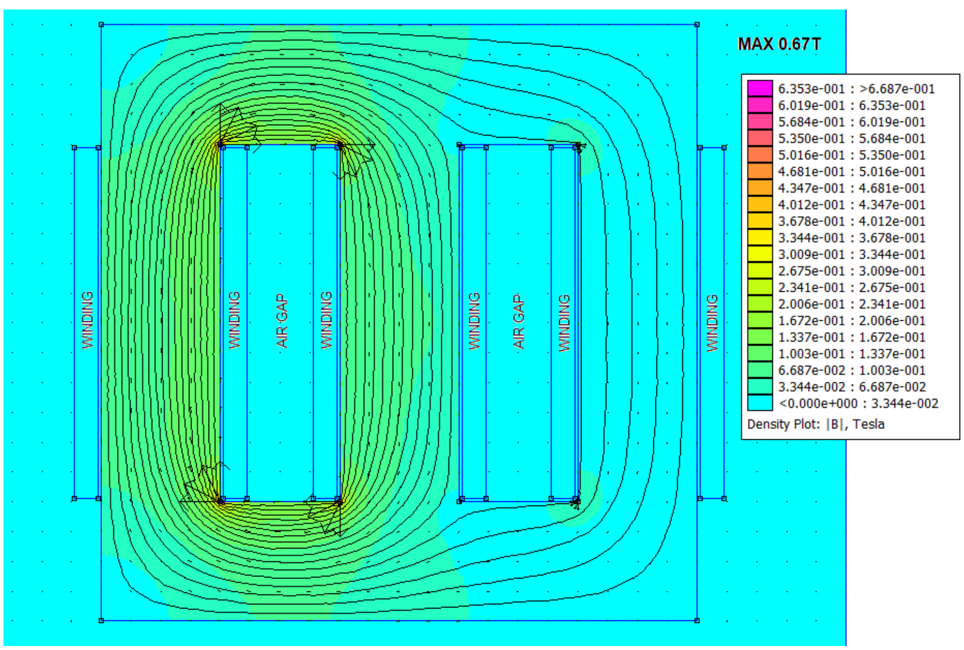

Figure 3.6. Flux Density Path in Three-Phase Core Form Transformer, 10% Additional Current on One Limb, DC-only

While Figure 3.5 exhibits an obvious asymmetry in flux density, this example's small difference in flux due to DC would not likely be sufficient to result in core saturation.

When the three-phase core-form transformer is placed within a steel shell, the shell becomes the primary return path for the DC magnetic flux. While the flux density is still low in the core, the shell that surrounds the transformer exhibits significantly more flux density than the core. This phenomenon can be expanded to other steel items within the transformer such as support brackets and flitch plates. Figure 3.7 shows the flux behavior when the transformer is enclosed in a steel shell. In this example, the shell is approximately 10% of the width of the transformer limb, but carries 100% of the available flux. The thickness of shells on substation power class transformers may be 2% or less than the width of a transformer limb.

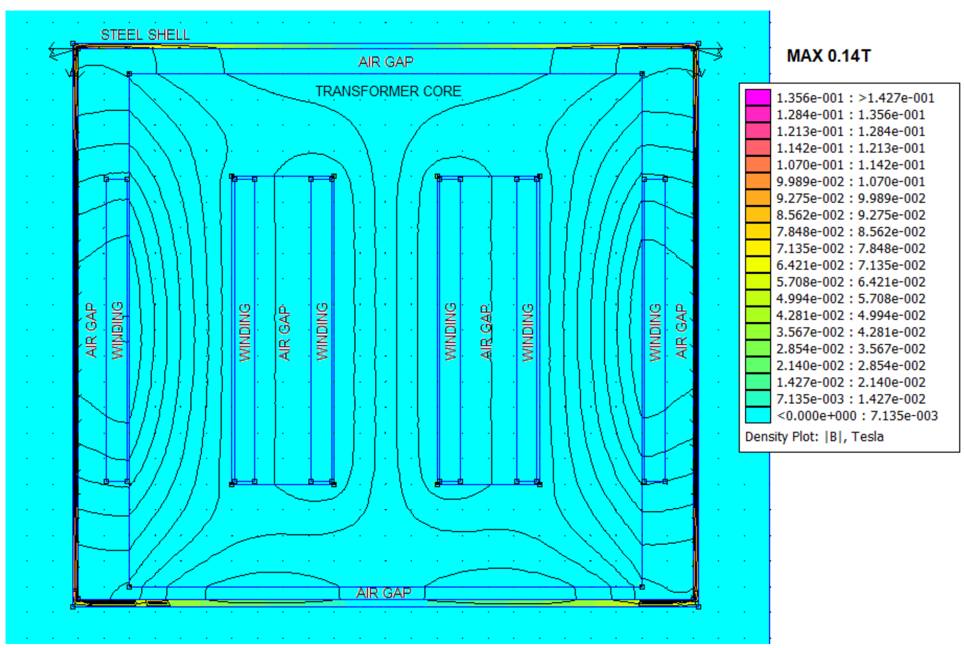

Figure 3.7. Flux Density Path in Three-Phase Core Form Transformer with Shell, DC-only

Core design thus plays a critical role in the susceptibility of transformers to saturation under DC. Single-phase transformers show a much higher susceptibility to saturation than three-phase three-limb transformers due to the difference in the reluctance of the magnetic flux paths in the core.

Design of Transformer Test Bench and Calculating Modeling Parameters

Series Transformers

A small-scale transformer DC-injection test bench was designed using a 208V three-phase laboratory voltage supply. A single line diagram for the network is shown in Figure 3.8. This diagram is representative of all three phases. Three single phase 2 kVA 120:240 step-up transformers were connected wye-wye to increase the available supply voltage. These three transformers were connected to three wye-connected 2kVA 220V single phase variable autotransformers. These three autotransformers were then wye-connected to three 1500VA single phase 1:1 isolation transformers (T1). This point of connection is referred to as the "Line" component of the network. The neutral was not connected across the isolation transformer.

The secondary side of the isolation transformer served as one half of the test "Loop". The isolation transformers were wye-connected to yet another set of wye-connected transformers (T2). Several transformer styles were available: a bank of (3) 250VA single phase, a bank of (3) 500VA single phase, and (1) 1kVA three-phase three-limb were available during this test period. Between the neutral connections of these transformers was a resistor in parallel with a switched battery. On the secondary side of the final wye-connected transformers (T2), light bulbs were used as a resistive "Load".

A National Instruments CompactDAQ with LabView 2015 was used to collect measurements during DC-injection tests. AC voltage was measured by AC voltage DAQ modules while currents were measured by AC current DAQ modules and Hall Effect current sensors. In Figure 3.8, data acquisition points for voltage and current are denoted by "V" and "I" respectively, and represent AC voltage inputs, AC current inputs, and Hall Effect current sensor inputs to the CompactDAQ system.

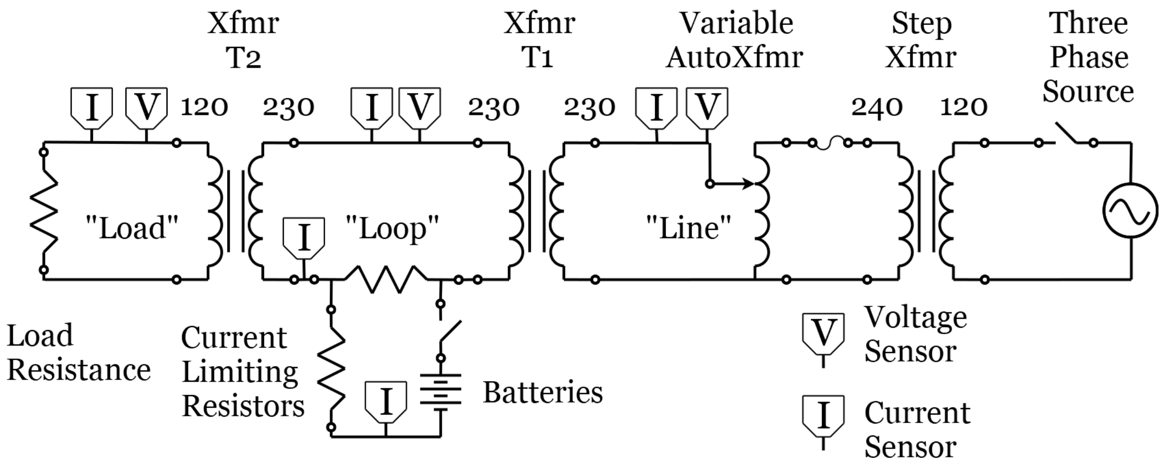

Figure 3.8. Transformer DC Injection Test Bench Single Line Diagram, Series Configuration

Initial tests were performed without the Hall Effect current sensors. It was observed that abnormal transient current measurements were present during the higher-level DC-injection periods. It was determined that these transients were due to the magnetic saturation of the small internal current transformers (CTs) used in the National Instruments current input modules. The Hall Effect current sensors operate on a different principle for measurement and are not subject to this magnetic saturation. Additionally, Hall Effect sensors are able to reproduce the DC offset of the current waveform, whereas the AC CT does not reproduce DC offset beyond a few power system cycles. With the Hall Effect current sensors it was possible to accurately measure the amount of DC flowing through each branch of the transformer network.

A picture of the test bench in an early stage of development is shown in Figure 3.9. During this phase, having both sets of transformers together on the bench led to magnetic field interference with the Hall Effect sensors, thereby causing excessive noise in the current measurement. Eventually the larger transformers were moved below the table to provide open space for the Hall Effect sensors, which helped reduce the noise on the measurements.

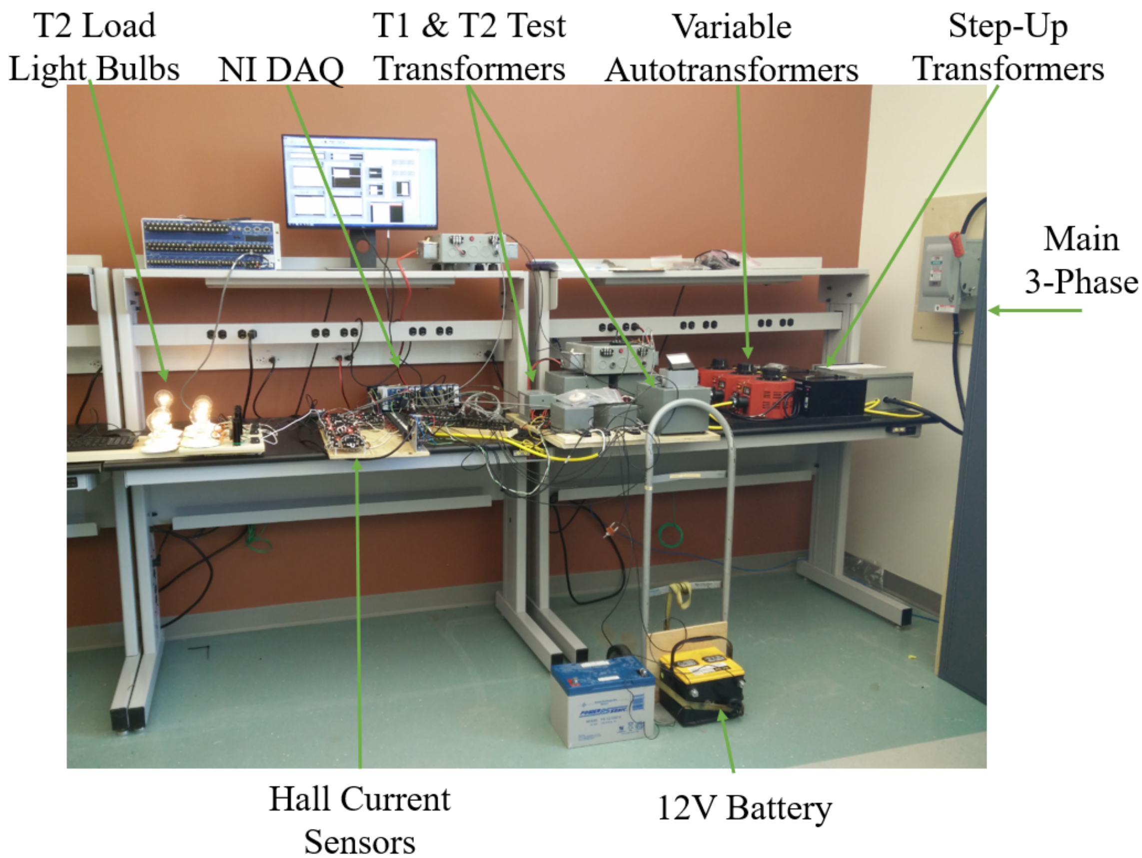

Figure 3.9. Transformer DC Injection Test Bench, Series Configuration, early 2018

Parallel Transformers

Following the success of saturation testing with the test bench configuration as transformers in series, the transformers were placed in parallel to more closely resemble the configuration of the Idaho National Labs testing. The single line diagram for this configuration is shown in Figure 3.10.

A neutral "Loop" exists in this configuration where DC current may be introduced into the network, but in this configuration the neutral connection of the "Loop" also included the variable autotransformer and the step-up transformer. This introduced the possibility for DC to enter the source side of the lab's power grid. Series DC blocking capacitors were installed between the source and the transformers

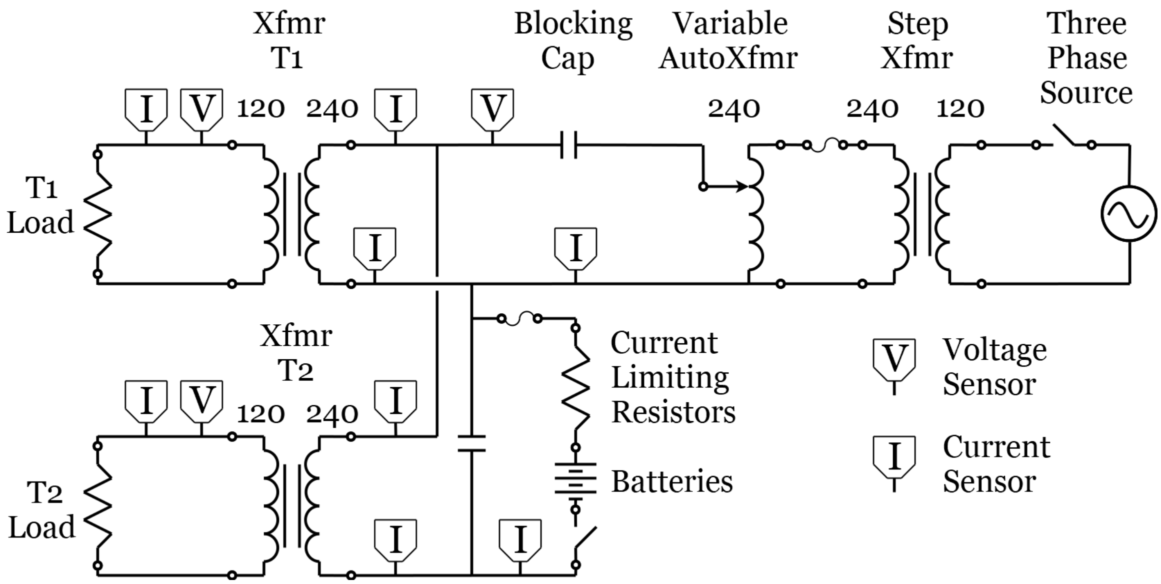

Figure 3.10. Transformer DC Injection Test Bench Single Line Diagram, Parallel Configuration

under test to resolve this problem. Another change was the addition of a series capacitor instead of the resistor in the neutral. The series capacitor permits AC neutral current to flow while blocking DC from circulating within the small parallel loop. A picture of the test bench as described is shown in Figure 3.11.

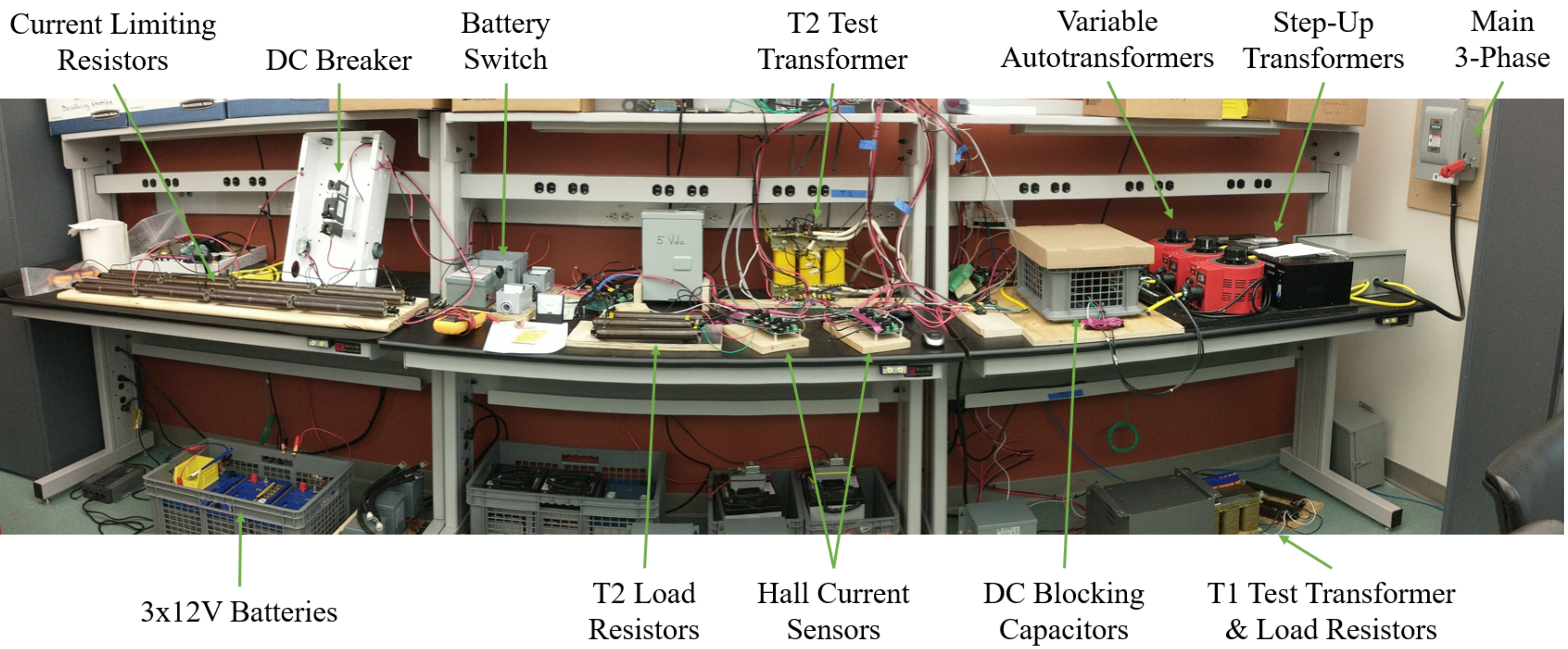

Figure 3.11. Transformer DC Injection Test Bench, Parallel Configuration, 2020

Transformer Parameter Calculations

Before software modeling is possible, transformer testing must be performed to calculate the series and shunt impedances of the windings. Open-circuit and short-circuit tests were performed on each size of transformer under test. In industry, typical open circuit testing involves 90%, 100%, and 110% of voltage rating. Because of the flexibility of the variable autotransformer and sophistication of the data acquisition equipment, open circuit tests were performed incrementally across the range from 10% to 115% of primary winding voltage. Likewise, short-circuit tests were performed to 150% of rated current.

Because tests in the laboratory can take a significant amount of time to run, it was necessary to create simulations in ATP/EMTP (Alternative Transients Program / Electromagnetic Transients Program). To create a saturable model in ATP, the magnetizing current is a required parameter. Magnetizing current is purely inductive, in contrast to the resistive nature of winding resistance. Transformer parameter calculations here rely on sampled values from the data acquisition system. Test data was acquired at a 25 kHz sampling rate resulting in 417 samples per power system cycle. Equations 3.6 and 3.7 are standard root mean square of sampled values, where v and i are the sampled data points and n represents the number of sampled values.

$$V_{RMS} = \sqrt{\frac{\sum_{k=1}^{n} {v_k}^2}{n}} \tag{3.6}$$

$$I_{RMS} = \sqrt{\frac{\sum_{k=1}^{n} {i_k}^2}{n}} \tag{3.7}$$

To determine the phase angle difference between the fundamental (60 Hz) voltage and current, Matlab was used to calculate the Discrete Fourier Transform (DFT) of the n samples, with the DFT calculation result being a set of complex values. Since these tests are performed with standard sinusoidal signals with very low levels of harmonics, the difference between the angles of the complex values found at the peak magnitude of the DFT accurately represents the phase angle difference between the voltage and the current.

$$\angle V = \angle(DFT(v)_m)\; where\, m = index(max(abs(DFT(v)))) \tag{3.8}$$

$$\angle I = \angle(DFT(i)_n)\; where\, n = index(max(abs(DFT(i)))) \tag{3.9}$$

$$\angle\Theta = \angle V - \angle I \tag{3.10}$$

The magnetizing current may now be found by Equation 3.11:

$$I_{MAG} = I_{RMS} \sin\Theta \tag{3.11}$$

The small transformers under test have various nameplate primary (H) winding to secondary (X) winding ratios, but the design of most smaller transformers (smaller than 1kVA per phase) is typically compensated to account for transformer losses due to the smaller design. Proper modeling to account for transformer compensation requires the actual ratio calculation in Equation 3.12, rather than the nameplate ratio from the transformer itself.

$$N = \frac{V_{RMS_H}}{V_{RMS_X}} \tag{3.12}$$

Finally, the transformer AC impedance, AC resistance, and reactance may be calculated from the short circuit tests using the following equations:

$$Z = \frac{V_{RMS}}{I_{RMS}} \tag{3.13}$$

$$R = Z\cos\Theta \tag{3.14}$$

$$X = \sqrt{Z^2 - R^2} \tag{3.15}$$

The open circuit tests in the laboratory were performed using scripted steps with a programmable voltage source. This permitted a consistent step interval of 10 volts across all phases and transformers. The magnetizing current curve for the three sizes of single phase transformers is shown in Figure 3.12. The magnetizing current required for the 250VA and 500VA transformers is very similar, while the larger 1500VA transformer is significantly greater. The nameplate rating for all three transformers is 240V for the primary winding.

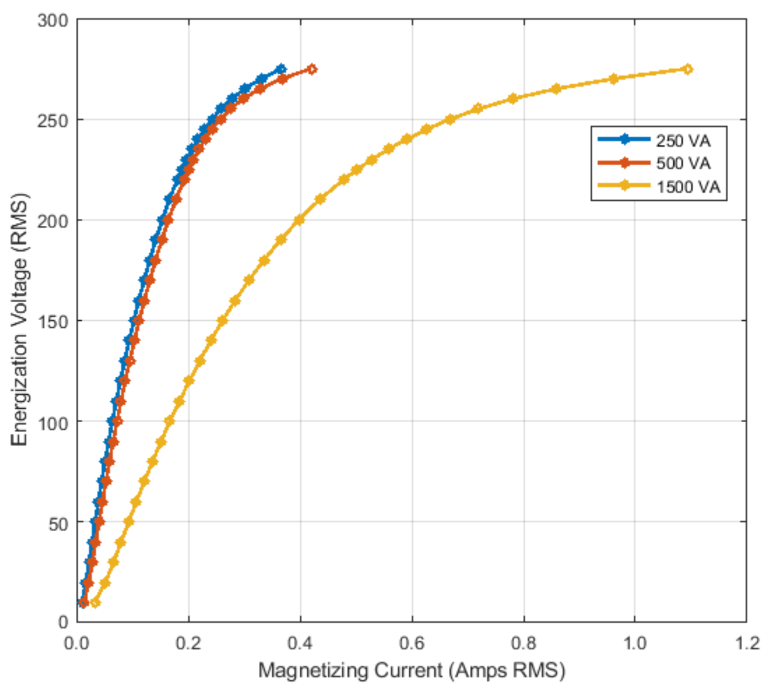

Figure 3.12. Single Phase Transformer Voltage vs Magnetizing Currents, AC-only

Single phase transformers allow for straightforward modeling of the magnetization curve since each unit functions as an individual and there is no magnetic circuit interaction between the phases. With a three limb three phase transformer, the center limb (in this case, B-phase) has a lower reluctance magnetic circuit because the center limb path uses the two outer parallel limbs (see Figure 3.5), while the outer limbs use a series magnetic circuit. Figure 3.13 shows the magnetizing current of a 1000VA (333VA per phase) three limb three phase transformer. Note that the magnetizing current magnitude is significantly lower for the three phase transformer than single phase transformer current magnitudes.

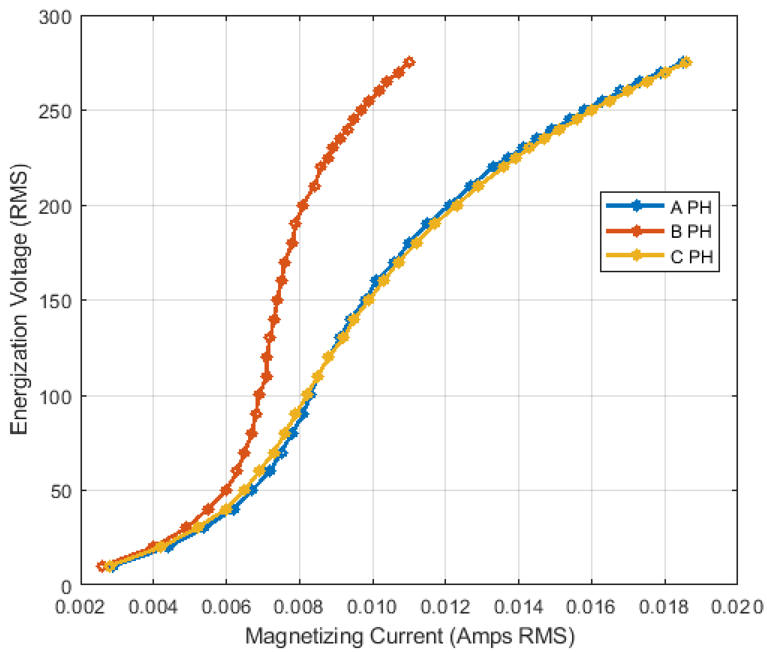

Figure 3.13. Three Phase Transformer Voltage vs Magnetizing Currents, AC-only

Creation of the ATP (Alternative Transients Program) Model

ATP was used to create a simulation model of the test bench. It was observed that the transformer winding resistance calculated from the AC circuit performance during the open- and short-circuit tests was greater than the DC resistance as measured using a digital multimeter. This result was not unexpected, as the skin effect phenomenon will cause AC resistance to be greater than DC resistance. Both resistance values were simulated in the circuit, and it was determined that for DC injection test modeling, a more accurate representation was observed using the DC resistance with AC inductance.

The Magnetizing Current vs Voltage curve values and impedances were used with the standard ATP TRAFO_S single-phase saturable transformer model. The first model created was based on the series transformer configuration shown in Figure 3.8. The ATP magnetizing curve for the 250VA transformer as configured in the TRAFO_S model is shown in Figure 3.14. ATP automatically creates the lower left quadrant symmetric with the user-configured upper right quadrant entries.

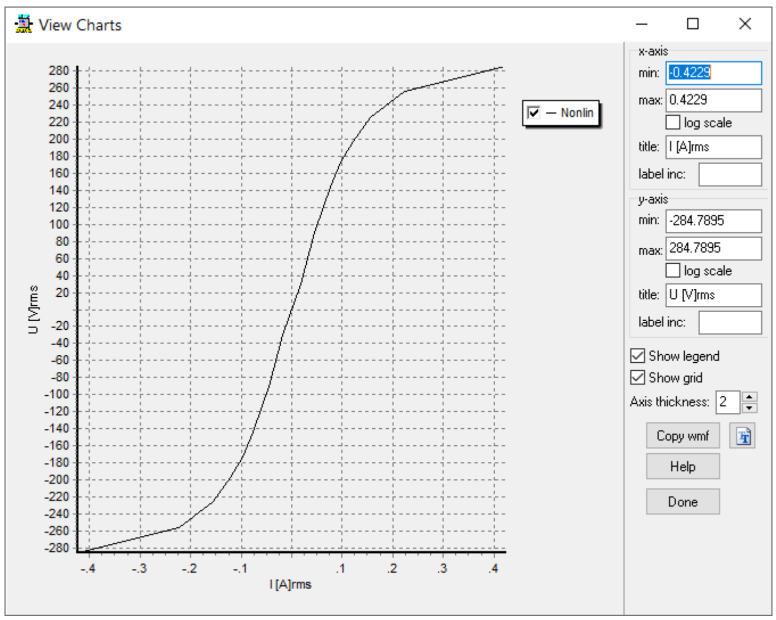

Figure 3.14. ATP TRAFO_S 250VA Magnetizing Curve

The simulated circuits consist of three single-phase voltage sources with 120 degrees of angular separation between phases. In the circuit shown in Figure 3.15, the 1500VA and 250VA single-phase transformer models are used in series. The transformers are wye connected with neutrals grounded except for the secondary of the first set of transformers. So that DC may be injected into this circuit, the neutral on these transformers is connected to the battery injection circuit instead of to ground.

In the series connection, the secondary windings of the source transformer and the primary windings of the load transformer are involved in the DC 'loop'. With

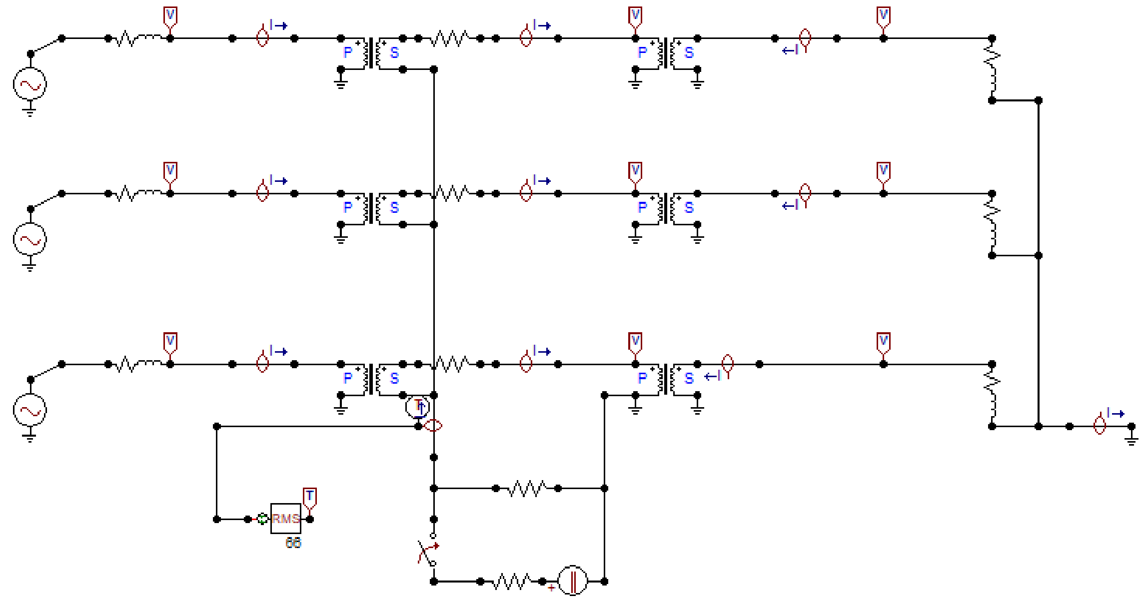

Figure 3.15. Three-Phase ATP Model, Series Transformer Configuration

a parallel connection, the primary windings of both transformers are within the DC ‘loop’. With this configuration, both banks of transformers may be evaluated under DC injection, whereas with the series configuration, only one transformer configuration could be tested at a time. The parallel transformer simulation circuit is shown in Figure 3.16.

With the parallel connection in the simulation circuit, the neutral of the primary winding for the larger (1500VA) transformer was not connected to ground. This allowed the DC to flow in the loop between the two sets of transformers.

In the ATP/EMTP modeling, it may be noted that the directional indicator of the secondary current metering appears to be in the opposite direction of current flow. The current metering polarization is arranged in this manner because differential relay protection uses opposing polarity current transformer connections on either side of a power system transformer. The series circuit was used to create test files for transformer differential relay testing, which will be discussed in detail in Chapter Six. Simulated waveforms will also be presented in Chapter Six.

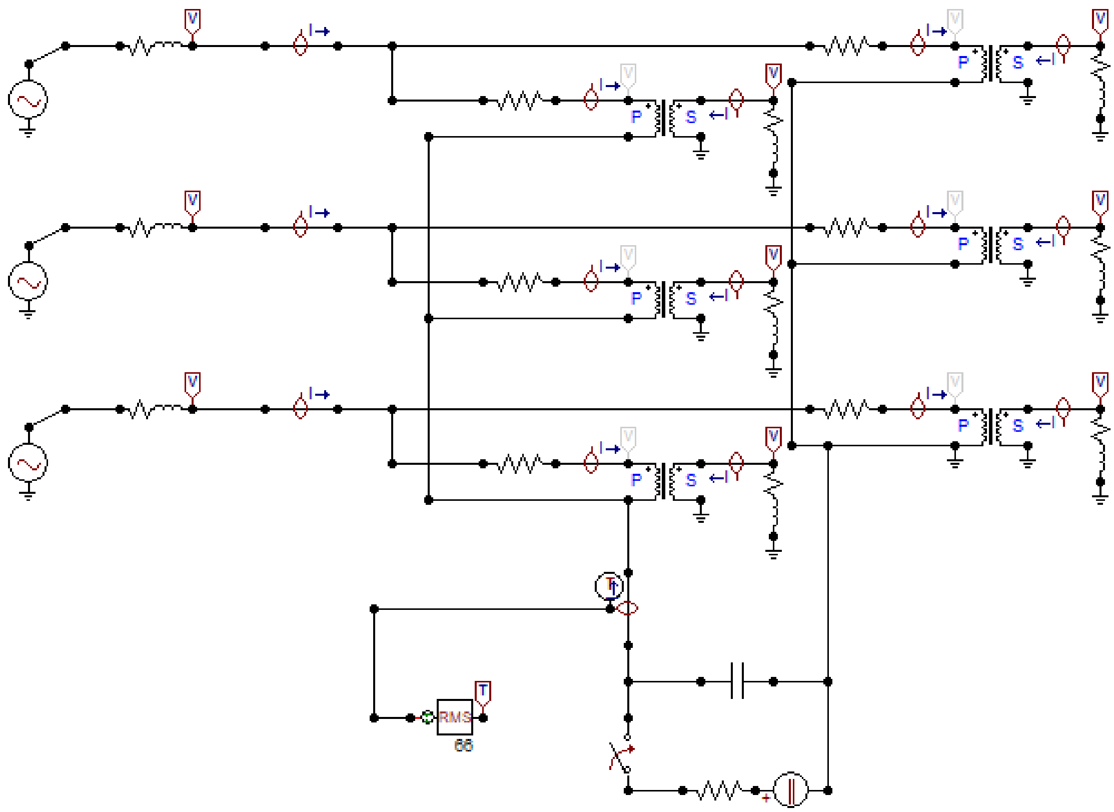

Figure 3.16. Three-Phase ATP Model, Parallel Transformer Configuration

CHAPTER FOUR

Transformer Test Bench Results

The goal of bench testing was to compare saturation characteristics between benchtop transformers and utility grade transformers under DC injection test conditions. Analysis of the data was to adequately address the questions:

(1) What is the harmonic response of a transformer during varying levels of DC injection while load is constant?

(2) What is the power response of a transformer during varying levels of DC injection while load is constant?

(3) Which characteristics of small transformers in the laboratory resemble observations from the Idaho National Laboratories / Defense Threat Reduction Agency (INL/DTRA) field tests of utility grid-scale transformers?

On the transformer test bench, six models of transformers were available that represented three styles of transformers, including autotransformers which have limited coverage in the literature. The nameplate information for these transformers is shown in Table 4.1.

Table 4.1. Benchtop Transformer Specifications

Rating (VA)	Phase	Description	Primary V (L-N)	Secondary V (L-N)
250	Single	2-Winding	240	240/120
500	Single	2-Winding	240	240/120
1500	Single	2-Winding	240	240/120
1000	Three	2-Winding YY	230/240	127
2500	Three	Auto-Y	240	120
7000	Three	Auto-Y	230	120

In a typical 60 Hz power system, even harmonic (2^{nd}, 4^{th}, etc.) currents are not present except during abnormal conditions. Transformer energization is one such condition where inrush currents result in even harmonics. When a transformer is energized, it is common to observe asymmetrical input currents and/or a 'flat' waveshape at the zero-current level for a half-cycle. The almost-flat waveshape phenomenon is shown in Figure 4.1, which is based on data that was collected by the author during energization of a 480V to 69kV three phase step-up transformer at a test facility. For the first 5-7 cycles, the waveform is highly asymmetric with the characteristic 'flat spot' near zero on the Current (Y) axis. As described in the V-I saturation curve discussion in Chapter Three, the saturation current may occur on either the positive half-cycle or the negative half-cycle but typically not both. In Figure 4.1, phase A is saturating during the positive half-cycle, while phase C is saturating during the negative half-cycle. The half-cycle saturation polarity depends upon the voltage polarity at the moment the switching device closes and upon remanent magnetism that may exist in the transformer core.

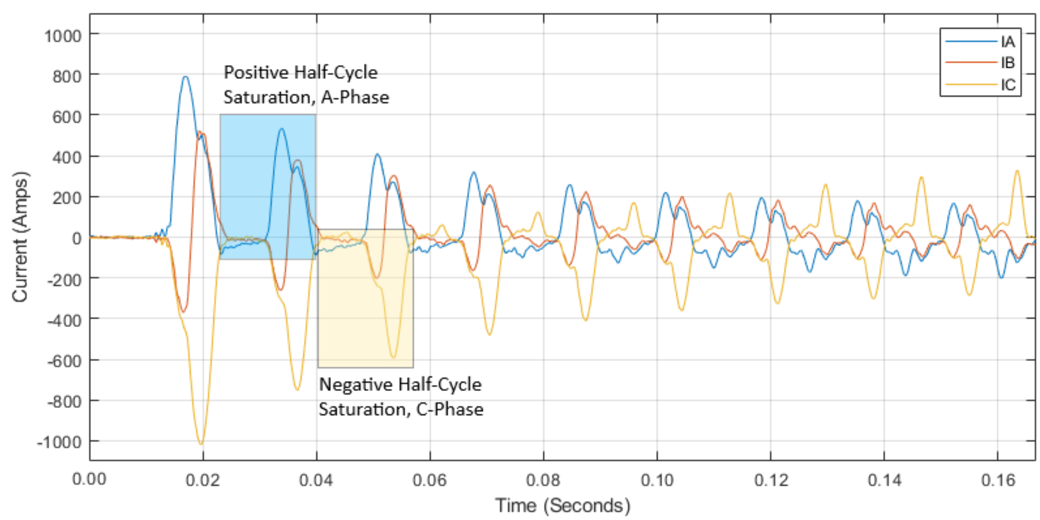

Figure 4.1. Transformer Inrush Current with High Second Harmonic Component: 45% 2^{nd} Harmonic A Phase and 72% 2^{nd} Harmonic C Phase

Why is the second harmonic component important in transformer analysis? In power system protection, transformer differential relays have settings based on harmonic content that can prevent differential relay operation during periods of energization inrush current. Protection is typically accomplished through two methods: harmonic blocking and harmonic restraint. These functions will be described in detail in Chapter Six, but for this discussion, the harmonic percentage value of 15% is used. In the context of protective relaying, this percentage value is described as the percent of *operating current* in a transformer differential relay. In practical terms and throughout this chapter, the operating current is referred to as the *loss current* within a transformer – the scaled difference between transformer primary current input and transformer secondary current output. The loss current is a combination of copper losses, magnetizing current, core losses, harmonic losses, and in the case of an internal transformer fault, the change in current flow as a result of an internal open or short circuit.

The loss current is calculated by subtracting the ratio-scaled transformer secondary current from the transformer primary current as shown in Equation 4.1, where V_S is the secondary voltage and V_P is the primary voltage.

$$I_{LOSS} = I_P - \frac{V_S}{V_P} I_S \tag{4.1}$$

The significance of the loss current is in terms of protective relay operation. For consideration as a common threshold within industry, when the second harmonic content of the loss current reaches 15% of the fundamental loss current, a transformer protective relay may block or restrain tripping on differential current. Testing has shown that this threshold is quickly achieved when the transformer is subjected to low levels of DC. For this reason, harmonic component percentage analysis is included in the discussion of test results. Harmonic blocking or restraint prevents relay operation during energization but also reduces the sensitivity of transformer differential relays because of harmonics due to transformer saturation. This phenomenon will be discussed in Chapter Six.

For DC-injection transformer tests performed in the laboratory, the load on the transformer was purely resistive. The reasons for this are to simplify calculations for loss current and to minimize external harmonics. Inductive, capacitive. and nonlinear loads would introduce harmonics that would complicate analysis of the acquired data.

The transformers tested may be categorized into three groups based on winding configuration and core design:

(1) Single phase, 2-winding, shell-form core construction (250VA, 500VA, 1500VA)

(2) Three phase, 2-winding, core-form core construction (1000VA)

(3) Three phase, Autotransformer, core-form core construction (2500VA, 7000VA)

As described in Chapter 3, core construction is influential in the susceptibility to magnetic saturation. This was confirmed during bench tests. While the three-phase core-form transformers required more DC to saturate the core, it was possible to introduce sufficient DC on the test bench to cause elevated harmonics and limited magnetic saturation of the core.

Group 1: Single Phase, 2-winding Shell Form

Early testing involved connecting two banks of single-phase shell form transformers in series (Figure 3.8). The three 1500VA single-phase transformers were connected with primary windings on the line side, and the load transformers (either 250VA or 500VA single-phase transformers) were connected with their primary winding attached to the secondary of the 1500VA transformers. This secondary-primary connection had an isolated neutral loop that included the DC injection source.

The single phase transformers all showed the characteristics of saturation at low DC levels, and were in deep saturation well within the limits of the injection test bench current capability. For example, in this test, the lightly-loaded single phase 250VA transformer crosses the 15% second harmonic loss current at 5% per unit of rated current (DC injection at only 0.045A). The characteristic second harmonic-related saturation region waveshape (highlighted in red) is evident from the graph in Figure 4.2 with a response similar to the simulated waveform from Figure 3.3. When examining the harmonic spectrum of the waveform, elevated levels of second, third, fourth, and fifth harmonics are evident. The second harmonic is the important indicator of approaching saturation, as it does not typically occur in power systems except during transformer inrush. The third harmonic component is common in slightly unbalanced three phase power systems and in this instance is associated with the second harmonic positive half-cycle impulses causing a current imbalance between the phases. The fourth and fifth harmonics, while detectable and used by some protective relay systems, do not present a problem and are not of as much interest as the second harmonic.

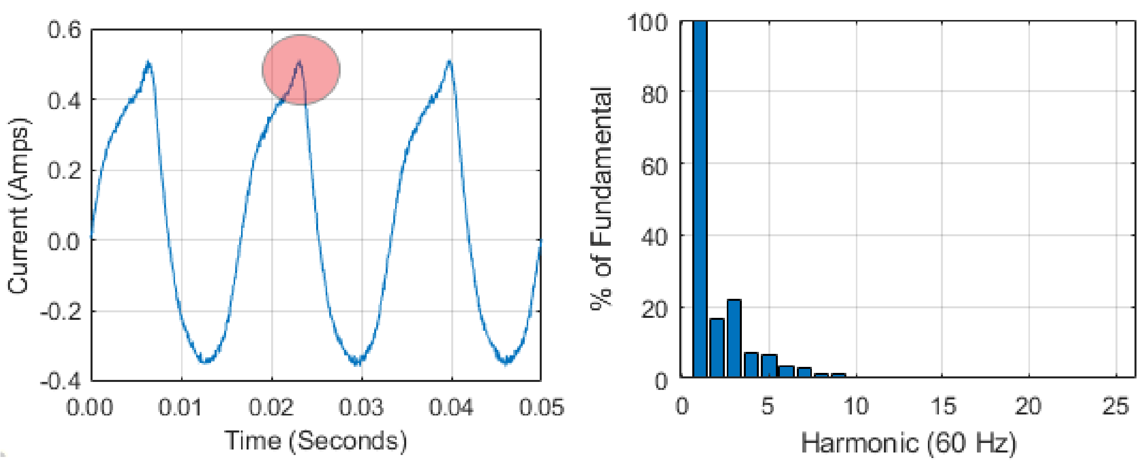

Figure 4.2. Source Current Waveform and Loss Current Harmonics, Single Phase 250VA

The series-connection injection tests were the basis for initial protective relay current testing. Tests of the three 250VA single-phase transformers resulted in a collection of data representing a stepped series of harmonic-rich current waveforms.

These waveforms were converted to test files, scaled, and injected into various current-sensitive protective relays in order to evaluate the response. As DC increases, the second harmonic characteristic becomes more pronounced. An example of the increase in second harmonic influence related to increasing DC is shown in Figure 4.3, and the results of this relay testing is the subject of Chapter Five.

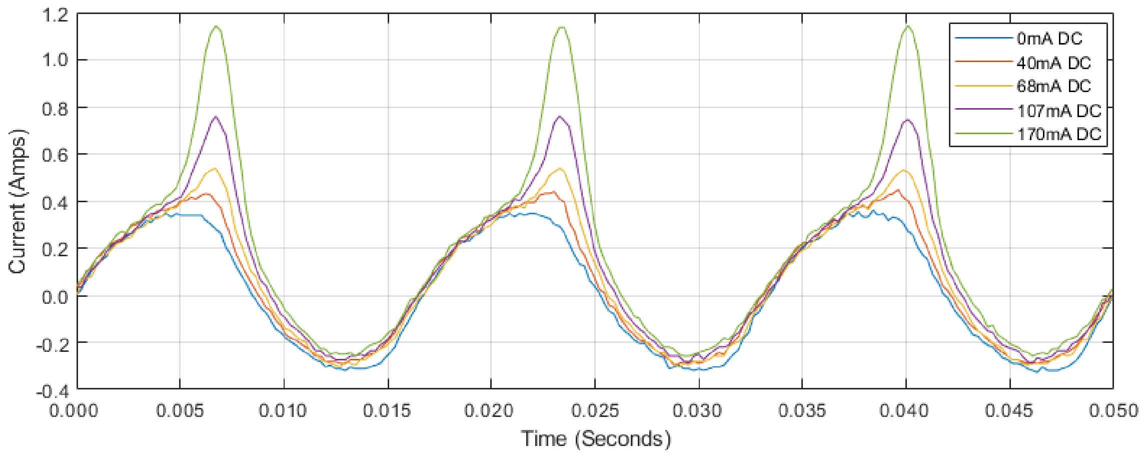

Figure 4.3. Transformer Current Waveforms with Varying Levels of DC, Single Phase 250VA

Current and voltage distortion were evident during higher levels of DC saturation. Figure 4.4 shows the voltages and currents during a series configuration three-battery test of the 1500VA (Source) and 500VA (Load) single phase transformers with positive voltage half-cycle saturation. The load voltage distortion waveshape has similar characteristics on both the rising and falling edges to voltage waveshapes logged in the Idaho National Laboratories testing, examples of which are shown in Figure 4.5. At these levels of voltage distortion, transformers are in deep saturation as the core has begun to absorb power and is unable to effectively transfer as much power to the secondary of the transformer. The INL voltage graphs are scaled from the original 277 V_{LN} to 120 V_{LN} for comparison purposes.

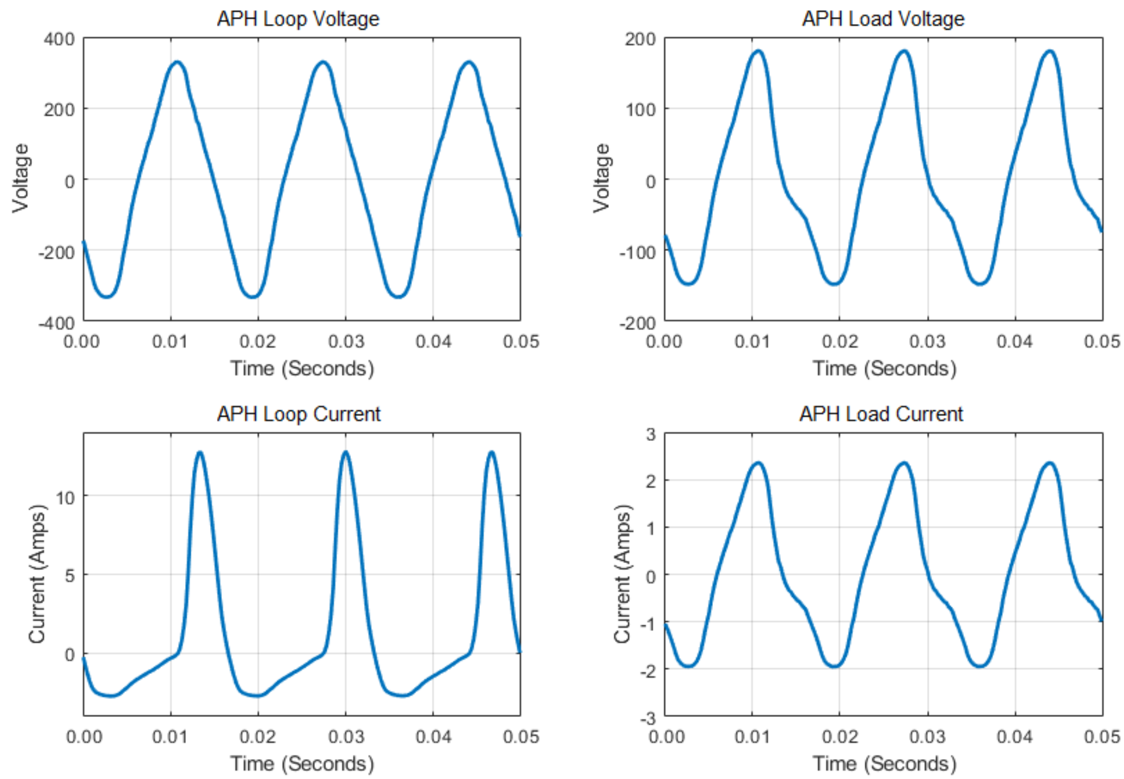

Figure 4.4. Voltage and Current Waveforms During Three Battery Test, Single Phase 500VA

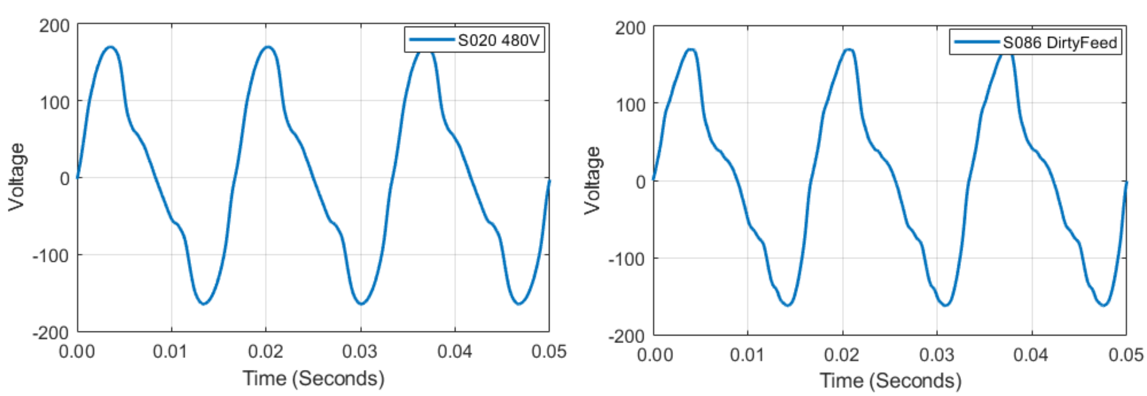

Figure 4.5. Load Voltage Waveforms from INL Tests

Group 2: Three Phase Three Limb Core Form Transformer

A three phase, three limb, YY configuration core form transformer was purchased for testing. This transformer proved difficult to saturate. The primary winding input resistance of each winding was high (over10 ohms on the DC multimeter), which limited the DC to around 2.5-2.6 amps per phase with 3 batteries on the parallel configuration test bench. Additionally, the transformer was designed with multiple taps to use higher voltages than the available bench test voltage levels. Bench voltages were a maximum of 240 volts line to neutral (415 volts line to line). This transformer had taps ranging from 220 volts line to line through 480 volts line to line (277 L-N), with the 400 and 415 volt taps being used on the test bench. Increasing the DC supply with additional batteries was not considered safe at the time of testing. Loading on the transformer was 10% of its rating (100 watts resistive, 33 watts per phase).

Figure 4.6 shows the results of a 3-battery 2.5A per phase test: slight distortion of the primary winding input current, a clean output current waveform, a fair amount of third harmonic on the primary current, and a large amount of third harmonic in the loss current. The reason for the spike in third harmonic in the loss current was because the loss current was of very low level - this 1000VA transformer has a low loss current design, so a small amount of third harmonic can make up a high percentage of the overall loss current. Similar to the previously described 500VA transformer, the third harmonic in the loss current is an artifact of the saturation characteristics created by the second harmonic. There was enough second harmonic content in the loss current to enter harmonic blocking/restraint mode of a differential relay, but this test is barely entering the saturation region.

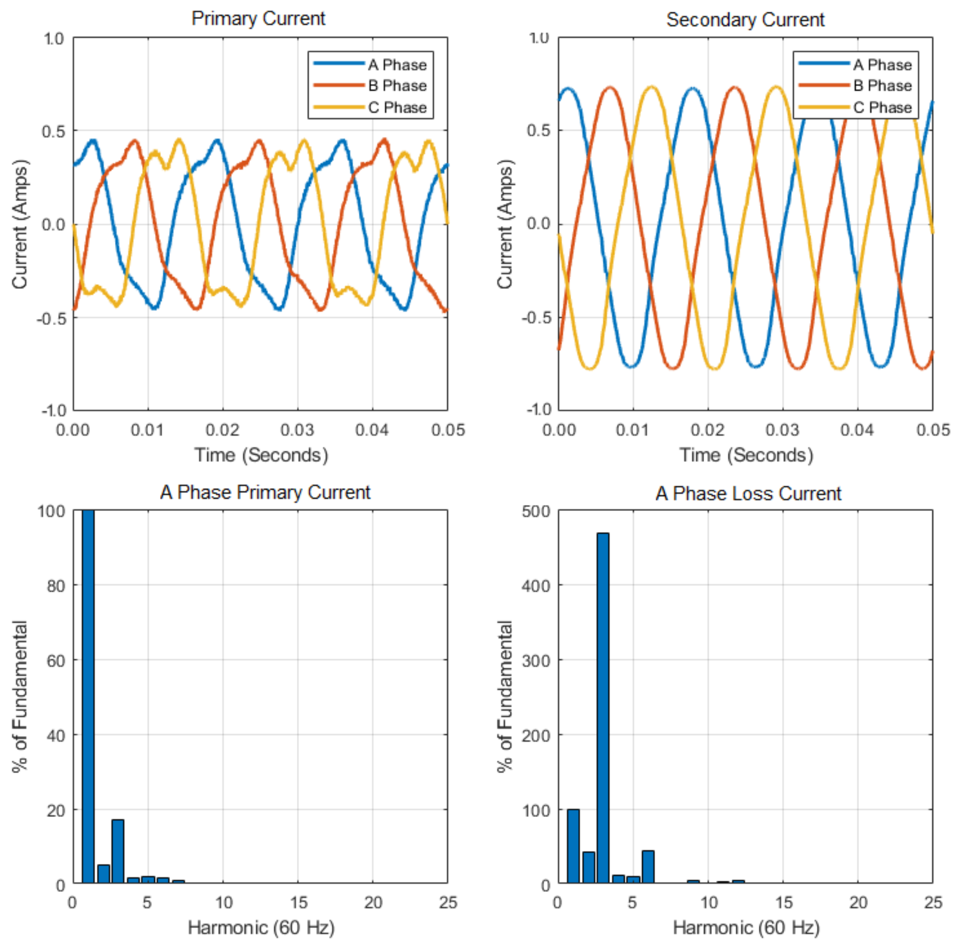

Figure 4.6. Primary and Secondary Currents with Primary and Loss Current Harmonics, 1000 VA Three Phase Three Limb Core Form Transformer (1.8 PU Amps / 2.5 Amps per Phase DC)

Comparison with Idaho National Laboratories Test, 2012

The two main power transformers tested at Idaho National Laboratories were both three phase three limb core form transformers with a grounded-wye primary winding and a delta secondary winding. Penn (named for the manufacturer, Pennsylvania Transformer) is a 15 MVA transformer, while West (named for Westinghouse Electric) is a 3.75 MVA transformer. These transformers are typical of generator step-up or industrial pump load stations. The primary windings of both transformers were connected in parallel at 138kV. Varying levels of DC were injected into the common neutral between the transformers and data was collected by Schweitzer Engineering Laboratories engineers using SEL protective relays. The data acquisition rate was 8 kHz. Depending on the test, loading on each transformer was either 10% or 50% of the transformer capacity using a resistive load. Figure 4.7 is a picture of the INL test facility during the 2011-2012 testing, and Figure 4.8 is a diagram showing how the two transformers were interconnected with the DC source between them [43].

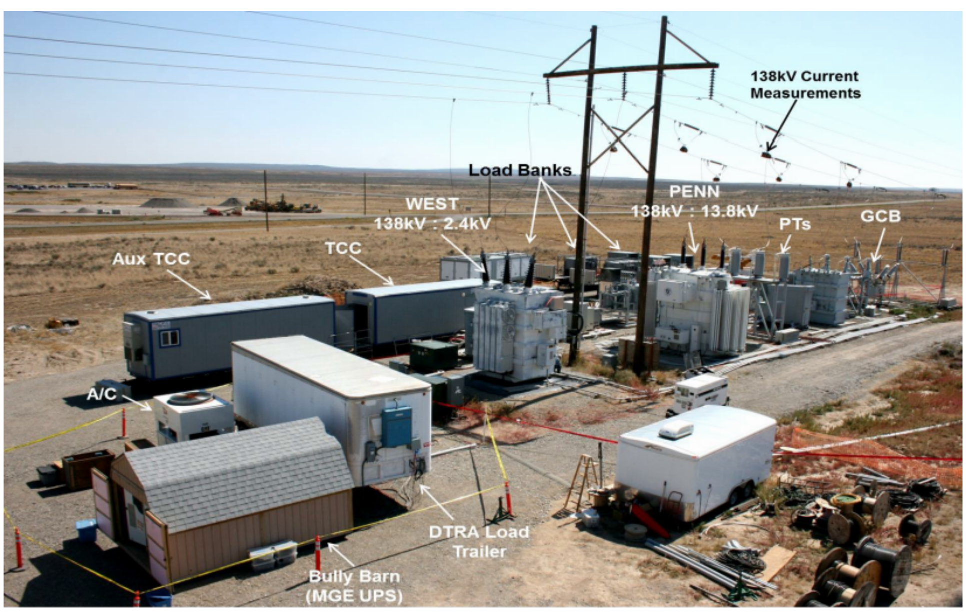

Figure 4.7. Picture of Phase IV-B Test Facility at Idaho National Labs

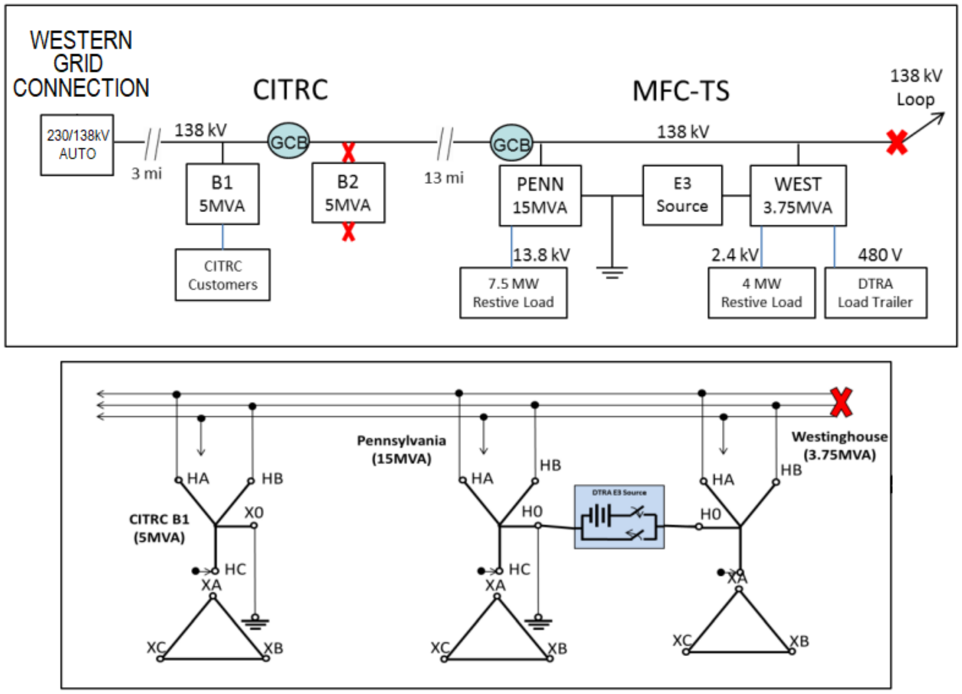

Figure 4.8. Diagram of Phase IV-B Test Facility at Idaho National Labs

Because of the connection of the DC injection system at INL, all DC would flow through the Westinghouse transformer, but only 75% of that current would flow back through the Pennsylvania transformer. The remaining current would flow out towards CITRC and the Western Grid connection. The return path for this DC was through the shared ground connection present at the neutral of the Pennsylvania transformer.

The closest per unit DC injection test data to compare the three transformers (1kVA benchtop, West, and Penn) was used to compare West and the 1kVA benchtop. Test S021 was a 1.9 per unit DC test for West and a 0.37 per unit DC test for Penn at 10% resistive load. Figure 4.9 shows the waveform for the primary currents for West and Penn along with the harmonic component percentage of the primary winding currents. Between the 1kVA benchtop transformer and the two INL transformers, the biggest differences are the second and third harmonics. The benchtop transformer has low second / high third, while both Penn and West have higher second / lower third harmonics.

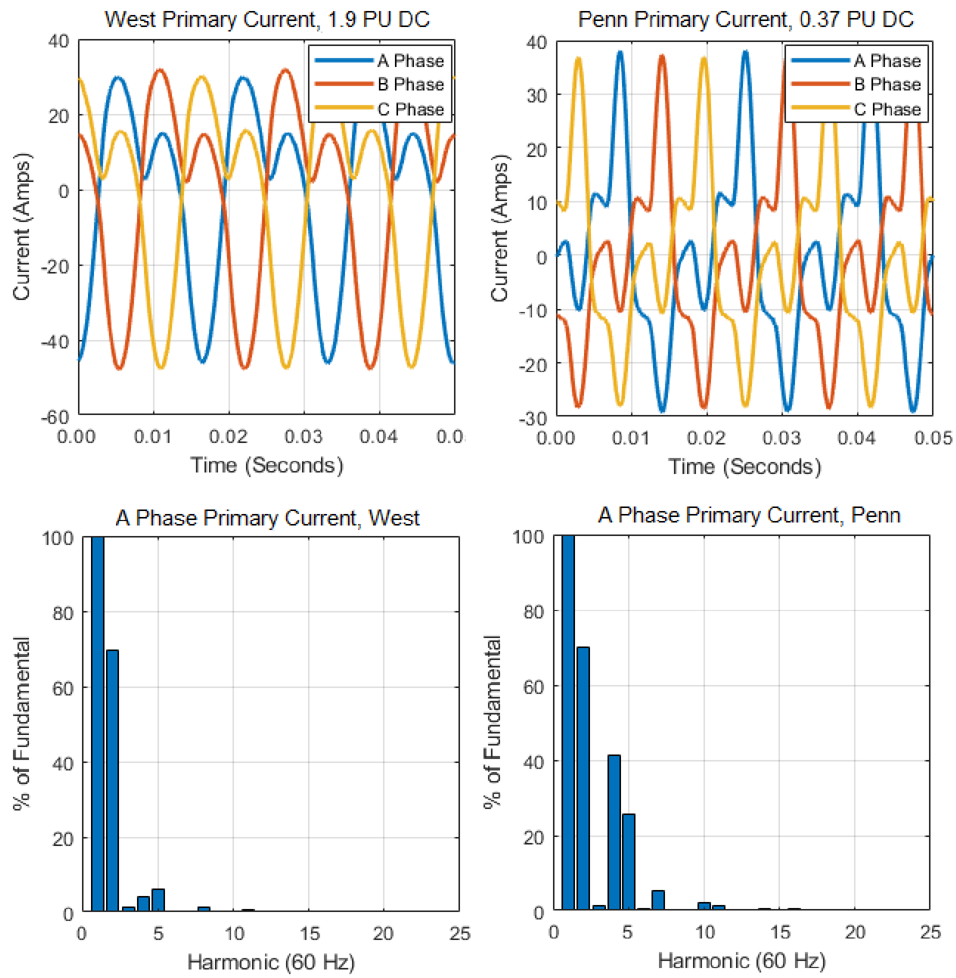

Figure 4.9. West and Penn Current Waveforms and Harmonic Content, 1.9 (West) and 0.37 (Penn) Per Unit Amps DC Test

It is apparent that both West and Penn transformers were saturating by examining the magnitude off the second harmonic component and the primary winding current. Both transformers were near 70% second harmonic content on the primary winding current. At 10% resistive load, primary winding load current would be under 2 amps on West and 7 amps on Penn. During the DC test, RMS current (which includes harmonics) increased to 24 amps on West and 17 amps on Penn, which is a 1,200% and 240% increase respectively.

This level of saturation is in contrasts to the three phase 1kVA transformer in the laboratory. It had low second harmonic content in the primary winding current and was not in saturation. It is believed that the design of the transformer itself is the reason for this. The 1kVA transformer, which was designed as a low voltage control systems component, has multiple taps on the primary winding. During laboratory testing, the 415V tap was being used, while the maximum winding voltage tap was 480V. It is likely that the transformer was designed to operate at 480V and would not saturate until closer that level of voltage even with the DC injection. The remaining test transformers are not designed to operate at this level of voltage, so this was not tested.

Group 3: Three Limb Core Form Autotransformers

There were two autotransformers available for testing: a 7kVA transformer and a 2.5kVA transformer. Because of the three limb core form design, these transformers also proved difficult to saturate. Unlike the 1kVA wye-wye transformer, these transformers have a low input resistance, so the DC injection bench was capable of supplying over 15 amps per phase of DC to the transformers during a three battery test. Testing at this level was limited as it put the neutral circuit of the test bench at risk for equipment failure, as it was not designed to handle over 45 amps of current. Fortunately no damage occurred but a blown fuse in the DC circuit during testing did require replacing.

The 2.5kVA autotransformer did begin to exhibit characteristics of saturation at the maximum levels of testing, but no secondary voltage or current harmonics were observed. It was expected that harmonics would appear on the common winding of the autotransformer because of the direct electrical connection between the windings, but this was not the case. All of the current distortion appeared in the primary (series) winding.

Figure 4.10 shows the result of a 3-battery, 15A per phase (4.3 PU DC) test on the 2.5kVA autotransformer: negative voltage half-cycle transformer saturation with high second harmonics, yet no distortion on the secondary load side of the transformer. When examining the three phase current waveforms in Figure 4.11, there is an imbalance in the depth of the second harmonic-related current impulse, as was implied in the unbalanced finite element model in Chapter Three. For Figure 4.10, DC offset was removed from the current waveform graph, while Figure 4.11 contains the DC offset as measured by the Hall Effect current transducers. The difference in current waveshapes between Figure 4.10 and the 500VA single phase transformer in Figure 4.4 is because of DC polarity during injection. The autotransformer in Figure 4.10 was subjected to negative DC polarity thus entering the negative half-cycle saturation region. The single phase transformer in Figure 4.4 was subjected to positive DC polarity therefore entering the positive half-cycle saturation region. If the current waveform in Figure 4.10 is inverted, the distinctive waveform spike will be positive and the waveshape is comparable to Figure 4.4.

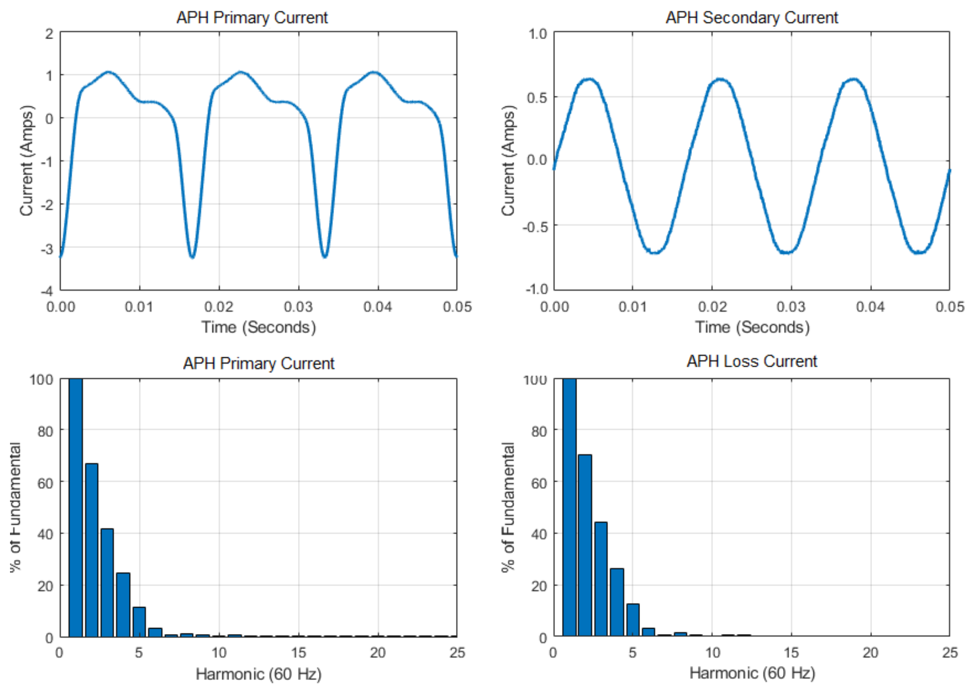

Figure 4.10. Primary and Secondary Currents with Primary and Loss Current Harmonics, 2.5kVA Autotransformer

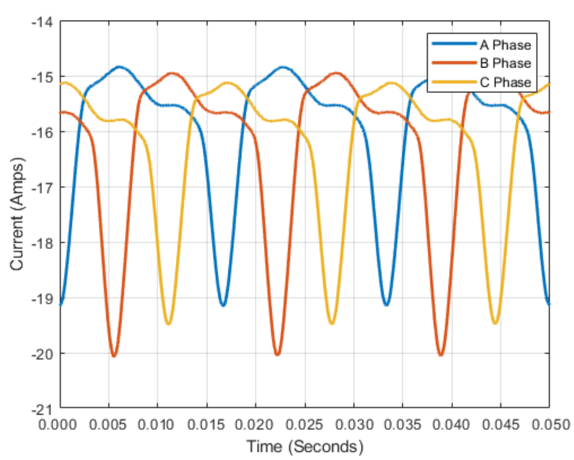

Figure 4.11. Phase Currents during 15A DC Test, 2.5kVA Autotransformer

During this sequence of testing, the 7kVA autotransformer was also subjected to a with and without metal shell tests. Two 15A per phase tests were performed on the transformer, one with a metal shell, one without the shell. A picture of the 7kVA transformer and the metal shell are shown in Figure 4.12.

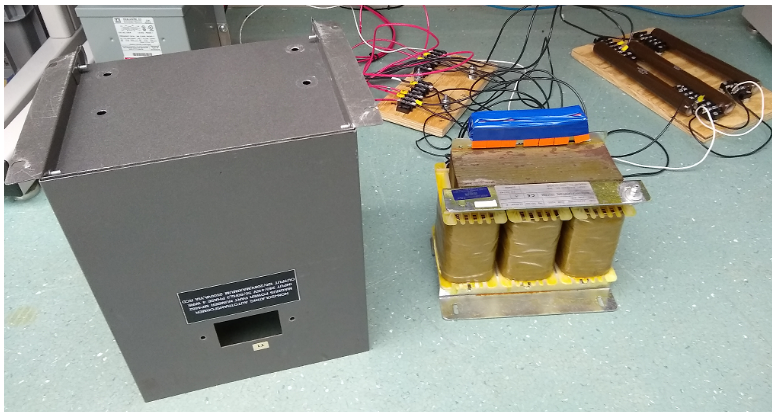

Figure 4.12. Metal Shell and Transformer, 7kVA Three Phase Autotransformer

As shown in Figure 3.7, flux paths due to DC will change when a transformer is surrounded by a steel enclosure. When there is no shell or enclosure, only the high reluctance flux paths through open air are available. When placed in a ferromagnetic shell, the flux from a saturating transformer will seek the lowest reluctance path and that path will include the shell. While the enclosure being tested only had 5 sides (it lacked a bottom), there was a difference in the primary current waveforms and the harmonic response of the transformer. The current waveforms are shown in Figure 4.13, and the harmonic components are shown in Figures 4.14 and 4.15. The RMS current decreased by 7% on phase A, 17% on phase B, and 22% on phase C when the shell was installed, likely because of the lower reluctance path requiring less magnetizing current in the transformer core. The second harmonic content of the primary current also decreased when the shell was applied. During these two tests, the 2.5kVA autotransformer was in the parallel test position and showed no difference in its waveform characteristics or harmonic response.

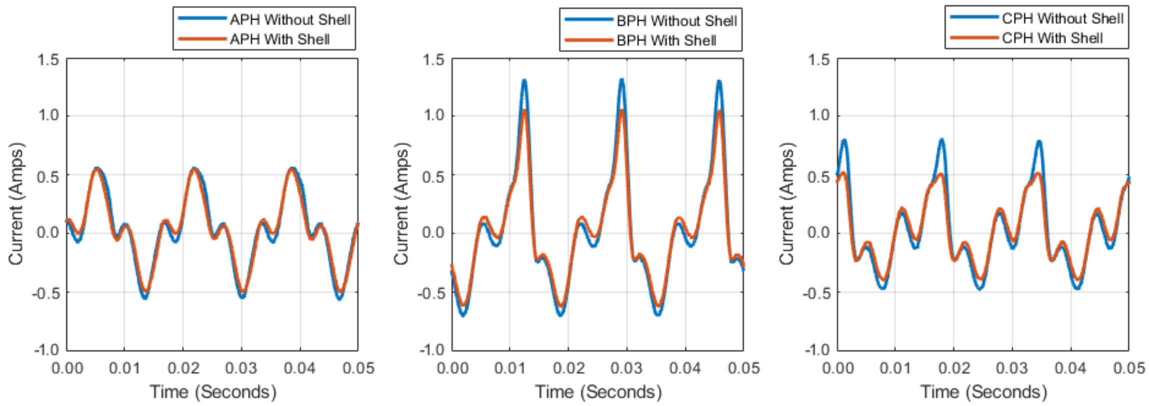

Figure 4.13. Primary Current Waveforms Per Phase, 15A Tests With and Without Shell, 7kVA Three Phase Autotransformer

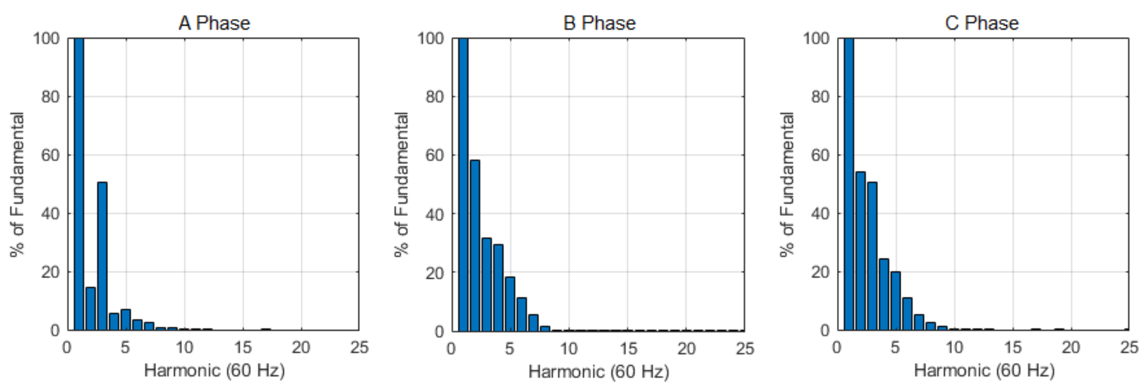

Figure 4.14. Primary Current Harmonics, 15A Test Without Shell, 7kVA Three Phase Autotransformer

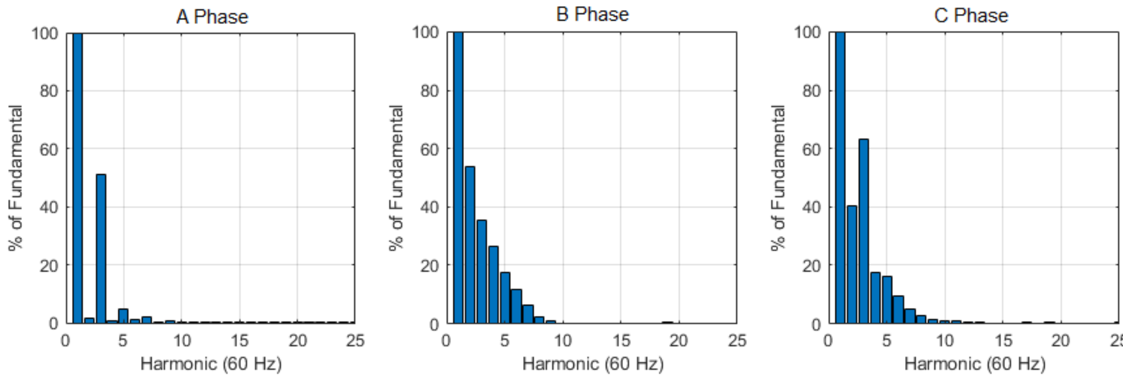

Figure 4.15. Primary Current Harmonics, 15A Test With Shell, 7kVA Three Phase Autotransformer

For the testing process, the shell was loosely placed over the top of the transformer. During the test, the stray flux would interact with the shell and the shell would move towards the transformer, resulting in a clunk followed by a buzzing sound due to vibration of the loose shell. This easily demonstrates that there is a strong interaction between the core's electric field and the shell of a transformer.

While the 2.5kVA transformer of Figures 4.10 and 4.11 displayed second harmonic characteristics of saturation that were similar to the single phase transformer, the 7kVA autotransformer did not exhibit saturation characteristics in this manner during the 15A per phase testing. Instead, the phase harmonics were highly distorted dissimilar primary current waveforms. The current waveforms in this instance resembled the distorted currents of Waveforms 2 and 3 found in Chapter Five, which proved problematic for protective relays that operate on RMS value and not the filtered fundamental component of the current.

The Hysteresis Response of Transformers under DC

It is possible to examine the hysteresis response of a transformer to DC injection by accurately sampling the voltages and currents. The physical transformer parameters of the core, windings, and structural members that may impact the flux during saturation need not be known, as the parameter of interest is relative transformer loss which is proportional to the area of the hysteresis loop.

As mentioned in Chapter 3, the magnetic flux density B is proportional to the voltage, and the magnetic field intensity H is proportional to the magnetizing current. While H is a direct calculation from the current (Equation 3.1, Ampere turn per meter, with number of turns and meter being constants), B is defined as the Volt-Second divided by the surface area (a constant in square meters). The Volt-Second is the flux in Webers, and flux is related to voltage through Equation 4.2 (Faraday's Law).

$$V = N\frac{d\Phi}{dt} \tag{4.2}$$

Integrating both sides yields the flux linkage in Weber-turns, as shown in Equation 4.3.

$$N\Phi = \int_0^{\pi} v(t)dt \tag{4.3}$$

N (the number of turns) is a constant and generally unknown for most transformers, while the flux will vary with the electromotive force, which in this case is the applied AC voltage. For this analysis the area is considered as combined with the flux density (Φ=BA). While this procedure does not provide a direct calculation for the actual B value in Tesla, it does provide a value that is very useful for loss comparison purposes.

When analyzing a hysteresis loop, the loss current is one of the parameters required. While mentioned earlier in this chapter, it is relevant to mention in this section. The loss current is calculated by subtracting the ratio-scaled transformer secondary current from the transformer primary current as shown in Equation 4.4, where V_S is the secondary voltage and V_P is the primary voltage.

$$I_{LOSS} = I_P - \frac{V_S}{V_P} I_S \tag{4.4}$$

When using sampled values from a data acquisition system and wye-wye connected transformers, the loss current is a straightforward calculation based on the primary and secondary sampled currents and the fixed transformer ratio. One cannot use measured instantaneous voltage for the ratio calculation because the data is invalid when the primary voltage approaches its zero crossing (divide by zero error).

The loss current in this case includes magnetizing losses, eddy current losses, and real power copper losses. As normal loading increases, loss current will increase due to copper losses, even when magnetizing losses remain relatively constant. It will be shown that during DC injection, these losses increase dramatically, well beyond load current losses.

For the sampled value voltage, the process to calculate the integration of Equation 4.3 is to perform a sum of the previous half-cycle of voltage measurements and multiply that value by the sampling time interval. If there are integer n samples per half-cycle and a sampling rate of SR with a present sampled value v_s, the flux linkage may be found as shown in Equation 4.5.

$$N\Phi(t) = \frac{1}{SR} \sum_{k=0}^{k=n-1} v_{s-k} \tag{4.5}$$

For consistency when analyzing calculations based on sampled values, the best results are obtained when the starting voltage sampled value is at a zero crossing.

Hysteresis Analysis and Results

During normal transformer operation, the loss current is low when compared to the primary and secondary currents. Figure 4.16 shows the primary current, the scaled secondary current, and the loss current for a 500VA single phase transformer during normal (no DC) operation.

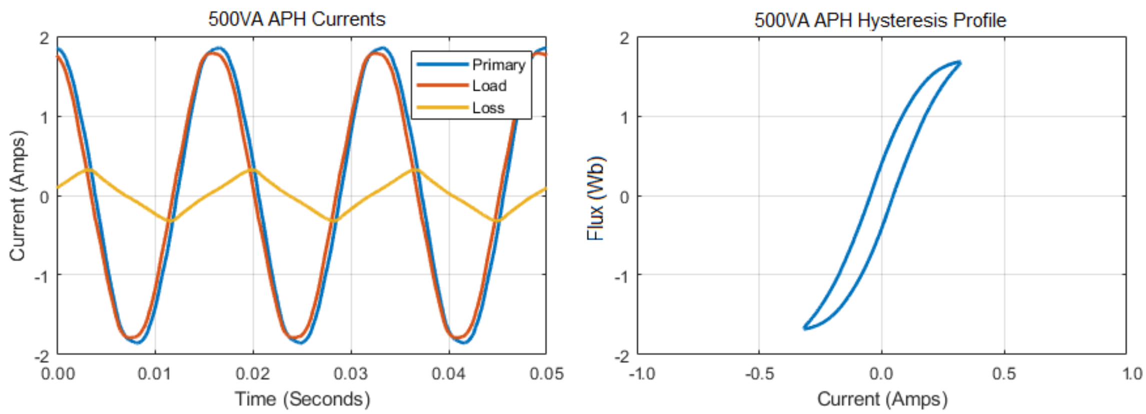

Figure 4.16. Current Waveforms and Hysteresis Loop, Normal Operation, Single Phase 500VA Transformer

When applying the procedure for creating a hysteresis loop as described in the previously in this chapter, the result is shown in Figure 4.16. The hysteresis graphs presented represent Webers - the flux density B times area A - on the Y axis, and current - flux intensity H divided by turns per meter - on the X axis. With area, turns, and length being constant, the shape and area of the hysteresis loop are proportional to the B and H values. For this test, each single phase transformer was supplying 275 watts per phase to a load while input power was 293 watts per phase, for a loss of approximately 18 watts per phase.

As DC is applied, the primary and magnetizing currents begin to exhibit the characteristics of positive half-cycle magnetic saturation as shown in Figure 4.17. During this test, power supplied to the load dropped very slightly to 271 watts per phase while the transformer loss increased slightly to 22 watts per phase. This low increase in power absorption is reflected by the relatively small area encompassed by the half-cycle saturation region.

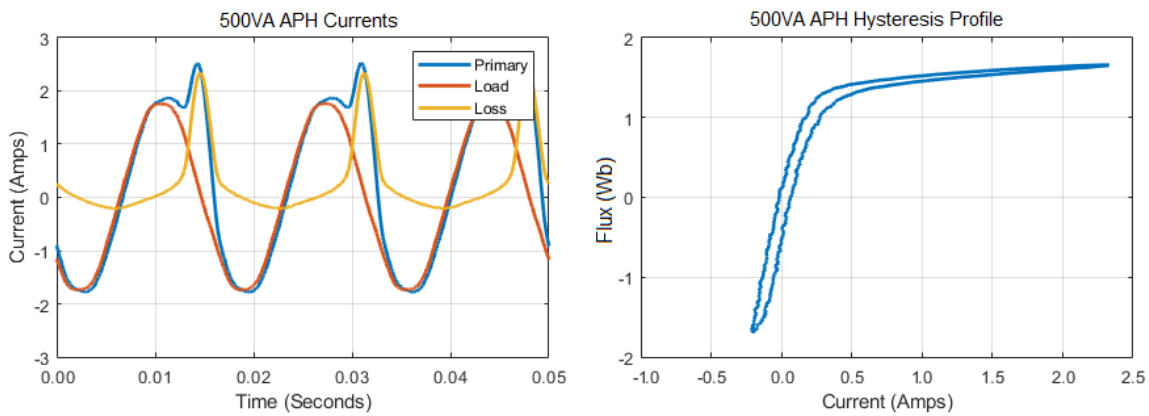

Figure 4.17. Current Waveforms and Hysteresis Loop, Low Level of DC, Single Phase 500VA Transformer, DC Bias Removed

At deep saturation, the transformer absorbs much higher levels of power. While delivering 287 watts per phase to the load, the 500VA transformer in this test was absorbing 410 watts per phase during the test – a factor of 22 times regular losses. The currents and hysteresis loop are shown in Figure 4.18. The area of the positive half-cycle saturation region of the hysteresis loop is now much larger, indicating a large increase of power absorption. The power loss values are based on the fundamental power components, which will be explained later in this chapter.

The area of the hysteresis loop increases as DC increases. Similarly, watt and VAR losses increase as DC increases. The area of the loop may be calculated using Matlab's *polyarea* function, and this was done for comparison purposes. Figure 4.19 compares watt loss, VAR loss, and loop area against per unit DC current. For this graph, the watt, VAR losses, and area at no-DC injection correspond to 1.0 and the graph plots the multiples of that base value as DC increases. For example, at 2 per unit DC current, VAR losses and area are nearly 30 times the no-DC VAR loss, while

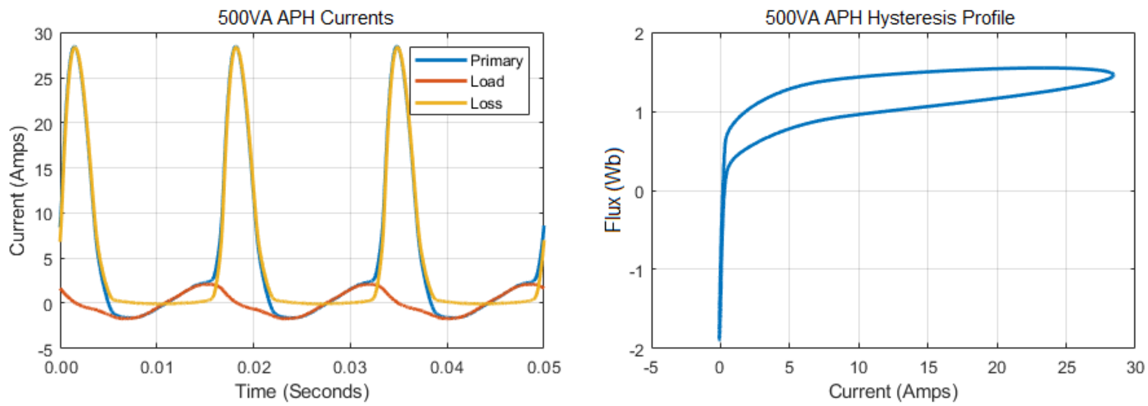

Figure 4.18. Current Waveforms and Hysteresis Loop, High Level of DC, Single Phase 500VA Transformer, DC Bias Removed

watt loss is approximately 15 times the no-DC watt loss. It may be observed that for levels of DC injection below 0.75 per unit, the area loss change and the watt loss change follow similar slopes, likely because the losses at lower levels are primarily resistive, but at higher current levels the reactive component is dominant.

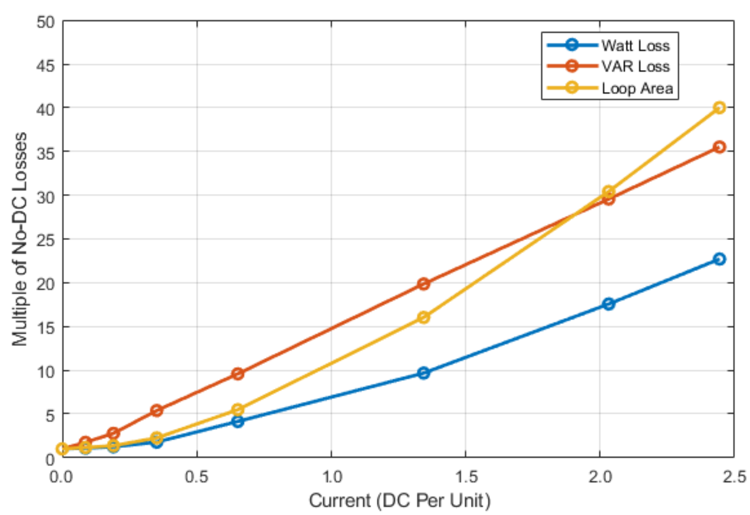

Figure 4.19. Comparison of Multiples of Loss Watts, VARs, and Loop Area, Single Phase 500VA Transformer

Three Phase Transformer Hysteresis

Single phase transformers have independent cores, so the magnetic circuits for each phase have no influence on each other. As shown in Chapter Three, three phase core form transformers do contain magnetic circuits that overlap and this influences the hysteresis and therefore the loss profile of the transformer. An example of per-phase hysteresis under normal loading for a 2.5kVA autotransformer is shown in Figure 4.20.

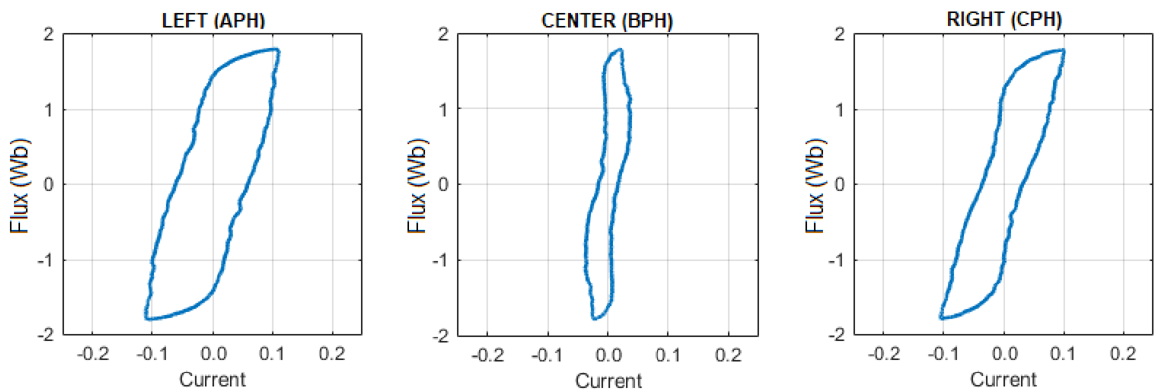

Figure 4.20. Hysteresis Loops for Left, Center, and Right Limbs of 2.5 kVA Core Form Autotransformer, AC Only

The center limb (B phase in this instance) has a significantly smaller hysteresis loop area than the two outer limbs. This reinforces the observation made with Figure 3.13 on a different three phase core form transformer – that the center limb magnetizing current is lower than the outer two limbs. In this case, the transformer is lightly loaded.

A three-phase core-form transformer such as this example being tested requires significantly more DC to saturate than the single phase transformer that was shown previously. When saturated, the current harmonics resemble the single phase harmonic characteristic. An example of this is shown in Figure 4.21. DC injection level during this test is over 3 per unit (10.8 amps per phase).

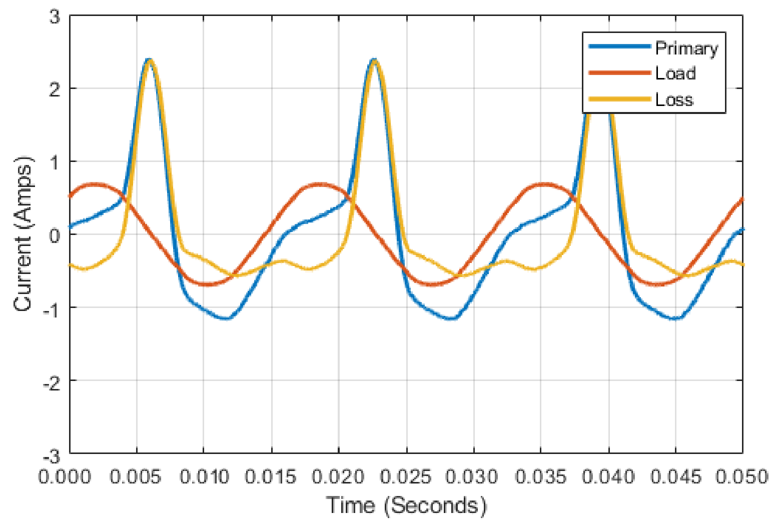

Figure 4.21. Primary, Load, and Loss Currents for 3-Phase 2.5kVA Autotransformer under DC Injection

The hysteresis graphs for this level of saturation are shown in Figure 4.22. Note that the center limb winding now resembles the outer two windings. The area of the loop has increased and the hysteresis characteristic is now comprised of three areas that have crossing intersections – the upper portion, the middle portion, and the lower portion. This is typical of a three phase three limb transformer, as the magnetic circuits interact with each other in the core during the three phase rotation of the 60 Hz power cycle.

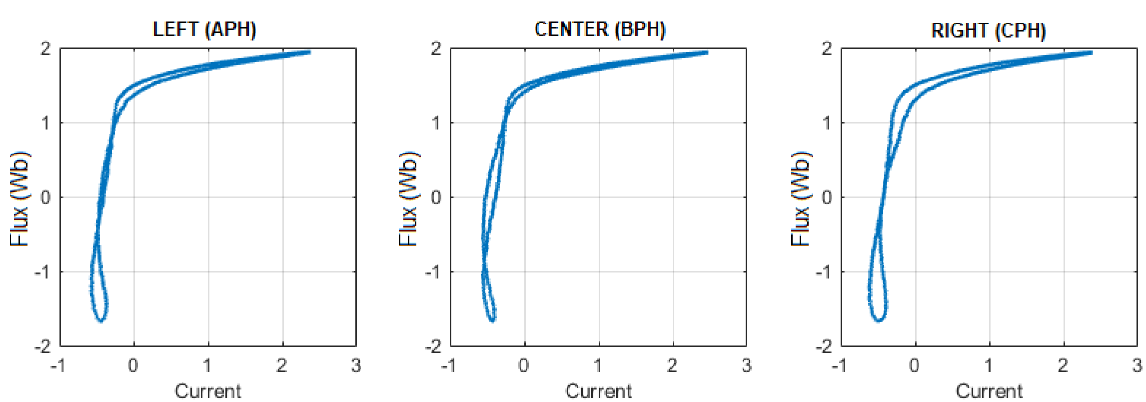

Figure 4.22. Hysteresis Loops for Left, Center, and Right Limbs of Core Form 2.5kVA Autotransformer with DC Injection, DC Bias Removed

Figure 4.23 shows a comparison of the hysteresis loop area versus watt and VAR loss. This figure reveals that the transformer is not yet into deep saturation.

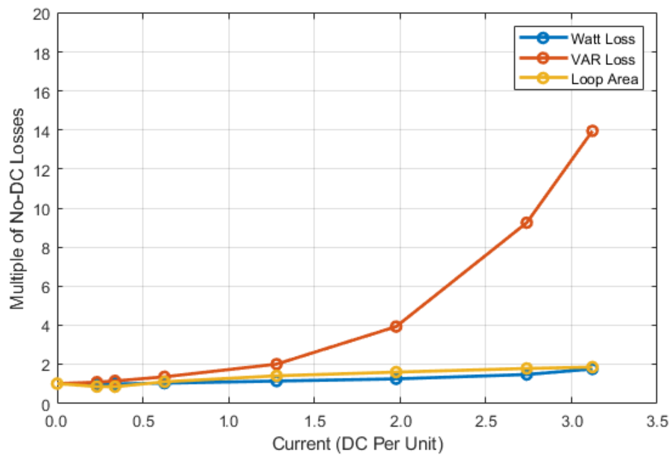

Figure 4.23. Comparison of Multiples of Loss Watts, VARs, and Loop Area for 2.5kVA Autotransformer

In Figure 4.23, the watt and loop loss are increasing at nearly the same rate, while the VAR loss begins increasing significantly at 1.25 per unit DC. During the final DC test, the VAR absorption was approximately 14 times the absorption rate with no DC.

Transformer Active and Reactive Power Absorption

VARs in the power grid constitute a reactive power that does not represent the transfer of real power. VAR flow is oscillatory and is influenced by inductive and capacitive characteristics of the power network and its primary influence on the grid is voltage stability and magnitude. Inductive loads such as motors will absorb VARs, decrease the power factor and eventually lead to a drop in voltage. Capacitors may be used to offset the decrease in power factor and thereby increase the voltage. The power grid is designed to be operated near equilibrium for VAR flow, with shunt capacitors, shunt reactors, and active VAR compensation devices being installed in strategic locations to either increase or decrease voltage depending upon the requirements of that specific region of the electric grid at any moment in time.

During a nuclear EMP MHD-E3 event, transformers under DC saturation will begin to absorb a significant level of both real power and VARs. This absorption of VARs may be sufficient to result in voltage instability because the equilibrium of the capacitor banks may be insufficient to offset this increased absorption of VARs.

Even though VAR flow is not real power, it is possible for VAR currents present in transformers during the MHD-E3 event to damage equipment in a substation. The following is a description of a VAR-related event wherein the author was the lead investigator.

VARs Causing Power System Issues

The first case is an example of localized VAR damage. The example substation contained two 20MVA delivery transformers, each having four 25kV distribution feeders connected. One feeder from each transformer is connected to an automatic transfer scheme. If the load is energized from Transformer A's feeder, and the scheme detects a voltage dip, a pair of downline switches will operate to automatically transfer the load to Transformer B's feeder and disconnect from Transformer A's feeder.

A fault on an adjacent feeder caused Transformer A's bus voltage to dip. The automatic transfer scheme operated and Transformer B's switch closed, but Transformer A's switch failed to open. The result was that the two transformers were tied together and operating in parallel with each other. The failure of the switch to open was not noticed by the system operator.

Current began to circulate between the two transformers as the on-load tap changer controls attempted to regulate voltage. Eventually, one tap changer went offline as significant VARs were circulating and voltage regulation ceased. For this customer, the normal feeder load was approximately 1.5 MW at 0.97 power factor (approximately 375 kVAR). Circulating VAR flow between the two transformers reached

13 MVAR (measured as +13 MVAR on one feeder/transformer and -13 MVAR on the opposite feeder/transformer). At 25kV, nearly 300A of VAR-related circulating current was flowing through 100:5 current transformers, which was well over their rating factor. After several hours in this state and about 24 hours after the initial event, a current transformer on one feeder catastrophically failed, damaging nearby equipment, tripping the protective relay systems, and dropping the customer load.

In this scenario, neither transformer was damaged. Several bus insulators were damaged, some jumpers were damaged, and all current transformers (3 for each feeder) required replacement because of the thermal overload. When the current transformer failed, the catastrophic equipment failure arc reached the distribution bus so the transformer protection operated and dropped all customer load on that transformer.

While not specifically related to nuclear MHD-E3 or GMD, this example does validate the assertion that excessive VAR flow at the local level can result in damage to equipment and subsequent power outages necessitating significant repair work when the equipment is exposed to reactive power beyond equipment ratings.

An example of wide area VAR issues is the 1989 Hydro Quebec Event, as described in Chapter Two and documented in [30]. Protective relay systems were configured with settings that did not account for harmonic currents; the fundamental current remained unchanged, but harmonics led to an increase in the RMS current magnitude, and the protection systems did not incorporate harmonic filtering. As the capacitor bank protection systems tripped offline, the transformers were absorbing significant VARs because of the high level of DC in the grid. This VAR absorption reduced system voltage to the point that available generation was not capable of compensating and the grid collapsed. Reactive power played a major role in the system collapse during the 1989 event.

Idaho National Laboratories – Penn and West Power Absorption

When evaluating voltage and current samples with high levels of harmonics, the question of how to handle harmonic power is of consideration. The general method used in the following section is to perform a discrete Fourier transform on the sampled data values for currents and voltages to obtain a magnitude and phase for the fundamental and each harmonic. RMS values for the sample sets are also calculated. Using RMS and the Fourier series components, fundamental and harmonic active and reactive power may be calculated, with the fundamental values being the area of interest.

The data collected during the INL/DTRA testing provides interesting insight into the question of power and VAR absorption on grid-scale transformers. The data being presented was collected by Schweitzer Engineering Laboratories (SEL) engineers with SEL protective relays and is in addition to the other available data sources provided by Scientific Applications Research Associates (SARA) and INL. This distinction is important in that the SEL protective relays do not measure steady-state DC, as their input circuitry is designed to measure AC signals via internal current and voltage transformers. While magnetic AC coupling does allow the measure of a transient DC offset, once the DC has reached steady state the AC coupling will measure zero DC. Additionally, the common grid instrumentation that protective relays are connected to – potential transformers and current transformers – will only pass AC signals once DC transients have achieved steady state.

The data in these INL/DTRA examples are from the BHE (resistive) series of tests. This data was selected because it allows for analysis without requiring compensating for the reactive components of the load.

The loading of the transformers was approximately 50%. While load makes a difference in I^2R power losses a transformer will have, it does not influence the saturation of the core. Core saturation depends on applied DC and the applied excitation voltage. In these tests, the applied voltage was consistent and within design parameters, and the load was fixed at a constant magnitude. The only variable was the injection level of DC.

These graphs are presented in per unit rather than amps, watts, or VARs. Per unit represents a percentage of the rated value for an electrical parameter. For example, 0.5 per unit current for a transformer represents 50% of the rated current for that transformer. This unitization permits the comparison between transformers of different capacity more easily.

The DTRA tests were designed to inject up to 125 amps DC into the neutral conductor of the Westinghouse transformer, and as described previously, only 75% of this DC returns through the Pennsylvania transformer while 25% returns through the other grid and ground connections. Once the DC reaches the transformer neutral it is considered to be evenly split between the phases, so each phase of Westinghouse would be subjected to approximately 41.7 amps DC, while each phase of Pennsylvania would be subjected to approximately 31.3 amps DC. The ampere rating for Penn is 64 amps at 138kV for 1.0 per unit, while the ampere rating for West is 17 amps at 138kV for 1.0 per unit.

For the Penn transformer, while subjected to varying levels of DC, the power delivered into the transformer during the pre-test period (before DC injection) was very close to the power during the test period. Penn did not appear to absorb extra power during the tests, even at the highest DC injection level, as shown in Figure 4.24.

Observe that the injected DC did not exceed 1 per unit. The power shown is the fundamental component of the active power, as calculated in Equation 4.6.

$$P_1 = V_1 I_1 cos(\angle V_1 - \angle I_1) \tag{4.6}$$

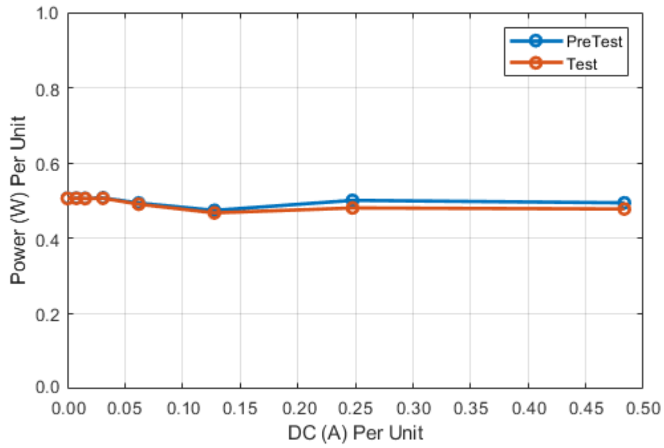

Figure 4.24. Pennsylvania Transformer: Per Unit DC Amps vs Per Unit Power Before and During Tests

For the smaller West transformer, power absorption – the difference between the load and the transformer absorbed power – began to increase upon exceeding 1 per unit current, as shown in Figure 4.25. At almost 2.6 per unit current, power absorption was approximately 50% of the rating of the transformer. A transformer the size of Westinghouse would have a typical rated loss of below 60kW under normal conditions. At a 50% power loss, this means that the transformer is absorbing approximately 30 times its usual rated loss component.

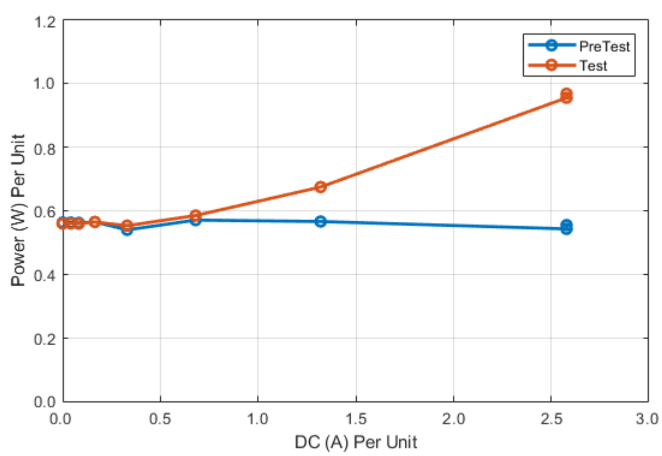

Figure 4.25. West Transformer Per Unit DC Amps vs Per Unit Power Before and During Tests

The reactive power considered here is also with respect to the fundamental frequency voltage and current components and based on the discrete Fourier transform components. For these graphs, the reactive power is calculated from Equation 4.7.

$$Q_1 = V_1 I_1 sin(\angle V_1 - \angle I_1) \tag{4.7}$$

For the Penn transformer, a small trend in increasing VARs is observed beginning at 0.25 per unit DC as shown in Figure 4.26. Mild saturation appears to begin at this level and an increase in VARs is observed between 0.25 and 0.48 per unit DC. With a maximum value of 0.2 per unit VARs (3 MVAR in this case), this would be considered a low level of VAR absorption and would not be detrimental to the transformer or associated equipment.

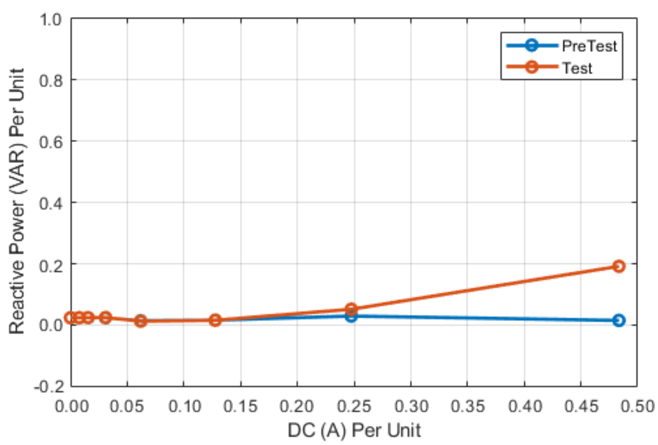

Figure 4.26. Penn Transformer Per Unit DC Amps vs Per Unit VARs Before and During Tests

The smaller Westinghouse transformer test data shown in Figure 4.27 shows a much greater response to DC for VAR absorption. This transformer is 25% the size of the Pennsylvania transformer, so higher levels of per unit DC were possible with the test configuration. DC up to approximately 41 amps per phase were injected into the transformers, and that level is over 2.5 times the rated current of the Westinghouse transformer, but well within range of a strong solar geomagnetic storm and far below anticipated current magnitudes during an MHD-E3 event.

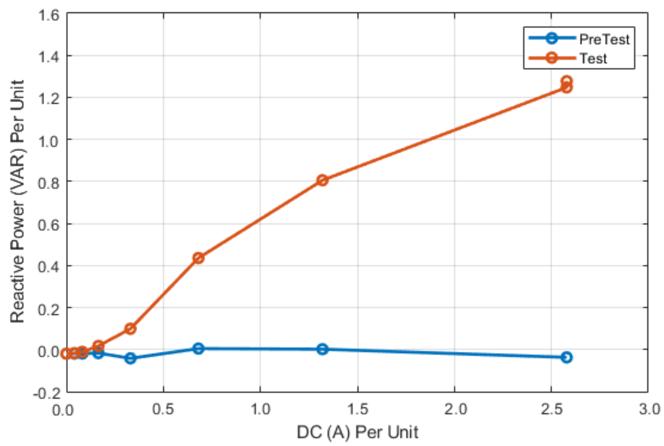

Figure 4.27. West Transformer Per Unit DC Amps vs Per Unit VARs Before and During Tests

Transformers are designed to operate at 1.0 per unit MVA indefinitely, and many may be capable of operating at 110% to 115% for periods of a few hours with possible slight reduction in service life due to insulation degradation. Recalling that S^2=P^2+Q^2, with the Westinghouse transformer loaded at 50% and the combination of real power and reactive power absorption, the transformer was at 100% capacity at about 1.3 per unit DC and at 150% capacity at 2.5 per unit DC.

Third Harmonic Power Oscillation

The instantaneous power measurement of a three phase transformer may be calculated by Equation 4.8.

$$P_{INST} = v_A i_A + v_B i_B + v_C i_C \tag{4.8}$$

During normal operation, this instantaneous power quantity will be relatively constant with little fluctuation in magnitude because of the sum of the balanced phases. With the introduction of saturation currents due to DC, the power becomes a product of the fundamental (60 Hz) voltage and the dominant second harmonic component (120 Hz) phase current, leading to a three phase power exhibiting a strong third harmonic. This is consistent across all transformers that exhibited the characteristics of saturation. For example, the Idaho National Laboratories West and Penn transformer instantaneous power behavior are shown in Figure 4.28.

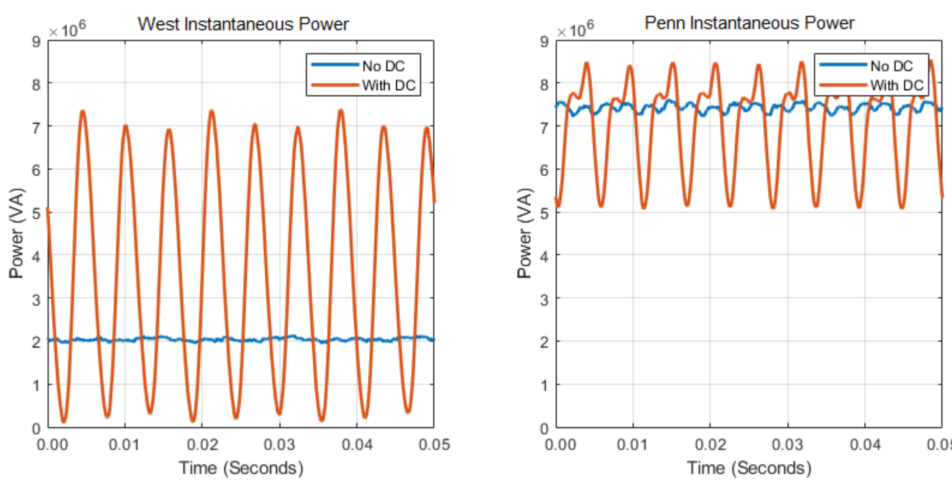

Figure 4.28. West and Penn Instantaneous Power Oscillations With and Without DC Influence

In the Baylor test lab, the three single phase 500VA transformers exhibited similar characteristics as it experienced deep saturation. This is shown in Figure 4.29. The 1kVA three phase three limb transformer did not saturate, so while its instantaneous power was less consistent while subjected to DC, it did not reflect as significant third harmonic oscillation.

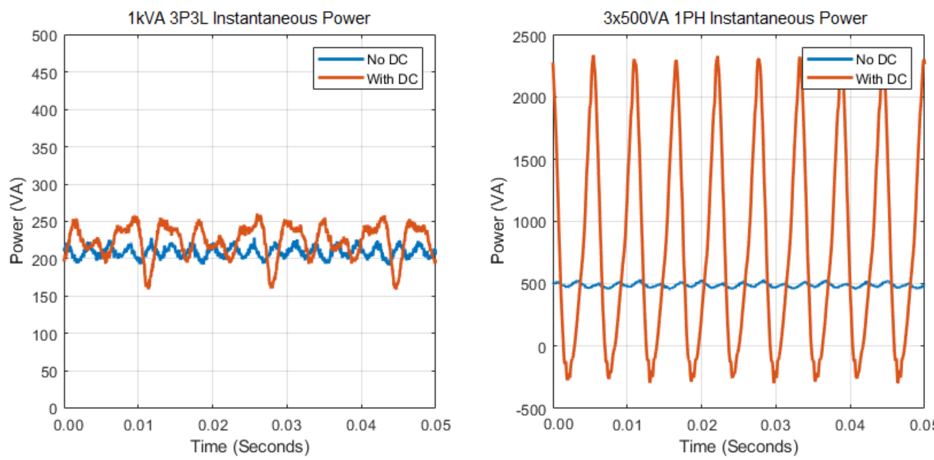

Figure 4.29. 1kVA and 3x500VA Instantaneous Power Oscillations With and Without DC Influence

During the period of testing as seen in Figure 4.30, the 2.5kVA autotransformer was beginning to saturate and showed the characteristic oscillation. The 7kVA autotransformer was not exhibiting the high-current impulses associated with saturation (see Figure 4.13 for current waveforms at this level of DC) but the instantaneous power was oscillating when compared to the case without DC influence. The harmonic content for the 7kVA transformer that was previously shown in Figures 4.14 and 4.15 indicate the presence of DC (via the elevated second harmonic), but the design of the transformer appears to be inhibiting the half-cycle saturation characteristic.

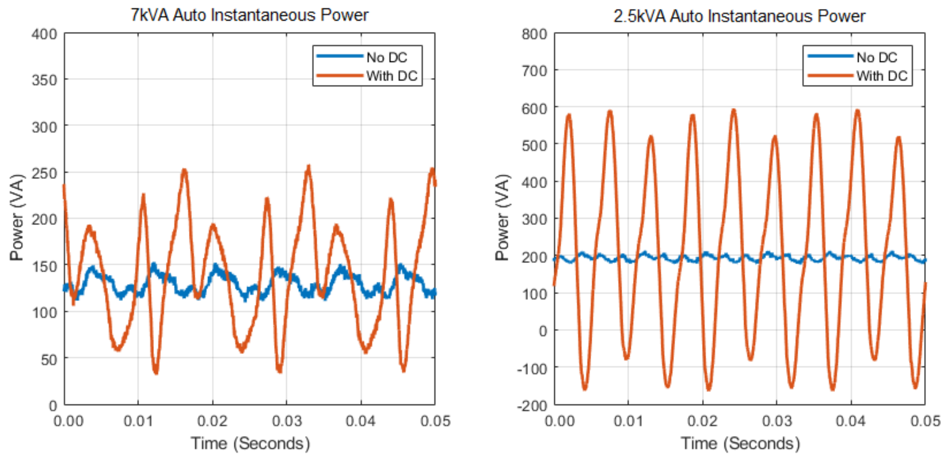

Figure 4.30. 7kVA and 2.5kVA Autotransformers Instantaneous Power Oscillations With and Without DC Influence

Discussion

On the test bench, the harmonic response of transformers to DC varied according to core design and winding characteristics. For single phase transformers, primary winding current harmonics become present with very little DC. Three phase core form transformers - whether they be autotransformers or conventional wye-wye winding configuration - require significantly greater DC before showing the characteristics of saturation. Secondary current and voltage distortion was only present at the highest levels of DC injection. Current harmonics did not propagate to the secondary circuit of the autotransformers, even when the primary current was heavily distorted.

Once transformer saturation begins to occur, power absorption begins to increase as DC increases. Transformer parameters such as core design and winding characteristics determine how much power may be absorbed, per its saturation characteristics. Transformers tend to absorb more VARs than watts, which is problematic from both a voltage stability standpoint. Additionally, a strong third harmonic oscillation of the input power during saturation may result in extreme vibration of the internal components of the transformer.

There are both similarities and differences between the Idaho National Laboratories test results and the benchtop system test results. Primary input current harmonic response is similar, albeit at different magnitudes and phasing. As DC increases, the harmonics increase. Likewise, the third harmonic power oscillation is similar between the two test configurations. What was not observed on the test bench was the significant current and voltage distortion on the secondary of the transformer that was observed during the INL testing. Chapter Seven contains graphs of the distorted voltage waveforms from some of the INL tests, and these waveforms reflect much more harmonic distortion than those waveforms obtained with the test bench.

There are two major differences that may have had an impact in the differences between the test bench and the INL test facility. The first major difference is in the battery configuration versus the test voltage. At INL, the maximum DC test was comprised of 61 automotive or marine batteries in series in the neutral of a 138kV_{LL} power grid. The series battery array used in this testing represents 1% of the line to neutral voltage, yet was capable of supplying 125 amps DC to the neutral of the transformers during testing. In comparison, the transformer test bench used up to three marine batteries in series in the neutral of a 415 V_{LL} power grid, representing about 16% of the line to neutral voltage, and in some cases was only capable of supplying 8 amps DC to the neutral of the transformers (when testing the 1kVA three phase three limb transformer in parallel with the three 500VA single phase transformers, for example). In theory, the voltage excitation curve of the test bench transformers should have led to more extreme levels of saturation because of this higher DC offset voltage.

The limitation of the DC injection current is directly related to the second difference: the high resistance / low X/R ratio of the primary winding of the transformers. The input resistance of the smaller transformers is significantly higher than the input resistance of the large transformers at INL, and have a much lower X/R ratio. Large power transformers are typically constructed with large copper conductors that offer very low input resistance in order to minimize load losses, while the smaller benchtop transformers are constructed with small 14 to 20 AWG enamel coated solid copper wire. This high input resistance limits the amount of DC that may be introduced. The single phase transformers on the test bench had a higher X/R (around 5), while the three phase transformers had low X/R, with the 1000VA transformer lowest at 0.58. The core design also had some influence on saturation. Had the autotransformers been of a shell form design as opposed to the core form design, there would have been saturation much more like was observed with the single phase transformers.

CHAPTER FIVE

Response of Power System Protective Relays to Solar and HEMP MHD-E3 GIC

This chapter revised from publication: A. K. Mattei and W. M. Grady, "Response of Power System Protective Relays to Solar and HEMP MHD-E3 GIC," 2019 72nd Conference for Protective Relay Engineers (CPRE), College Station, TX, USA, 2019, pp. 1-7, doi: 10.1109/CPRE.2019.8765893.

Selection of Protective Relays

While there is a broad spectrum of protective functions available in electromechanical, solid state, and microprocessor-based relays, the primary areas of concern for this investigation are transformer protection and line/feeder protection, though some relays are common for other applications.

Transformer protection traditionally relies on current differential as its primary protection, phase- and/or ground-time-overcurrent as its backup protection, and an unrestrained instantaneous overcurrent as a failsafe. Harmonic restraint and/or harmonic blocking is nearly universal as a supplement to differential protection. Other protection schemes such as restricted earth fault (REF) or negative sequence protection may also be implemented.

Creating / Selecting the Test Waveforms

The literature offers examples of relay performance under the influence of GIC [47], the influence of harmonics on protection systems [48], and IEEE PSRC Working Group K-11 presented some consensus recommendations for protection systems under the influence of GIC [10]. These tests explore the response of protective relays on measured waveforms with all associated harmonics included. Three waveforms were selected: one created using a DC-injection transformer test bench in the laboratory, one from the NERC 1989 Hydro Quebec Report [30], and one from a DTRA DC-injection field test at Idaho National Laboratories in 2012 [43].

Laboratory Test Bench Waveform

A three-phase DC-injection test bench was constructed using up to nine single phase transformers plus three variable autotransformers (see Figure 5.1). The test transformers were connected in wye-wye with the neutral of the loop containing batteries to serve as a DC source. Batteries were selected from an assortment of either single or multiple 12V automotive lead-acid or 6V 200 Ah VRLA solar energy storage batteries. Injection current magnitude is controlled by a high-wattage variable resistor.

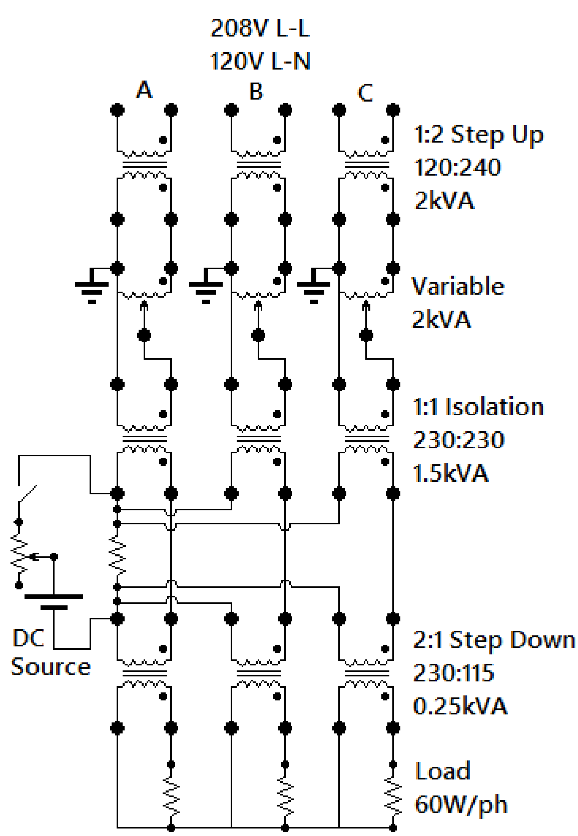

Figure 5.1. Laboratory Transformer Test Bench Diagram

Measurements for all lines were collected by a National Instruments (NI) CompactDAQ that was equipped with 9 phases each of AC current and voltage inputs. An analog input card with fourteen Hall effect sensors provided additional or backup current measurements. During testing it was found that the CompactDAQ AC current inputs were subject to magnetic saturation during the highest levels of DC injection (>2A/phase) and the Hall effect current sensors provided an effective secondary measurement source. It was also observed that the Hall effect current sensor signals were susceptible to distortion when placed near the magnetic field of a transformer, so steps were taken to mitigate this concern. For the waveforms in these tests, the DC injection magnitudes did not cause significant CT saturation in the NI AC inputs. The saturation occurs in the load-serving transformer.

Measured current waveforms from one of the phases formed by the looped DC injection circuit for an all-wye connection with low levels of DC injection are shown in Figure 5.2. This experimental data is nearly identical in appearance to the 500kV transformer response shown in Figure 2-44 of [7] and confirms the expected response per Figures 4 and 5 of IEEE Std C57.163-2015 [49].

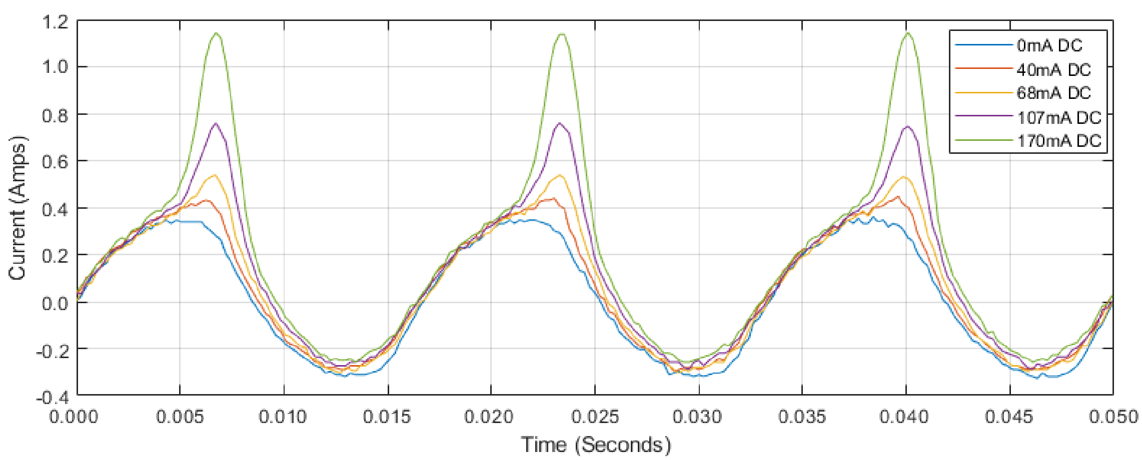

Figure 5.2. Laboratory Transformer Test Current Waveforms

Relay tests were created based on the waveforms shown in Figure 5.2. For transformer differential tests, the currents on both sides of the 2:1 Step Down transformers were used as the primary and secondary currents. The measured current on the secondary of the transformer was inverted to simulate the negative polarity of a transformer differential current transformer connection. Custom COMTRADE files were created as input to relay test set software. An example of the transformer differential relay current input is shown in Figure 5.3. Actual tests used values that were scaled appropriately for the desired relay settings. The peak magnitude of this waveform will be referred to as Waveform 1.

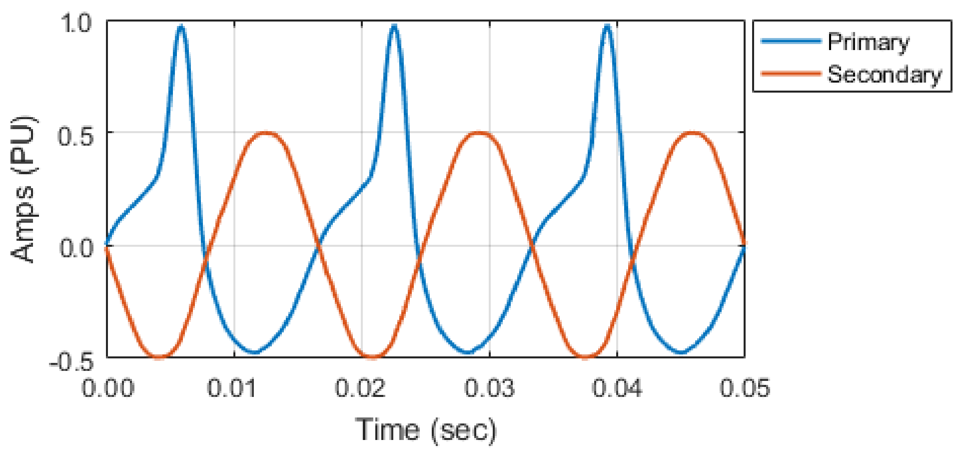

Figure 5.3. Transformer Differential Test Current (Waveform 1)

For the test bench generated waveform, one key thing to notice is the near-linear increase in second harmonic as the DC injection magnitude increases as shown in Figure 5.4. At the highest level of DC injection for this sample of data, the second harmonic is nearly 38% of the fundamental current and 77% of the calculated operate current. At 77% second harmonic in the operate current, the protective relay will be restrained or blocked from operating on normal differential current detection if the blocking and/or restraint functions are activated. Common blocking or restraint pickup settings in a current differential protective relay is in the range of 15% to 25% of the operate current.

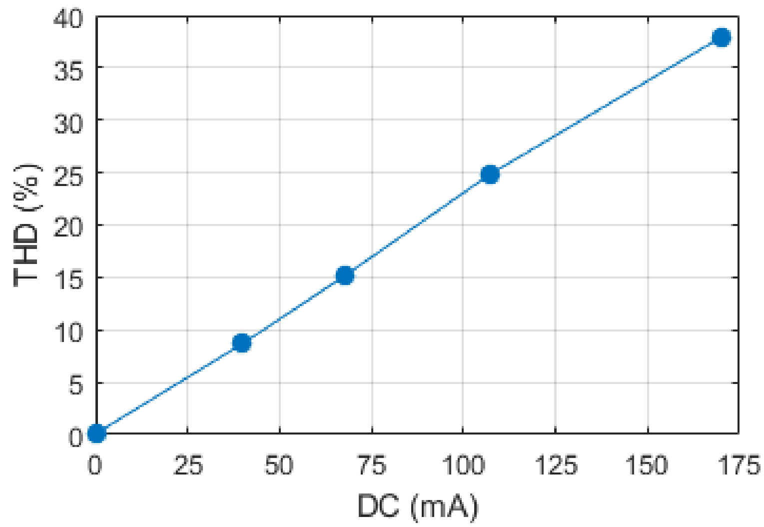

Figure 5.4. Second Harmonic Percentage vs. DC Injection

NERC 1989 Geomagnetic Disturbance Report Waveform

In the supporting documents for the NERC Transmission Planning Standard TPL-007 "Transmission System Planned Performance for Geomagnetic Disturbance Events," there are several current waveforms shown graphically with Fourier magnitude and phase included [30]. The three waveforms from this NERC report all exhibit high levels of second harmonics.

The test waveform used from this report was a reconstruction based on the FFT provided in the 1989 Report's Figure 15. This was a recorded current at the Albanel Static Var Compensator. This waveform is shown in Figure 5.5. This waveform was selected for testing because of its extreme level of second harmonic distortion and that its fundamental frequency magnitude is less than half of its RMS magnitude. The Albanel SVC waveform will be referred to as Waveform 2 in this document.

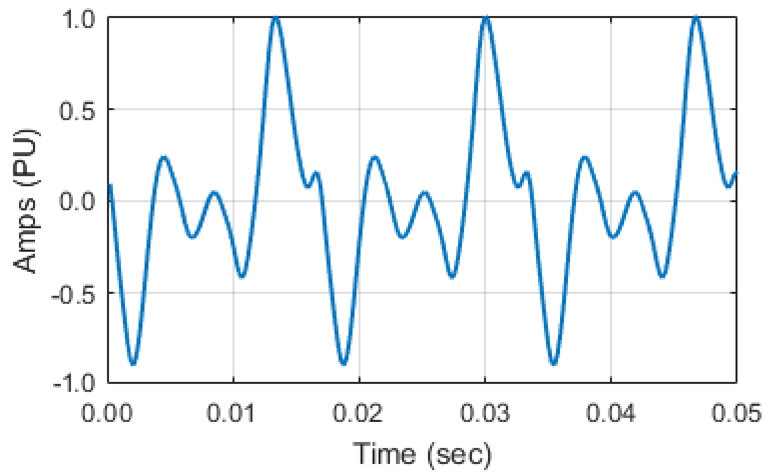

Figure 5.5. 1989 Event, Albanel SVC Current (Waveform 2)

DTRA / INL MHD E3 Waveform

In 2012, the Defense Threat Reduction Agency (DTRA) created a test grid that was attached to a 138kV transmission loop at Idaho National Laboratories (INL) [44, 42]. Presentations from NOAA's Space Weather Prediction Center conference materials are available that describe the test configuration and results [43]. All of the time-sampled voltage, current, and audio data from this series of tests was provided to the authors for analysis. There were many harmonic-rich waveforms to select from and the waveform selected was representative of the waveforms observed during the tests.

The waveform sampled for testing was developed from data acquired during a 120-amp (40A/phase) DC injection test into the neutral of a 15 MVA 138kV wye / 13.2kV delta transformer at Idaho National Labs in 2012. The current in Figure 6 was measured on the 138kV side of the transformer. The DTRA/INL waveform will be referred to as Waveform 3 in this document.

Fourier magnitude and phase for recreation of all test waveforms are included in Tables 5.3, 5.4, and 5.5 at the end of this chapter.

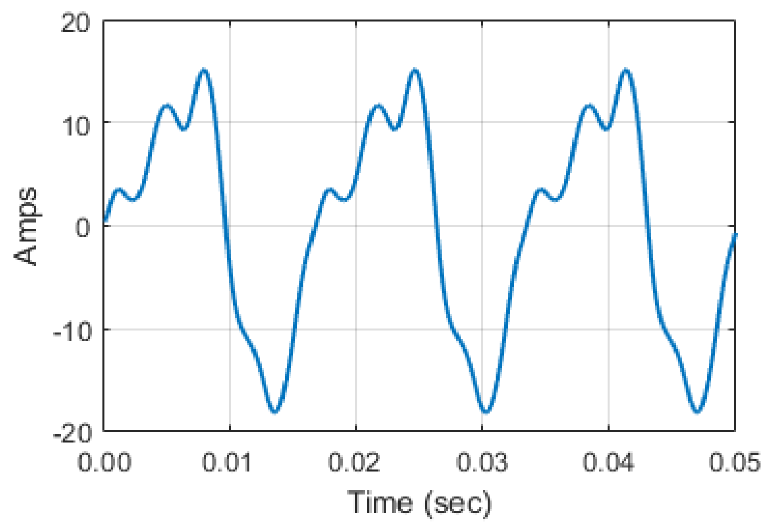

Figure 5.6. DTRA 138kV Current (Waveform 3)

Evaluating Current Magnitudes

Microprocessor-based relays are designed following the principle of operating on only the fundamental frequency. The input signal passes through hardware and software filters before calculations are performed using the measured signal data. A low-pass filter followed by a fundamental frequency-based cosine filter is typical for protective relay signal processing. Electromechanical and solid-state (static) relays may or may not contain harmonic filtering. For signal evaluation, characteristics of the current need to be analyzed.

In a power system with normal levels of harmonics (<5%), currents have little distortion and follow the approximation of Equation 5.1.

$$I_{RMS} \cong I_{FUNDAMENTAL} \cong I_{FILTERED} \cong \frac{I_{PEAK}}{\sqrt{2}} \tag{5.1}$$

In the case of a power grid with transformers subjected to DC current via GIC, the example above is no longer valid because of the elevated levels of harmonics. Significant differences may exist between the RMS, Fundamental/Filtered, and Peak/$\sqrt{2}$ magnitudes.

Though reconstructed via Fourier cosine coefficients, the waveforms presented in this article represent time-sampled data with minimal error from the original signal. The RMS magnitude of a time-sampled current measurement $\mathrm{i_k}$, with n samples per cycle, may be calculated Equation 5.2.

$$I_{RMS} = \sqrt{\frac{\sum_{k=1}^{n} {i_k}^2}{n}} \tag{5.2}$$

For filtered values, a full-cycle cosine filter was implemented in Matlab. This was done as a validation-check for comparison with FFT magnitudes and event records from microprocessor-based relays. For the three primary tests and the DC-injection graphs shown in Figure 5.2, the Test Amps RMS and the Fundamental/Filtered Amps RMS values are shown in Table 5.1. Table 5.1 also reinforces the difference between RMS, Filtered, and Peak/$\sqrt{2}$ current magnitudes.

Table 5.1. Test Current Magnitude Comparison

Test	I_{RMS}	$I_{FILTERED/FUNDAMENTAL}$	$I_{PEAK} \div \sqrt{2}$
Waveform 1	10.25	9.06	17.37
Waveform 2	10.25	5.03	16.79
Waveform 3	10.25	9.46	12.81
DC 0mA	6.73	6.70	6.24
DC 40mA	6.93	6.85	6.75
DC 68mA	7.31	7.13	8.26
DC 107mA	8.18	7.72	11.48

Time-Overcurrent Relay Testing

Time-overcurrent relaying response to harmonics is of interest because of the potential to mis-operate during elevated levels of GIC. The NERC 1989 report highlighted a number of mis-operations for overcurrent relays during the geomagnetic disturbance event. While on the decline, there are still a number of electromechanical protective relays on the grid today. The testing system configuration for time-overcurrent consisted of an AVO Multi-Amp Pulsar protective relay test set, Megger's AVTS software, and an in-the-loop SEL-421 protective relay to serve as a data acquisition and trip timing device. The COMTRADE test files that were created were single phase current at 4200 samples per second (70 per cycle) for tests under 7 seconds, and 1980 samples per second (33 per cycle) for tests up to 20 seconds in duration. This is a result of the compromise between test set limitations and waveform harmonic resolution.

Two induction-disc based electromechanical relays were available for testing – a Westinghouse CO-9 and a General Electric IAC-53B. The SEL-421 that was being used as a data acquisition device was also programmed to respond to time-overcurrent. While each device has its own characteristic time-overcurrent curve (the SEL-421 was programmed for U3/Very Inverse), the pickup was set to 5 amps and the Time Dial was set to 2 for all three relays.

Harmonics will play little role in the current waveform amplitude for faults of high magnitude. For high magnitude faults, the system provides significant fault current at the fundamental frequency. The primary area of concern for these time-overcurrent relays is for load or ground current near the pickup value. An example of this is shown in Figure 5.7. The RMS magnitude of Waveform 1 was varied while holding THD constant and the resulting operate times for each relay are graphed in blue.

The fundamental operating times are graphed in orange. For the microprocessor-based relay, there was no difference. The electromechanical relays operated at approximately half of their calculated pickup time at 5.75A fundamental (6.5A RMS). Harmonic currents do play a role in the operate time of the relay, and the result will vary according to the individual relays.

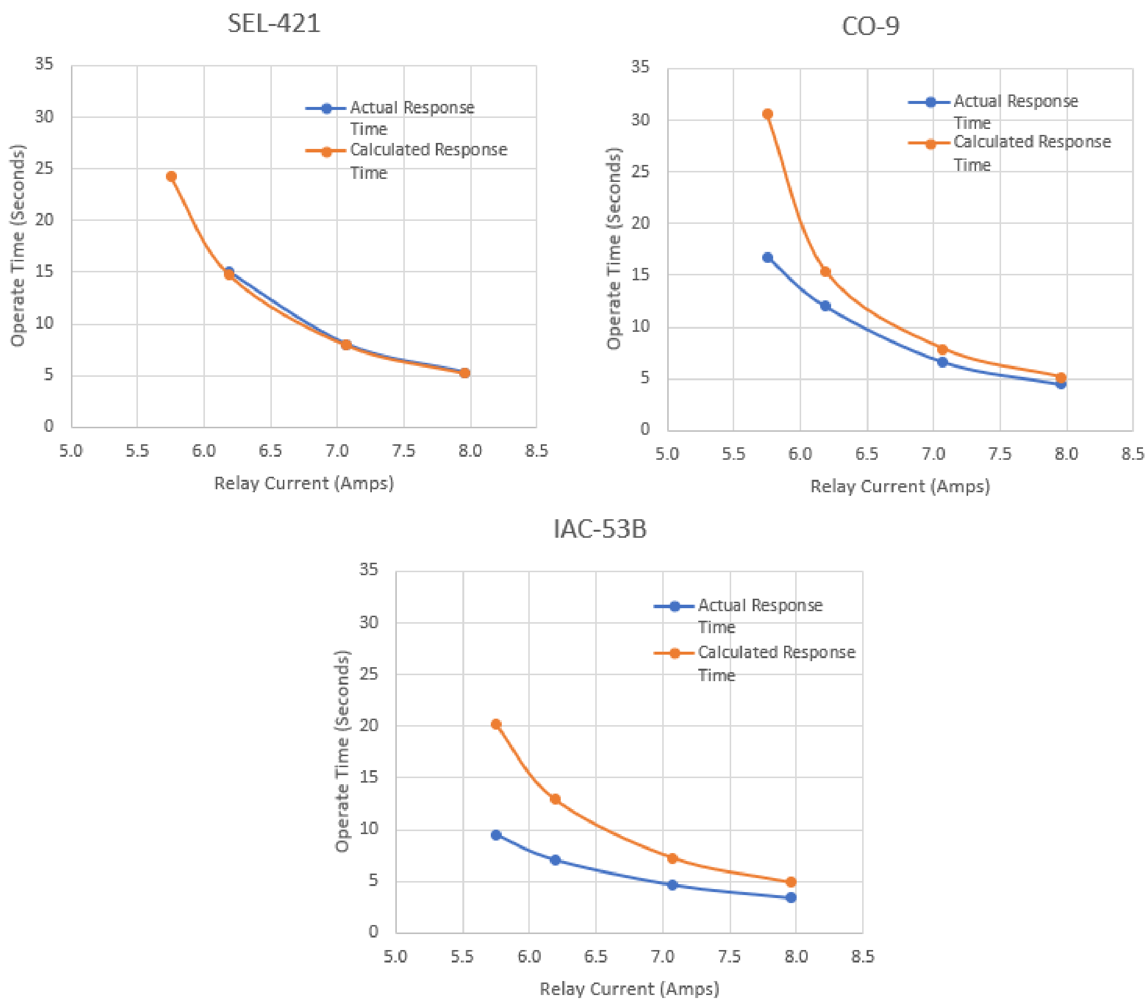

Figure 5.7. Time-overcurrent Operate Timing for SEL-421, ABB CO-9, and GE IAC-53B Relays

Because of the difference between RMS and fundamental magnitudes for distorted waveforms, operate times on the unfiltered electromechanical relays become unpredictable. While Waveforms 1, 2, and 3 were tested using the same IRMS magnitude, the operate times varied because of the variation in harmonic distortion. Table 5.2 contains the operate times for each of the relays for each test. Note that for Waveform 2, the SEL-421 did not operate within the test window (7 seconds). The estimated operate time based on fundamental frequency RMS would have been between 480 and 650 seconds.

Table 5.2. Operate Times for Waveforms 1, 2, & 3

Waveform 10.25A RMS	THD	CO9 Time (s)	IAC53B Time (s)	SEL421 Time (s)
1	53%	3.08	2.445	3.587
2	177.5%	4.994	2.281	480+
3	41.8%	2.738	2.425	3.2

THD in Table 5.2 is calculated based on the second through tenth harmonics from the FFT parameters in Tables 5.3, 5.4, and 5.5 at the end of this chapter using Equation 5.3.

$$\%THD = \sqrt{\sum_{h=2}^{10}(\frac{\%I_h}{I_1})^2} \tag{5.3}$$

Differential Relay Testing

The principle behind differential relaying is that the per-unit current in is approximately equal to the per-unit current out. Protection settings for differential relays do incorporate some margin for CT errors, transformer losses, and security. During a period of geomagnetically induced currents (and confirmed on the test bench), magnetizing losses in the transformer can increase dramatically and increase the potential for a protection system mis-operation because of the nature of a transformer differential relay monitoring the difference between input and output currents.

Typical transformer differential protection incorporates second harmonic restraint or blocking. This feature is protection against tripping during the imbalance of transformer inrush. Of the four relays available for testing, all incorporate second harmonic restraint. The four relays include a Westinghouse HU, a General Electric BDD16, a General Electric STD15, and an SEL-487E.

There were three questions considered: (1) Will the relay operate during the elevated magnetizing loss period? (2) Will the relay still operate for an internal fault? (3) Will the harmonics of the transformer impact the operation of the transformer?

A rather simple test was devised to check relay operation. This test simulates a low-magnitude internal transformer fault. Balanced 60 Hz current was injected into the transformer primary and secondary windings of each relay, and then the secondary side current injection was turned off while the primary side winding current injection continued. All four relays tripped immediately upon losing secondary winding current injection.

A COMTRADE file using the waveforms in Figure 5.3 was created, and a similar drop-out test was performed. In these tests, all four relays were restrained from tripping when the secondary winding current injection was stopped. The elevated level of the second harmonic held the restraint for the duration of the test and the relays did not operate for the 'internal fault'.

Discussion of Observations

Time-overcurrent Protective Relaying

The 'rule of thumb' in the literature is that electromechanical relays need to be examined on a case-by-case basis, as the electromagnetic and mechanical construction varies by manufacturer and by relay [48]. The tests performed by the authors confirms that two electromechanical time-overcurrent relays that use similar induction-disc construction exhibit substantially different behavior. The GE IAC53B consistently operated at close to RMS current values, while the CO9 was more influenced by the change in harmonic content.

The microprocessor-based SEL-421 performed predictably by operating solely on the fundamental current magnitude. The only concern with the SEL-421's performance is with currents that resemble Waveform 2 – extremely high harmonics that are much greater than the fundamental in magnitude. The fundamental of Waveform 2 was barely above the pickup of the relay (5 amps), while the peak magnitude of Waveform 2 was nearly 24 amps. There could be situations where this peak current would be damaging (i.e., capacitor bank protection) yet the relay would not operate on the harmonics due to the filtering.

Differential Protective Relaying

While second harmonic restraint does disable the sensing of low-level internal faults by the differential protection scheme, it does not completely disable the protection system. All of the relays tested feature an unrestrained high-current instantaneous element that will issue a trip for a strong internal transformer fault. Unfortunately, the time delay between a low-level fault and an instantaneous trip for a high-current fault may mean additional transformer damage that may not have occurred otherwise.

Selection, Detection, and Mitigation with Protective Relays

A commonly overheard question within ERCOT (the Texas grid, where the authors participate in industry discussions) is "How do I know if a relay is potentially going to be impacted by GIC?". The best practice currently is to examine the DC current magnitudes produced by the TPL-007 model created by the regional planning authorities based on the NERC Benchmark and Supplemental GIC events. These models contain DC current flow for transformers in the grid. Should a transformer have more than 30A of DC neutral current as a result of the simulation, the protection system should be evaluated for the possibility of harmonic susceptibility [10]. If there exist electromechanical overcurrent relays or relays without harmonic filtering, these relays should be tested for performance in a manner similar to this article. Relay pick-up settings also need to be examined for proximity to load; low settings may cause protection systems to operate unnecessarily.

Both MHD-E3 and solar GIC will result in additional second, fourth, and fifth harmonics being introduced into the power grid. While these harmonics are not normally part of the grid, many microprocessor-based relays are capable of calculating the harmonic content of the current and/or voltage. These measurements may be sent as analog values to a control center via SCADA or synchrophasor (PMU) data as part of a real-time harmonic monitoring system [50]. The authors have been using microprocessor-based differential relays for several years to log harmonic content of the operate current in the differential circuit on several 345kV/138kV autotransformers. An example of this type of data is shown in Figure 5.8. For this figure, the protective relay value for calculated percent second harmonic operate current for differential protection for each level of DC injection from Figure 5.2 is scaled by 100,000 and transmitted via synchrophasor protocol to a phasor data concentrator. The multiplier (100,000) is so large because the harmonic content is typically very low, so increasing the resolution permits observing small changes in harmonic content and, if using SCADA with deadbanding, permits more frequent measurement updates. This multiplier is beneficial for research but may be reduced during an actual implementation. With such a wide variance in range (from 0 to 12% in this figure, but can go higher), establishing alarm or actionable thresholds is easily accomplished. While there are waveform similarities between this test and Figure 5.3, the harmonic content is different because of the secondary current phase shift applied during this instance of relay testing. Figure 5.8 represents two seconds of high speed synchrophasor data.

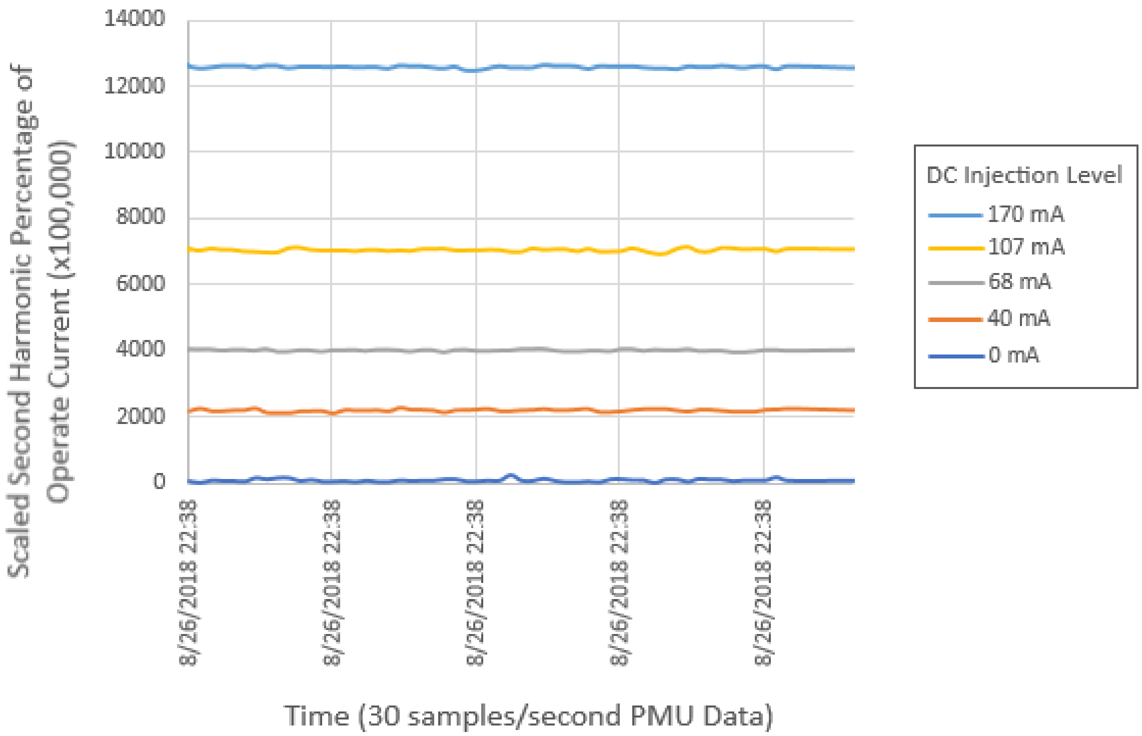

Figure 5.8. Operate Current Second Harmonic Percentage x100 from Differential Relay for Figure 5.2 Waveforms

Because elevated second harmonics can disable the fast operation of a differential relay protection system, it is recommended that a harmonic threshold timing alarm be created in logic in capable differential relays. For example, if the second harmonic restraint threshold is surpassed for more than 30 seconds, activate a logic output that can alert a system operator that transformer fast operation protection may have been disabled.

Conclusion

The introduction of quasi-DC currents via solar or MHD-E3 GIC into the electric power grid will result in harmonic currents and voltages that are not observed during normal grid operation. With the creation of test waveforms based on benchtop transformers with DC injection, waveforms from the literature, and field data from a grid DC injection testbed, several relays were tested for response to these harmonic-rich signals.

For time-overcurrent relays, electromechanical relays such as the Westinghouse/ABB CO-9 and the GE IAC53B tended to operate on fundamental plus some components of the harmonic current, as opposed to fundamental-only of the microprocessor based SEL-421. While the induction-disc technologies of the electromechanical relays were similar, their operations differed, with the GE tending to operate more closely to the RMS magnitude of the current.

Differential relays, whether electromechanical or microprocessor based, typically include second harmonic restraint or blocking which will disable tripping once the second harmonic reaches a pre-set threshold. With these relays, once that threshold is reached in a GIC scenario, differential protection via the traditional operate/restraint curves is disabled and the relays default to their high-current unrestrained element alone.

While the consideration of harmonics in GIC-prone substations is important for determining effective relay settings, protective relays may also be used to detect and monitor these harmonics. A monitoring system using already-installed protective relays provides operational awareness of possible harmonic issues and can alert system operators and engineers of possible device or protection compromise so that mitigating techniques may be applied.

Table 5.3. Waveform 1 Cosine FFT Components

Harmonic	Magnitude (%)	Phase
1	100	-90.52
2	37.9	107.3
3	29.03	-17.88
4	17.85	-144.26
5	11.91	85.39
6	7.09	-38.96
7	4.16	-161.3
8	1.64	64.51
9	0.46	-65.43
10	0.22	-30.53

Table 5.4. Waveform 2 Cosine FFT Components

Harmonic	Magnitude (%)	Phase
1	100	86.5
2	144.6	123
3	38.7	149.4
4	90.3	-15.8
5	28.3	1.1
6	7.8	-8.1
7	2.9	-78
8	1	-10
9	5.6	-0.9
10	5.5	69.1

Table 5.5. Waveform 3 Cosine FFT Components

Harmonic	Magnitude (%)	Phase
1	100	-102.03
2	36.25	29.62
3	0.93	62.99
4	17.63	54.56
5	10.91	-110.59
6	0.32	-109.7
7	0.7	-50.26
8	0.95	-95.3
9	0.07	-84.42
10	0.96	-43.88

CHAPTER SIX

The Response of a Transformer Differential Relay to Internal Faults While Influenced by Geomagnetically Induced Currents

This chapter revised from publication: A. K. Mattei, D. Haas, J. Candeleria and W. M. Grady, "The Response of a Transformer Differential Relay to Internal Faults while Influenced by Geomagnetically Induced Currents," 2020 Western Protective Relay Conference (WPRC), [Online]. Available: https://selinc.com/api/download/132014/

The Concern Regarding Differential Protection

During a geomagnetic disturbance period such as a strong solar storm or MHD-E3 event, transformer saturation will result in the production of harmonics within the winding that is being subjected to direct current. This will cause an increase in harmonics in the "operate current", which is the per unit magnitude of the sum of the winding phase-compensated currents between the primary, secondary, and if applicable, additional windings. Transformer saturation as a result of DC injection has a second harmonic characteristic that increases linearly as the DC increases [1]. Strong solar storms may induce over 100 amps per phase of DC [51], while an MHD-E3 event may induce over 300 amps per phase [8].

During transformer energization, the high levels of inrush current will tend to saturate the transformer core for a period of a few cycles up to perhaps a few seconds. Within this period, the transformer phase currents will exhibit a second harmonic characteristic with a high level of current towards each polarity and a flat section at the zero crossing (see Figure 4.1). At this time the transformer core is absorbing energy and if permitted, the differential protective relay may operate. Tripping a transformer during energization is an undesired result, so differential protection has traditionally utilized second harmonic restraint or second harmonic blocking to prevent tripping during energization.

Preventing the operation of the differential relay during periods of elevated second harmonics raised the questions: what happens to the differential protection when there is a fault within or near the transformer during a period of geomagnetic disturbance, and does protection vary as fault magnitude varies? We set out to explore the sensitivity, selectivity, and dependability of a pair of modern transformer differential relays through the use of modeling, simulation, and testing.

Transformer Protection and Transformer Differential Elements

For large transformers, several types of protection are often applied. For speed, selectivity, and sensitivity, phase differential protection (87) is applied for phase faults and, in some cases, for ground faults as well, particularly in solidly grounded systems where dedicated ground fault protection may not be applied. Because of the 87 element's broad use and very specific concerns about the response of the 87 element during periods of high GIC, we focus on this element in particular.

Traditionally, phase fault protection has involved only the phase differential and overcurrent elements. However, with modern microprocessor-based relays, more sensitive detection of phase faults and detection of turn-to-turn faults is possible using a negative-sequence differential element (87Q) [52]. We evaluate the 87Q element as well in our testing and analysis.

There are other elements present, particularly for more sensitive detection of ground faults or turn-to-ground faults. These include the ground differential element (87G) or, alternatively, restricted earth fault (REF) schemes. Since the focus of our investigation is phase fault detection, and since some utilities still rely on the phase differential element for protection of ground faults, we did not evaluate the performance of these ground protection schemes in this paper.

In addition, sudden pressure or Buchholz relays are often applied to detect internal transformer faults where the fault currents are difficult to detect with traditional phase differential elements.

The two relays analyzed in this paper are microprocessor-based relays of varying vintage, both with phase 87 elements using the adaptive slope characteristic described in [53].

The phase differential elements in these relays use Equations 6.1 and 6.2 to calculate operate and restraint current, shown for just A-phase, respectively.

$$IOPA = \mid \sum_{m} IAmCFC \mid \tag{6.1}$$

$$IRTA = \sum_{m} \mid IAmCFC \mid \tag{6.2}$$

In Equations 6.1 and 6.2, *IOPA* is the A-phase operate current in per unit, *IAmCFC* is the A-phase filtered (no harmonics), winding-configuration compensated current per unit, *IRTA* is the A-phase restraint current in per unit, and m is the specific three phase winding set of inputs on the relay, labeled S, T, U, W, and X.

The method of calculating restraint current in Equation 6.1 is referred to as an average or weighted average restraint [54], and may vary according to relay or manufacturer. The 87Q element uses a single-slope characteristic with a slightly different method of calculating restraint current. Equations 6.3, 6.4, and 6.5 outline how the 87Q element in both relays calculates negative-sequence, operate, and restraint currents respectively. In these equations, a is a phasor of $1\angle 120°$ and *IAmCFC*, *IBm-CFC*, and *ICmCFC* are the individual phase filtered and compensated currents in per unit.

$$3I2mC = \begin{bmatrix} 1 & a^2 & a \end{bmatrix} \cdot \begin{bmatrix} IAmCFC \\ IBmCFC \\ ICmCFC \end{bmatrix} \tag{6.3}$$

$$IOP87Q = \mid \sum_{m} 3I2mC \mid \tag{6.4}$$

$$IRT87Q = max_m(\mid IAmCFC \mid) \tag{6.5}$$

For clarity, the older microprocessor-based relay is referred to as Relay 1. The newer microprocessor-based relay with additional algorithms and enhancements is referred to as Relay 2. They are both of the same manufacturer and model line, but Relay 2 has updated hardware and different firmware.

Both microprocessor-based relays have several methods to restrain incorrect tripping during inrush conditions. Both had the traditional methods of harmonic blocking and harmonic restraint applied. Relay 2 has an additional method of inrush restraint known as waveshape recognition that does not rely on harmonics. A comparison of these inrush restraint techniques is included in a later section.

Model Used for Simulation

Core construction influences the susceptibility of a transformer to saturation during the quasi-dc currents that occur with a GIC event. Single-phase, five-limb, and shell-form transformers provide low-reluctance return paths to the magnetic flux and permit more rapid core saturation than the higher-reluctance path present in three-limb core-form transformers [49].

A laboratory test bench was constructed using six single-phase wye-wye connected transformers. In the test region of the circuit, the secondary winding of the first set of three transformers was connected to the primary winding of the second set of three transformers, with a balanced resistive load on the secondary side of the second set. Within the loop formed by this connection, a switched battery-based dc source was placed in the neutral. When the switch was closed, the dc current saturated the transformers, and a GIC-like harmonic response was observed.

Data from the actual current waveforms collected from this laboratory test bench were used to create COMTRADE test files. These waveforms were used to evaluate the response of different types of relays to GIC-induced harmonic distortion [1]. To evaluate the response of the transformer differential relay to varying levels of GICs and different fault magnitudes and locations, a software model was necessary to generate test files. Open- and short-circuit tests were performed on these bench-top transformers, and a saturable transformer model of this laboratory test bench was created in Alternative Transients Program-Electromagnetic Transients Program (ATP-EMTP).

The saturable transformer model in ATP-EMTP provided a response that was similar to the test bench data under dc injection. This allowed the placement of a variety of faults both internal and external to the differential zone of protection.

Faults were placed in the following locations with varying GIC levels and resistance values, with the locations noted in Figure 6.1.

- Internal transformer primary phase-to-ground (F1)
- Internal transformer primary phase-to-phase (F1)
- Internal transformer secondary phase-to-ground (F2)
- Internal transformer secondary phase-to-phase (F2)
- External secondary phase-to-ground (F3)
- External secondary phase-to-phase (F3)

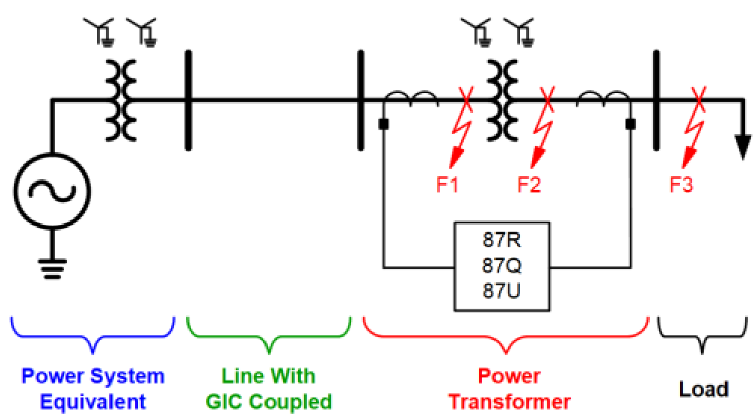

Figure 6.1. One-Line Diagram with Fault Locations

Other protective elements, such as sudden pressure protection and REF, are commonly used schemes within transformer protection but are not considered here because of the focus on the differential element and the potential for differential tripping to be inhibited by GIC harmonics.

Figure 6.2 shows a simplified three-line schematic diagram of the model, simulating specifically the phase-to-phase fault on the secondary winding of the power transformer. The portion outlined in blue represents the source system equivalent. The portion outlined in red represents the power transformer model and the phase-to-phase fault with fault resistance. Similarly, in green is the ground return and GIC source equivalent. Lastly, in black is the portion that represents the transformer load.

The response of the ATP-EMTP model exhibited elevated levels of the second harmonic at magnitudes similar to the test bench. As previously mentioned, the second harmonic is not normally present in power systems except for during the temporary period of transformer inrush.

Relay Configuration

The relays are configured for a wye-wye connection with single-phase transformers. And while the test bench and model validation discussed in the previous section were based on laboratory transformers, the model was adjusted and scaled along with the relay settings to look at the response of a 100 MVA, 138 kV-to-69 kV transformer bank and representative power system.

Tripping elements include an unrestrained element (87U), a phase element (87R), and a negative-sequence element (87Q). The unrestrained element has no supervision within the relay (no blocking or restraint). Both harmonic restraint and cross-harmonic blocking are enabled. Waveshape recognition with waveshape-based harmonic unblocking is also enabled in Relay 2. Table 6.1 outlines the specific settings that were used for 87U, 87R, and 87Q in the testing.

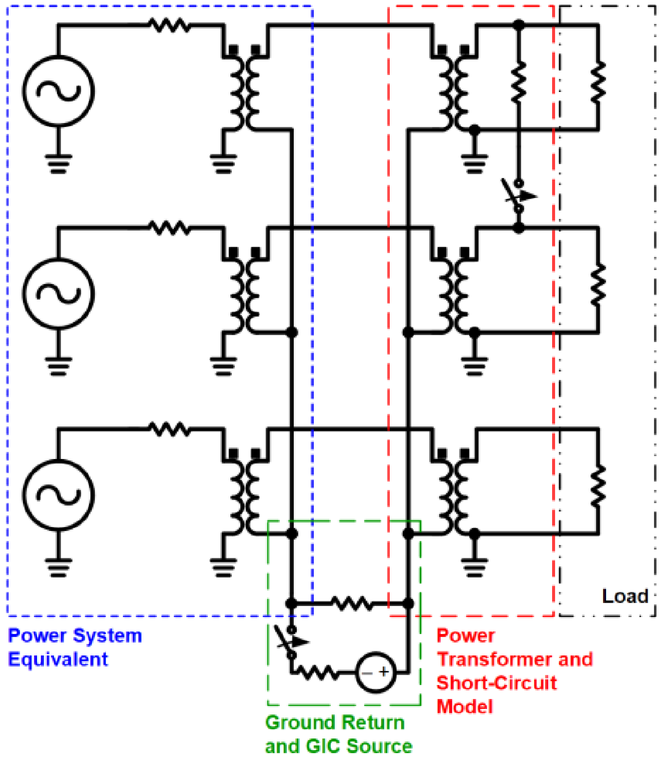

Figure 6.2. Three-Line Schematic Diagram of Model Used for Phase-Phase Fault on Secondary Winding

Harmonic Restraint and Harmonic Blocking

Harmonic restraint and harmonic blocking are commonly used to prevent the transformer protection system from tripping due to asymmetrical currents present during transformer energization current inrush. In general, the differential protection system is based on the ratio of operate current to restraint current, with operate representing the current unbalance and restraint representing the balanced current. For harmonic restraint, the harmonic magnitudes are extracted from the unfiltered differential current magnitude and used to increase the tripping threshold by adding them to the filtered restraint current. This additional restraint current added to the calculation provides security against tripping during an event (e.g., energization inrush) that causes the transformer to create harmonics.

Table 6.1. 87U, 87R, and 87Q Settings Used for Testing

Setting	Value
87U pickup	8 pu
87R pickup	0.5 pu
87R primary slope	20%
87R high-security slope	37.5%
Second-harmonic blocking pickup	15%
Fourth-harmonic blocking pickup	15%
87Q pickup	0.3 pu
87Q slope	25%

Harmonic blocking uses the calculated percentage of harmonics in the operate current and compares it to the preset pickup value. If the calculated percentage exceeds the setting threshold, the relay blocks tripping for that differential element.

Cross-harmonic blocking provides an additional level of security in that it restrains the relay if any of the three phases are above the harmonic blocking set-point threshold. It is commonly recommended to enable harmonic restraint, harmonic blocking, and cross-harmonic blocking as a set, so this combination is widely used.

Waveshape Recognition

Waveshape recognition is a time-domain protection algorithm that performs calculations based on sampled data rather than traditional phasor calculations. The theory, logic, and performance of waveshape recognition are outlined in [55].

During an inrush event, the differential currents are unipolar. Inrush differential currents based on the sampled waveform have predominantly positive or negative values. In Figure 6.3, we see energization inrush current measured from an overcurrent relay protecting a 480V to 69kV step-up transformer. The current on the A-phase in blue is offset positively, the current on C phase in yellow is offset negatively, and the red B phase trace has very short peaks in both regions. All three phases exhibit a characteristic flat spot between peaks.

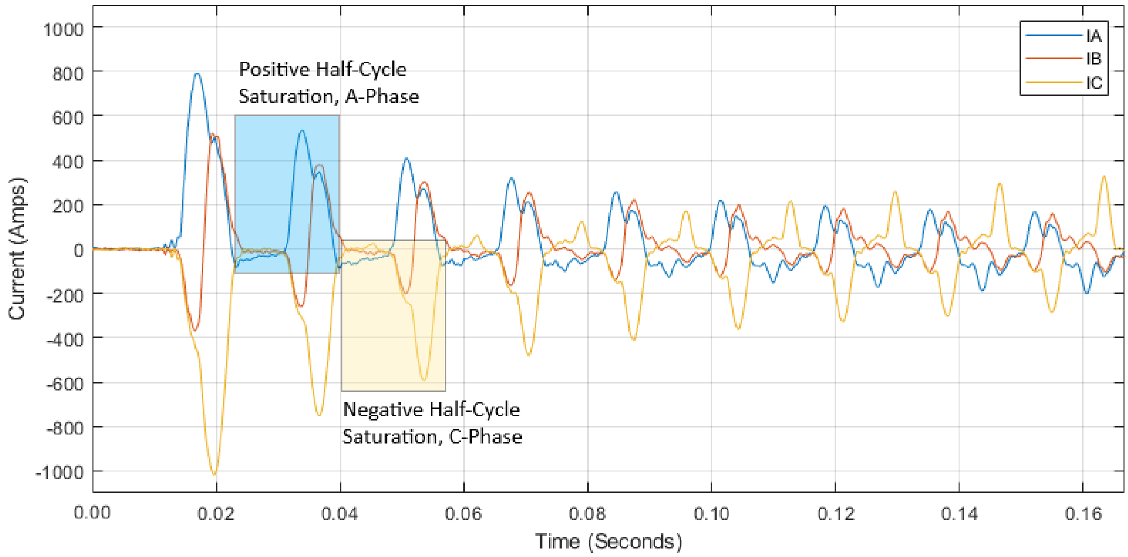

Figure 6.3. Transformer Inrush Current with High Second Harmonic Component

For the event in Figure 6.3, the transformer was unloaded during energization, so the phase currents and differential currents are the same. The waveforms for GIC-induced saturation are different than energization inrush, as noted in [56] and [1]. In Figure 6.4, the phase currents feeding a loaded transformer during GIC-induced saturation conditions are plotted on the top axes.

The raw differential currents are plotted on the middle axes, with positive (BLTH_P) and negative (BLTH_N) waveshape blocking threshold markers. The status of the waveshape blocking is plotted on the bottom axes. In the phase currents on the top axes, we can see a unipolar component but also the impact of the load currents, which are not unipolar. The differential currents, in the middle axes, are more unipolar. In addition, as [55] describes, the algorithm looks at the derivatives of the differential currents as well. For brevity's sake, we do not plot all signals and components of the logic, but we can see in the bottom trace that the waveshape

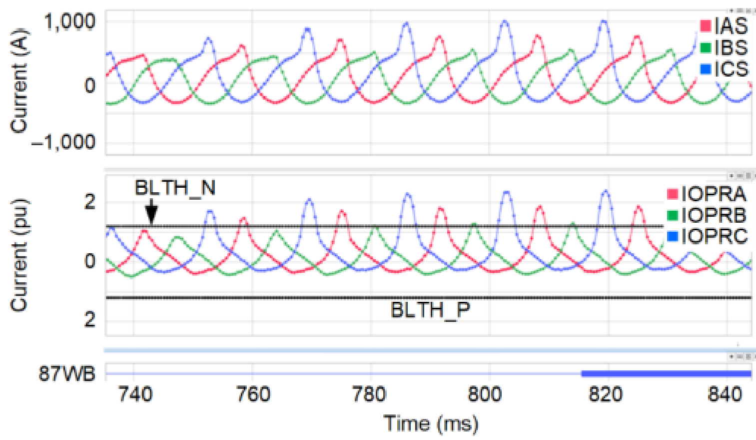

Figure 6.4. Phase Currents, Differential Currents, and Waveshape Blocking Logic Status During GIC-Induced Saturation

blocking algorithm sees the relatively flat parts of the differential currents and the unipolar nature of the waveform and asserts the waveshape blocking bit, denoted as 87WB in Figure 6.4.

For an internal fault during the inrush period, the waveform of the differential current for the faulted phase assumes a bipolar shape with both positive and negative peaks. Figure 6.5 shows the phase currents on the top axes, the raw differential currents in the middle axes, and the status of the blocking and unblocking elements on the bottom axes. We can see that for the case of the fault, the currents on the middle axes in particular go both above and below the thresholds. The fault makes A-phase and B-phase differential currents no longer unipolar but go above and below the unblocking thresholds.

The waveshape unblocking logic is also described in [55]. A simplified version of a critical portion of the unblocking logic is shown in Figure 6.6. We highlight the bipolar overcurrent detector that essentially looks for current both above and below a positive and negative threshold, respectively, within a certain time frame. The additional portions of the unblocking logic are discussed in [55], namely the sudden change in differential current detection.

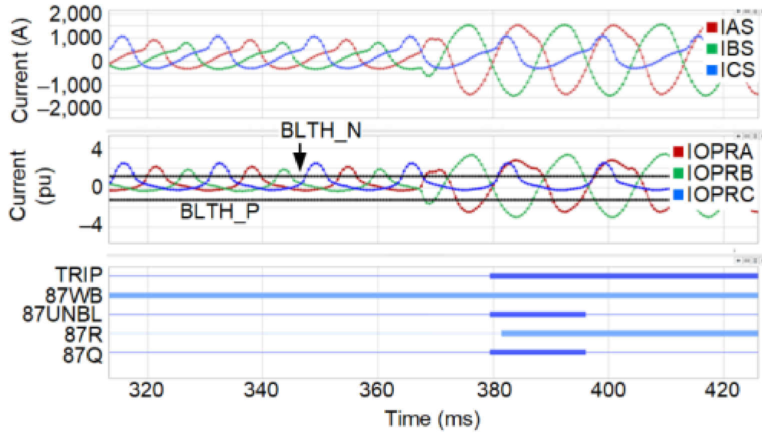

Figure 6.5. Phase Currents, Differential Currents, and Waveshape Blocking Logic Status During GIC-Induced Saturation and Internal Phase-to-Phase Fault

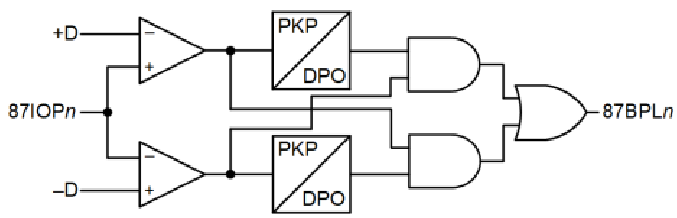

Figure 6.6. Simplified Unblocking Logic Showing Bipolar Overcurrent Elements

Based on this principle of symmetry and with some additional security checks and a supervising timer, a bipolar unblocking element is available in the relay. This unblocking element removes cross-harmonic blocking, waveshape-based inrush blocking, and the harmonic magnitudes from the calculations for harmonic-restrained differential elements. For negative-sequence protection, cross-blocking and waveshape-based inrush blocking are canceled, and the negative-sequence delay timer is bypassed.

Test Results

The test concept was to build a series of tests for comparing varying GIC levels with varying fault resistance values. For test Cases 1–6 in this section, we evaluate and compare two relay designs: Relay 1 with harmonic restraint and cross-harmonic blocking, and Relay 2 with waveshape recognition combined with harmonic restraint and harmonic cross-blocking.

Fault resistance was varied according to the location of the fault. Our goal was to observe if there were thresholds in fault resistance at which the relays would or would not operate. As the relays were tested, an operation or no operation was noted, as well as the first tripping element from the sequential events recorder (SER) report.

Each test simulation consisted of three well-defined periods in time. In Figure 6.7, we have a representative example of the currents from a simulation where all three periods are identified. The first period is a brief period of normal power system load following the start of the simulation, where normal transformer energization inrush is seen. This period is the left shaded section (red) in Figure 6.7. The second period is when the GIC current begins in the simulation. This is the middle highlighted section (green) in Figure 6.7. The final period of simulation is when the internal fault is applied, shown in the right highlighted section (blue) in Figure 6.7. While the primary goal of each simulation was to examine the relay's response to a particular fault scenario, we also were able to evaluate the response of the relay to the GIC current and the half-cycle saturation it caused, as well as ensure the simulation was initialized properly.

Restraint for GIC-Induced Saturation

For all of the cases simulated, the GIC-induced saturation alone did not result in a trip. For smaller values of GIC, the impact on the currents was barely noticeable. For larger values of GIC, the inrush restraint algorithms, along with the pickup of the differential element, prevented tripping. As described in [1], the harmonic content and general waveshape of the GIC currents matched other publications and the laboratory transformers. These results, however, may not be able to be generalized to all transformer types because, as previously mentioned, the single-phase construction

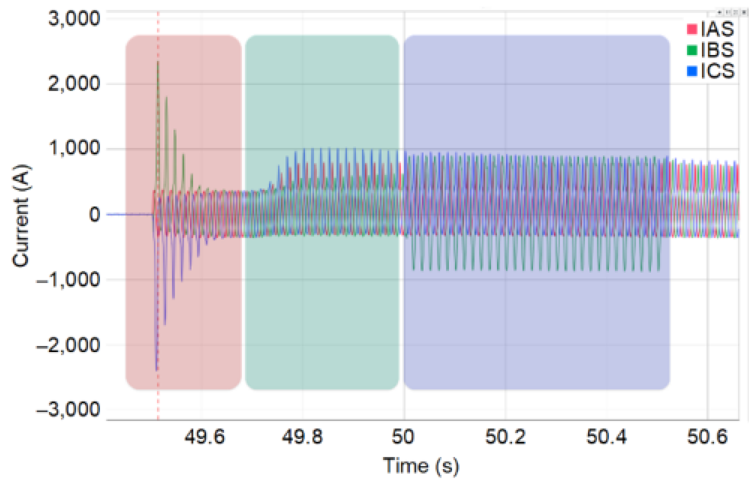

Figure 6.7. Oscillograph Showing Currents from Example Simulation and the Three Different Periods of Each Simulation

of the transformer impacts the saturation characteristics. In addition, we did not model all possible loading conditions that the power system or load may present to the transformer during periods of high GIC. But for all example cases modeled, both Relay 1 and Relay 2 were secure with GIC saturation during the simulation period when no faults were applied.

Fault Resistance Coverage

The simulated faults are discussed in the following subsections, organized by the location and type of fault simulated.

We performed an initial round of internal phase-to-ground fault simulations on the transformer primary while enabling only harmonic restraint, only harmonic blocking, or both harmonic restraint and harmonic blocking. The relay configuration included cross-blocking enabled without independent-pole harmonic blocking. We observed that with only harmonic blocking enabled, the relay did not operate while exposed to harmonic distortion unless the unrestrained element (87U) asserted. The minimum level of dc-related harmonic distortion from the test configuration was sufficient to enable harmonic blocking on all tests. None of the results for harmonic blocking only are highlighted in the following sections, as we had to turn on at least harmonic restraint to get any dependable operation for the test scenarios where any level of GIC was present.

Case 1: Internal transformer primary winding phase-to-ground faults. The transformer primary phase-to-ground case was constructed with a total of 60 tests, with the fault resistance varying from 50 to 500 ohms (50, 100, 200, 300, 400, and 500). Ten levels of dc were used for the GIC simulation. While typical fault resistance is lower than the maximum values in the simulation, we were interested in the sensitivity of the protective relays to abnormally high-resistance faults. For the low-resistance end of the spectrum (50 ohms), the assumption that relays will trip for a low-to-zero resistance fault was validated by testing.

The performance of both relays is shown in Figure 6.8 for the tests with both harmonic restraint and harmonic blocking enabled. The horizontal axis reflects increasing dc current, and the vertical axis reflects the maximum fault resistance where the relay still tripped dependably for an internal fault. A higher resistance data point on the graph indicates that the relay was sensitive to faults up to that point. Relay 2 was more sensitive across the range of faults than Relay 1.

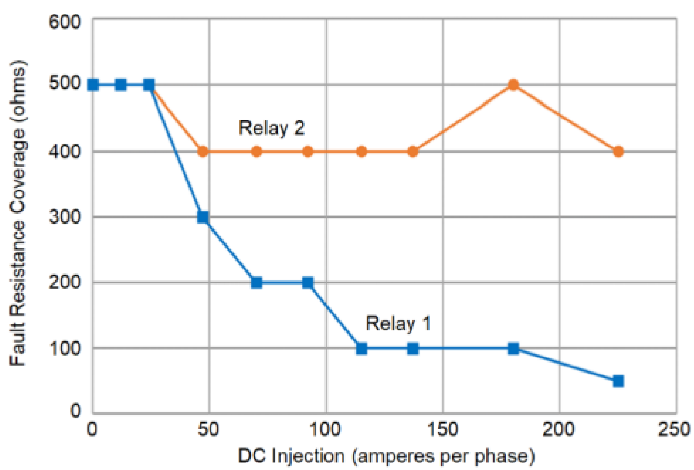

Figure 6.8. Fault Resistance Coverage vs. Increasing GIC Levels for Internal Phase-to-Ground Faults on the Primary Winding

Case 2: Internal transformer secondary winding phase-to-ground faults. For this set of tests, a different set of resistance values was selected (50, 100, 125, and 150 ohms) because the currents on the secondary of this transformer configuration are naturally higher than the primary winding currents. While fewer tests were performed for this case (40), the results once again indicated that Relay 2 was more sensitive than Relay 1. The fault resistances used again revealed a threshold of operation. Figure 6.9 shows the transformer secondary phase-to-ground response of the relays.

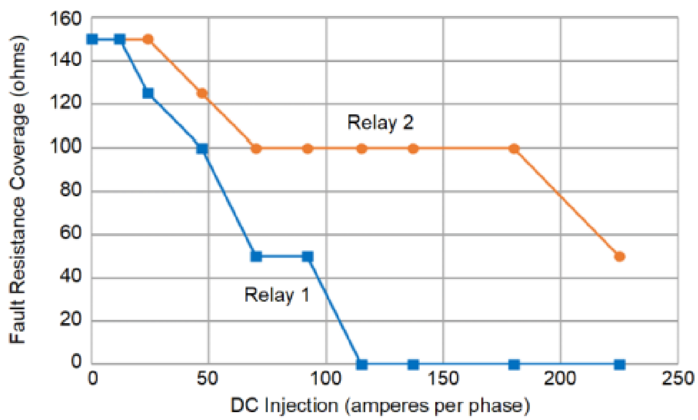

Figure 6.9. Fault Resistance Coverage vs. Increasing GIC Levels for Internal Phase-to-Ground Faults on the Secondary Winding

Case 3: Transformer primary winding phase-to-phase faults. For this set of tests, 20 tests were performed with varying fault resistances (50, 300, 400, and 500 ohms). Relay 2 tripped for all tests. Figure 6.10 shows the transformer primary phase-to-phase response of the relays.

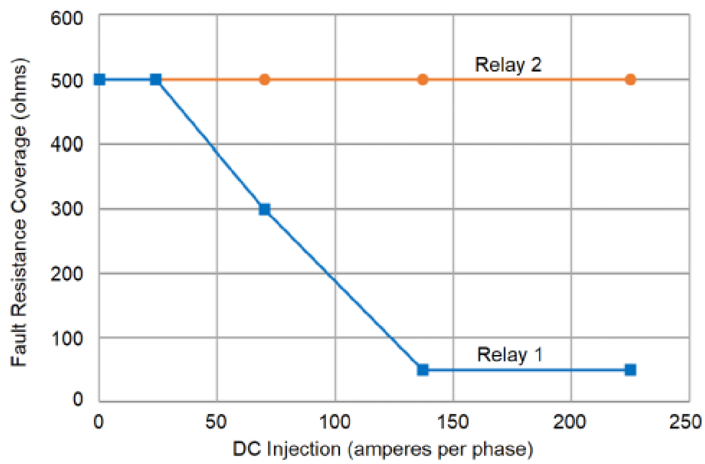

Figure 6.10. Fault Resistance Coverage vs. Increasing GIC Levels for Internal Phase-to-Phase Faults on the Primary Winding

Case 4: Internal transformer secondary winding phase-to-phase faults. For this set of tests, 20 tests were performed with varying fault resistances (50, 100, 200, and 300 ohms). Figure 6.11 shows the transformer primary phase-to-phase response of the relays.

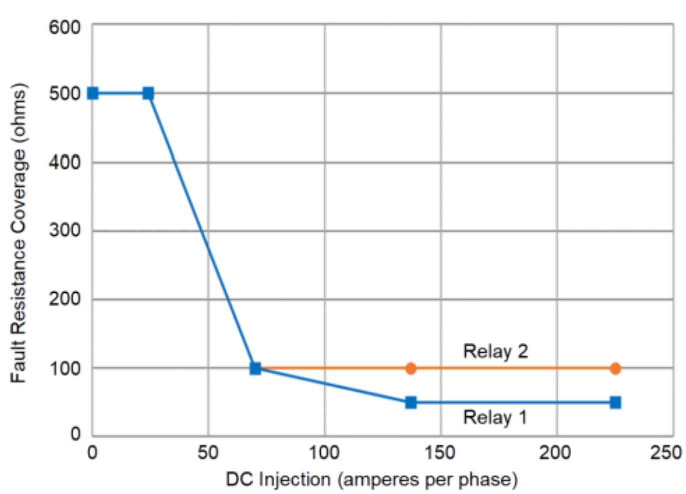

Figure 6.11. Fault Resistance Coverage vs. Increasing GIC Levels for Internal Phase-to-Phase Faults on the Secondary Winding

Cases 5 and 6: External secondary winding phase-to-ground and phase-to-phase faults. External faults were modeled to validate relay security during external fault conditions. Neither relay tripped for any of these faults. This demonstrated the security of both relays. It is important to note that we assumed ideal CT performance and did not account for the impact of CT saturation in our modeling. CT performance, as mentioned previously, is treated and analyzed in [41].

Observation of Tripping Elements

For Relay 1, the tripping elements were limited to the unrestrained (87U) and restrained (87R) differential elements. The negative-sequence element (87Q) did not trip the relay for any of the tests performed on Relay 1. The negative-sequence element in Relay 1 has a time delay and is also blocked or restrained from tripping by the second-harmonic setting.

For Relay 2, there were numerous instances of simultaneous or very near tripping of all three elements (87U, 87Q, and 87R). It was common to see 87Q and 87U with the same time stamp in the SER log, with 87R trailing these asserted elements by 2 milliseconds. Waveshape unblocking was key to the fast response and is briefly described in the next section.

Importance of Unblocking Logic and Unrestrained Elements

During a strong geomagnetic disturbance, elevated harmonics assert harmonic blocking while the second-harmonic currents are added to the differential restraint. This desensitizes the relay to low-magnitude internal faults.

An additional enhancement to the unrestrained differential element operated the relay during high-current faults. The unrestrained element may operate as usual on the fundamental current, but a bipolar element and a scaled Sampled Values-based element are available. In this testing, the waveshape-based bipolar logic operated more quickly than the standard differential elements.

Detailed Analysis of Elements for Example Case

To illustrate the points made in the previous two sections (restraint and unblocking), we analyze the response of the three elements—harmonic blocking, harmonic restraint, and waveshape recognition—for a particular test scenario. We selected an internal phase-to-phase fault, with 70 A of GIC and 100 ohms of fault resistance.

The results of Relay 1, highlighting harmonic blocking in particular, are shown in Figure 6.12. The phase currents on the high-voltage side of the transformer are plotted on the top axes. The second-harmonic content on the A-, B-, and C-phases is plotted on the middle axes against the second-harmonic threshold setting (PCT2). The states of the individual phase blocking elements (87ABK2, 87BBK2, and 87CBK2), as well as the combined cross-harmonic blocking element (87XBK2), are plotted on the bottom axes.

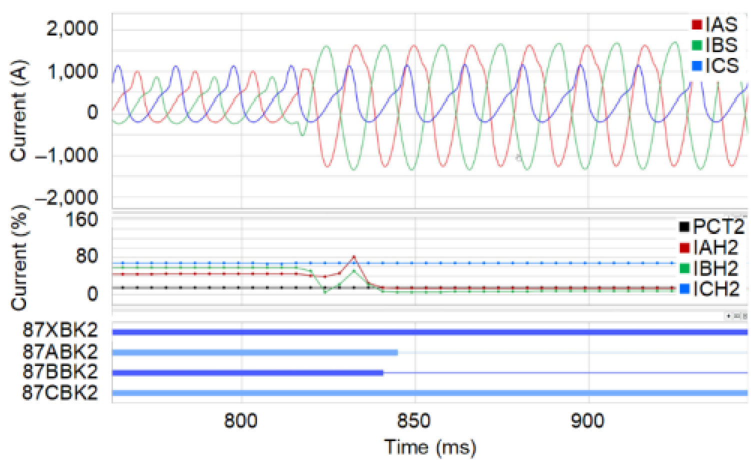

Figure 6.12. Phase Currents, Second-Harmonic Content, and Cross-Blocking Element Statuses for Internal Phase-to-Phase Fault

We can see in Figure 6.12 that in all three phases, the harmonic content is above the threshold settings before the internal fault is applied at around 820 milliseconds. After the internal fault, the harmonic content on the A-phase and B-phase (the faulted phases) drops just below the setting of 15 percent, at approximately 14 percent and 5 percent, respectively. The A-phase and B-phase harmonic blocking elements (87ABK2 and 87BBK2) drop out accordingly. However, since this relay used harmonic cross-blocking and the C-phase harmonic content stays above the threshold setting throughout the duration of the event, the differential element would not trip if supervised by harmonic blocking alone. One possible solution would be to consider applying a relay that has independent harmonic blocking instead of cross-blocking. And certainly, for this particular event, it would have allowed the A-phase and B-phase differential elements to trip. However, it is well-documented in [57] that using independent harmonic blocking alone compromises security during periods of inrush, or similarly for high GIC, where the harmonic content on a single phase drops just below the setting.

Reference [57] suggests using harmonic restraint as a preferred method when only the two methods of harmonic blocking and harmonic restraint are available. In these particular relays, as mentioned previously, both harmonic blocking and harmonic restraint operate in parallel.

Figure 6.13 shows the filtered high-voltage-side currents on the top axes and then the digital element statuses. We can see the harmonic restraint element on the B-phase asserted.

To get a better understanding of why the harmonic-restrained elements operated, we plot the operate and restraint current for each of the phase elements against the threshold settings in 6.14. The dashed line represents the differential characteristic without the impact of added harmonic restraint and is plotted strictly for informational purposes. The solid line represents the differential slope characteristic, including the added harmonic restraint. We can see from 6.14 that IA (red) comes close to the threshold of operation but never crosses. We can see that IB (green)

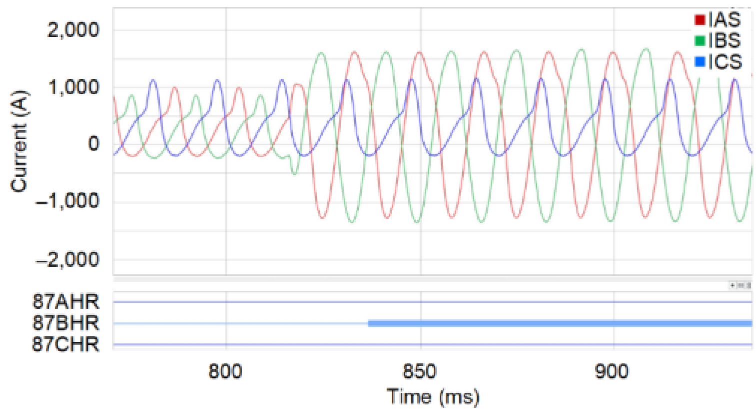

Figure 6.13. Phase Currents and Harmonic Restraint Differential Elements for Internal Phase-to-Phase Fault

crosses the threshold, and IB is the element in 6.13 that asserts. The unfaulted phase, IC, never comes close to the threshold of operation and never asserts.

For this particular phase-to-phase fault, simply enabling harmonic restraint is enough for the relay to trip. However, it is still instructive to see how the waveshape recognition impacts the relay operation.

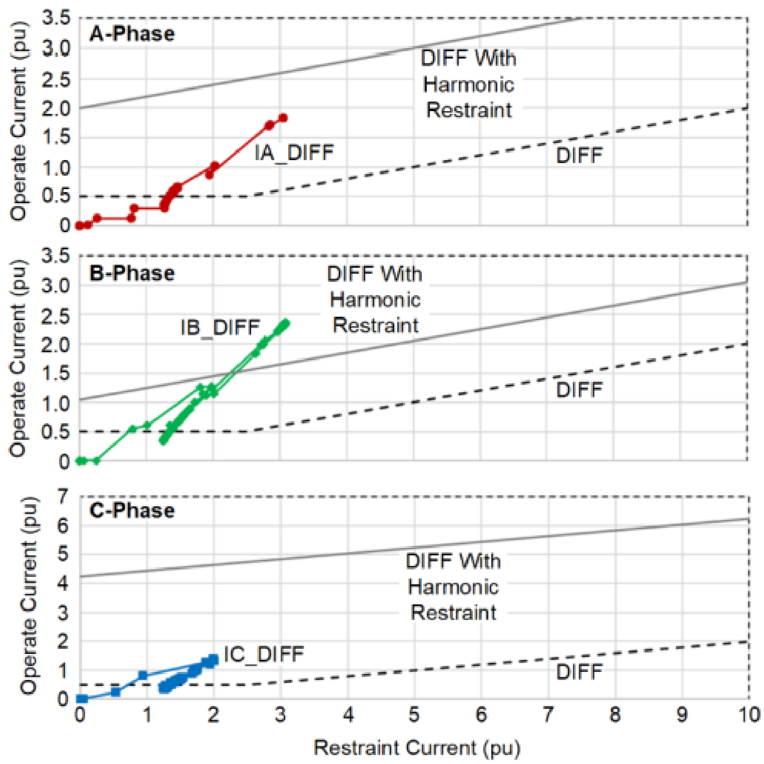

Figure 6.14. Operate Current Plotted Against Restraint Current for Internal Phase-to-Phase Fault for A-, B-, and C-Phases

Figure 6.15 shows, for the same event, the phase currents in the top axes, the differential currents in the middle axes, and the waveshape blocking and unblocking bits along with the tripping elements in the bottom axes.

In Figure 6.15, when the waveshape recognition unblocking element recognizes the bipolar overcurrent, all of the differential elements pick up.

A significant lesson learned in the analysis of this particular fault scenario is that by enabling several methods of inrush restraint and differential in parallel, multiple elements picked up, specifically the harmonic restraint and waveshape recognition elements.

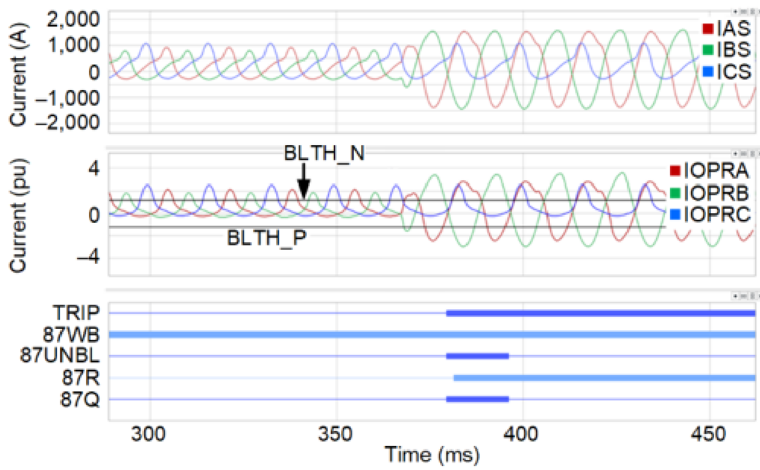

Figure 6.15. Phase Currents, Raw Differential Currents, and Digital Elements for Internal Phase-to-Phase Fault

Conclusion

Additional refinement and investigation into the model for the transformer and the model's applicability to various construction types for power transformers will help determine how well this dynamic modeling and the results can be generalized to all power transformers.

Both traditional and new methods of inrush restraint kept the relay secure during inrush conditions, including inrush due to half-cycle GIC-induced saturation.

Initial testing proved that applying only cross-harmonic blocking leads to dependability problems during high levels of GIC. Relay 1, which included harmonic blocking and harmonic restraint without the waveshape recognition logic, lost dependability and sensitivity as the levels of GIC increased and the fault current decreased due to fault resistance.

Relay 2, which included the traditional methods and enhanced waveshape recognition logic, did not see a significant change in dependability or sensitivity as the level of GIC current changed. The relay elements' sensitivity to fault resistance was impacted by GIC levels, though it was less impacted than Relay 1.

While the focus of this paper is solely on the phase differential element, other protective elements are available in modern microprocessor-based relays and could potentially trip for a fault where traditional blocking schemes fail to operate. In addition to more elements in microprocessor-based relays, additional relays, such as the sudden pressure or Buchholz relay, add dependability.

Additional testing and simulation are needed to evaluate the impact of GIC on other elements, such as REF.

The impact of GIC on a transformer differential relay based on the modeling and testing outlined shows only a small impact to the sensitivity and dependability of differential schemes, specifically only those schemes using traditional methods of inrush restraint, such as harmonic blocking and harmonic restraint.

CHAPTER SEVEN

Response of COTS-IT Equipment to Harmonic Voltages

A nuclear weapon explosion in the upper atmosphere would cause a disturbance in the Earth's geoelectric field such that direct current (DC) is induced into the alternating current (AC) power grid. DC currents in an AC network will alter the magnetic response of power system transformers such that significant harmonic distortion appears on the power system.

This chapter describes the testing of the impact of varying levels of harmonics on common electronic loads that may be found in an office or business environment. The Defense Threat Reduction Agency (DTRA) has provided a variety of Common Off-The Shelf Information Technology (COTS-IT) type equipment for testing with harmonic-rich voltage waveforms. The test waveforms are based on data acquired from the Phase IV-B DTRA/INL tests in 2012. These tests involved injecting stepped levels of DC current into an AC power system network and recording the response of power system equipment.

Voltage waveforms sampled during these tests were adjusted to single phase wall-outlet levels (nominally 120 VAC at 60 Hz for the United States, 230 VAC at 50 Hz internationally) for common electronic testing. A programmable voltage source with arbitrary waveform capability was used to act as the voltage source for the electronics under test.

The significant finding for testing to date is that no upsets of equipment have been observed under MHD-E3 test conditions. The majority of the equipment uses modern switched-mode power supplies with most having wide input ratings of 120-240 Volts AC at 50/60 Hz.

Testing Evaluation Process

The goal of the COTS-IT testing was to evaluate the impact of harmonic-rich voltage waveforms on electronic equipment. During testing, these impacts were evaluated on a scale from 0 to 3 and are described in Table 7.1 and recorded after each test.

Table 7.1. Test Result Impact Levels

Effect Level	Description
0	No effect observed
1	Device self-recovered (i.e., rebooted and recovered, etc.)
2	Operator intervention required (i.e., power off / power on recovery)
3	Device damaged and component or entire device is unrecoverable

The MHD-E3 period of an atmospheric nuclear blast may vary in length, but the standard for these tests is that it is 100 seconds in duration. Equipment functionality is checked before, during, and after this period of voltage variation. Computer network activity, screen functionality, keyboard and mouse response, radio and phone buttons or other forms of input response were examined before and after each test. For battery-operated devices such as cellular phones and handheld radios, charging indicators are also checked.

For the individual equipment tests, thermal assessment for each device was performed before and after each test and the temperature was recorded.

Source and Selection of Waveforms

Three sets of waveforms were created for equipment tests. These sets are listed in Table 7.2.

The Idaho National Laboratories data was recorded by the SANView data acquisition system from Scientific Applications Research Associates (SARA) with a

Table 7.2. COTS-IT Test Waveform Details

Waveform Designation	Description
AB through AG	• Derived from INL BHE resistive tests for 4, 8, 16, 31, 46, and 61 batteries • Waveform from Westinghouse transformer secondary (2400V) stepped to 120V. Small change in Fourier series higher harmonics calculation resulted in slight variation from original waveform. • Individual device testing complete before B-waveforms ready
BA through BG	• Derived from INL BHE resistive tests for 2, 4, 8, 16, 31, 46, and 61 batteries • Waveform from Westinghouse transformer secondary (2400V) stepped to 120V • Fourier series matches original waveform
CA, CD through CG	• Derived from INL BHE resistive tests for 2, 16, 31, 46, and 61 batteries • Waveform from pre-filter Dirtyfeed signal at 480V, stepped to 120V • Fourier series matches original waveform

sampling rate of 100 kHz. The A- and B- series tests were derived from the 3.75 MVA Westinghouse 132kV / 2.4kV wye-delta transformer, with measurements performed using a resistor bridge based on line-to-neutral on the secondary side of the transformer. The C- series tests were sampled from the secondary voltage of a 2400 / 480V transformer in the DTRA Load Trailer, again as line-to-neutral measurements. In the waveform descriptions, 'Dirtyfeed' refers to a 480V service that is before an electrical surge filtering device; 'Cleanfeed' refers to the same 480V service after the surge filtering device.

Creation of Test Waveforms

A Fourier series was calculated from DC to the 15th harmonic for each waveform and scaled for nominal 120 volt RMS level. For example, the 2400V Westinghouse secondary is a line to line voltage; this equals 1386 volts RMS line-to-neutral. The ratio of 1386/120 equals 11.55. This divisor of 11.55 was applied to the Fourier series components.

The scaled Fourier series components were used to calculate a 1024 samples-per-cycle harmonic waveform. This resulting waveform was then scaled for programming into the voltage test equipment.

Test Equipment

Device testing was performed using a California Instruments CSW-5550 programmable AC power source. This unit is capable of accepting a set of sampled values (1024 samples-per-cycle) for reproducing arbitrary harmonic waveforms. A laptop running California Instruments CSW software was connected via USB to the programmable source and used to load arbitrary voltage waveforms into the source. The unit was powered by a three-phase, 208 V_{LL} (120 V_{LN}) wall outlet. The programmable source is capable of generating three phase signals, though only single-phase mode was used for this set of tests. A macro scripting feature for changing test waveform, duration, and voltage magnitude is used with the programmable source for consistency of testing. An oscilloscope is used to monitor and verify the voltage output waveform of the programmable source.

Voltage and current data are collected with a National Instruments CompactDAQ 9133 running LabView. This CompactDAQ includes a NI-9220 +/- 10V input module and a NI-9244 400 V_{RMS} AC voltage input module. Hall effect current sensors are used to measure eight individual current channels, with the Hall sensor output using a 2.5V midpoint within a 0-5V range with +/- 15A input rating. The sampling rate is set to 25 kHz in order to achieve the most accurate representation possible of the current and voltage waveforms.

Temperature measurement was facilitated by a FLIR E5 thermal imaging camera with a 120x90 IR resolution and 4°F to 482°F range. The thermal imaging camera quickly locates and measures the temperature of hot spots on any device during testing.

A diagram of the test configuration is shown in Figure 7.1. The SEL relay shown in the diagram was used as a meter for fundamental and RMS voltage and current measurements during testing. When testing the harmonic waveforms, the fundamental values are not the same as the RMS values. A picture of the test system without the SEL relay is shown in Figure 7.2.

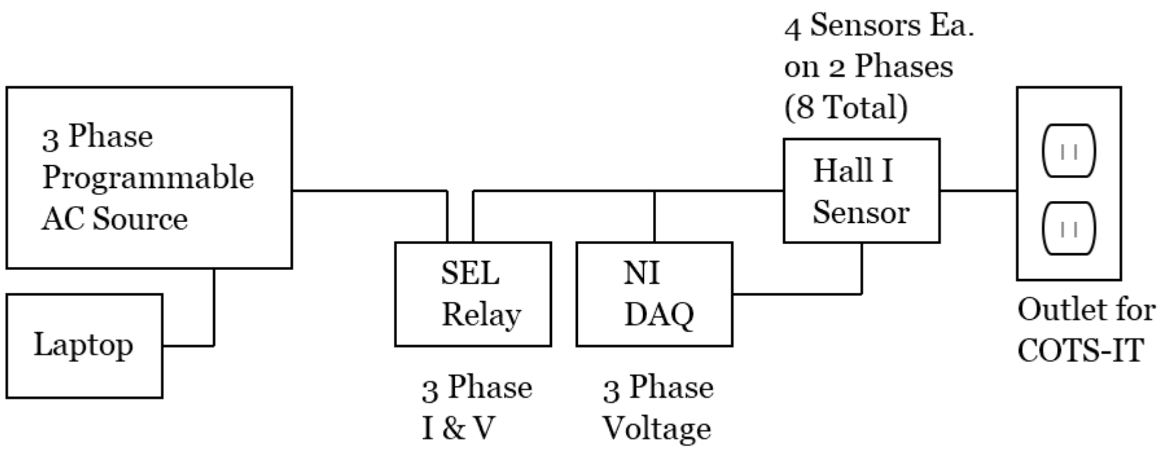

Figure 7.1. Diagram of COTS-IT Test Setup

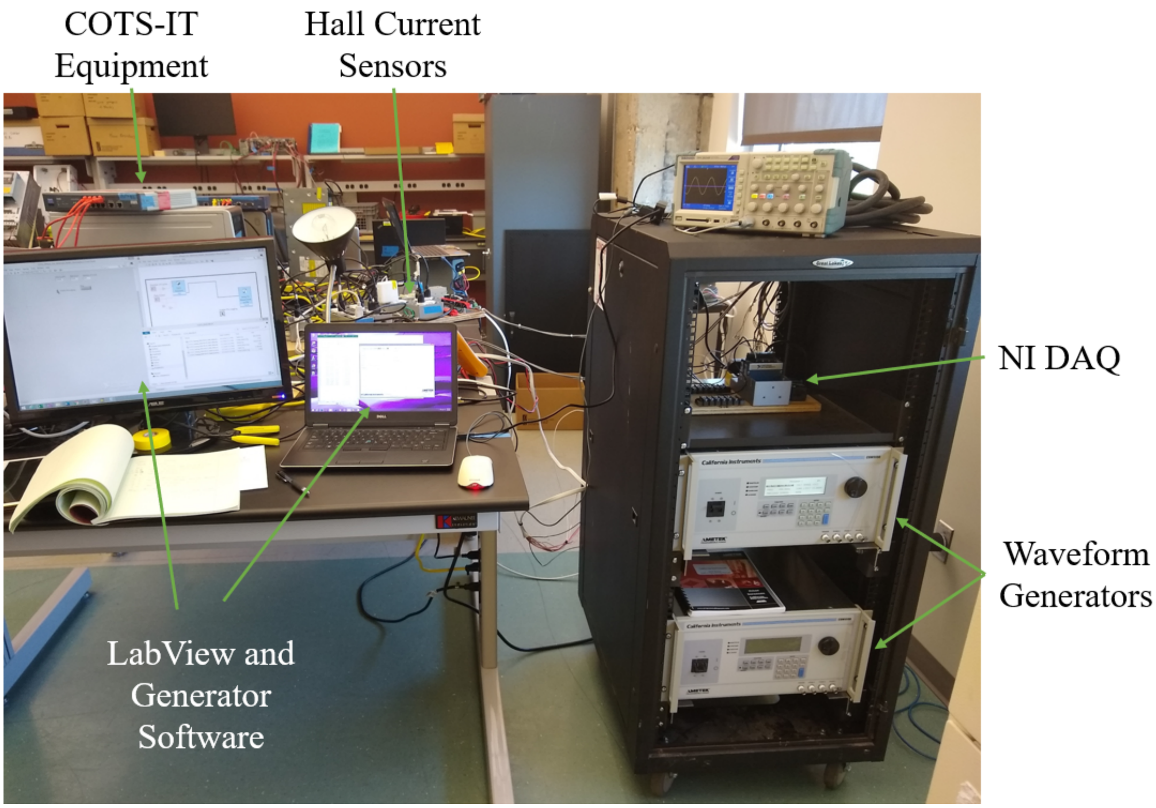

Figure 7.2. COTS-IT Test Setup

Test Requirements and Procedure

Pre-Test

(1) Power the equipment for at least 2 hours pre-test so that the equipment's power supplies reach steady-state working temperature. Apply power to the Hall current sensors so that they may also reach steady-state temperature (for calibration purposes). If possible, turn off all test equipment and create a zero-current Hall calibration file to find the actual 'center' voltage (2.5 VDC +/- 20mV is typical).

(2) Create arbitrary waveform files (.ABW) for all tests in advance. Pre-load these waveform files into the CSW-5550 programmable AC power source. Assign each waveform with a unique test name in the source.

(3) Create macro script files for each test. These will include 5 seconds of 120VAC clean sinusoidal waveform, then 100 seconds of the arbitrary waveform at the appropriate RMS voltage, and then a setting back to 120VAC. Each macro uses the unique test name of the waveform.

(4) Create Shot Sheets and if applicable, temperature record sheets. Place sheets next to equipment.

(5) Ensure CompactDAQ is ready for data acquisition and CSW Software is communicating with the programmable source. Open the macro function and prepare to run the test macro on the CSW software.

Test

(1) Check functionality of each piece of equipment and record its status on the shot-sheet. Check Ethernet network connectivity (PingTree), check input/output response (keyboard, buttons, touch-screen, etc)., check charging or power light. Mark Shot Sheet as appropriate.

(2) If necessary, record peak temperature observed through thermal imaging camera for each device.

(3) Start the CompactDAQ recording.

(4) Start the CSW software macro. Watch the oscilloscope screen to see that the voltage waveform changes after 5 seconds.

(5) For the next 100 seconds, monitor the equipment for any upsets, lost ping packets, or changes.

(6) Immediately after the end of the test, stop the CompactDAQ recording.

(7) Record temperatures using the thermal imaging camera.

(8) Evaluate functionality of each device – network, I/O, screens, lights, charging, etc.

(9) Change the name of the file on the CompactDAQ to reflect the name of the test that was run.

(10) Open the next test macro in the CSW software and prepare to go back to Test Step 1.

The COTS-IT tests were programmed into the voltage source as scripted, timed steps through a series of increasing distortion within the voltage waveform. The intent was to simulate the change in levels of distortion during the MHD-E3 event. In the example tests shown in Figure 7.3, the lower distortion tests of steps one through five were programmed to persist for five to ten seconds for each step, culminating with a 100 second test at step six. These waveforms represent tests AB through AG that were mentioned in Table 7.2.

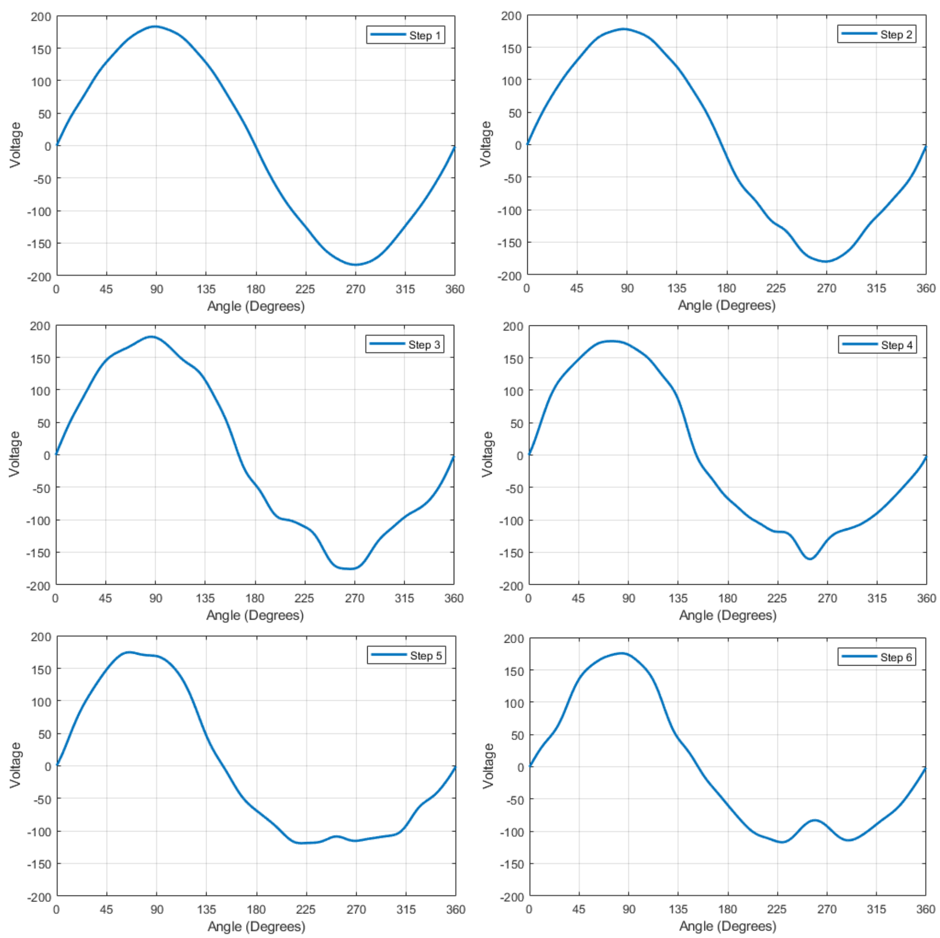

Figure 7.3. Test Voltage Waveforms for MHD-E3 Stepped Testing

Results and Observations

A ‘device upset’ would be assessed as an Effect Level 1 through 3. For these 120V tests, no device upsets were observed during the waveform testing. Since there were no upsets (all recordings are at Level 0), an effect matrix will not be presented.

Since the applied voltage directly impacts the device power supply, thermal imaging comparisons of the device power supplies (or ‘warmest location’ on the device) were performed before and after each test. No significant temperature change was observed during the waveform testing. A drift of a couple of degrees F may have been observed across the 100 second timeframe on occasion, but this does not necessarily indicate that the power supply was under stress by the voltage waveform. Devices equipped with fan-forced cooling were very consistent in temperature.

The majority (90%+) of devices in the test pool were equipped with switched-mode power supplies (SMPS). A characteristic of these supplies is that they will draw the current required to maintain correct output voltage and power levels through a wide range of input voltages. These supplies are designed with a feedback system that increases the current magnitude and/or duration of input current in order to maintain voltage and power output on the secondary side of the power supply. What has been observed with the SMPS design is that as the input voltage becomes asymmetrical - with one peak of lower magnitude than the opposite peak - the SMPS will only draw current only once per cycle, with the current level being just under twice the ‘normal operation’ current so that is drawing the same amount of power.

An example of ‘normal’ input voltage and input current for an SMPS device is shown in Figure 7.4.

Notice in Figure 7.4 that the current draw occurs as the voltage approaches a positive or negative peak. The current impulses are nearly symmetrical, with a peak of 0.8 amps.

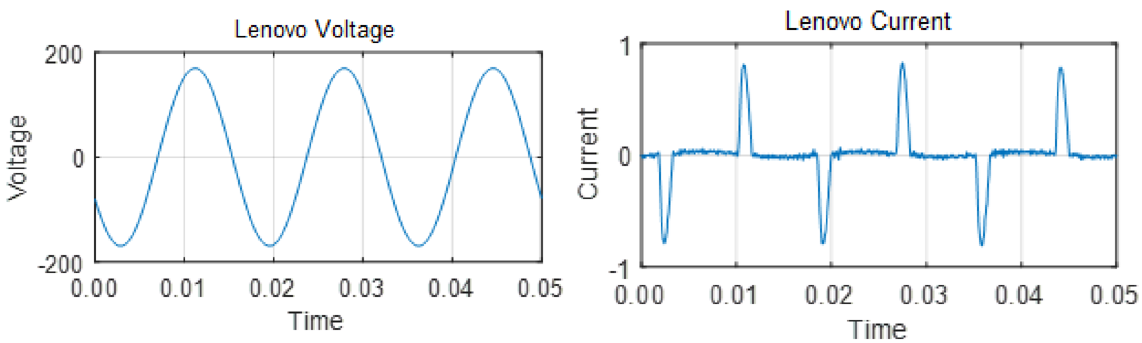

Figure 7.4. Normal Operation Voltage and Current Waveforms, Lenovo 15” Monitor

With an asymmetrical voltage waveform as shown in Figure 7.5, the positive peak is of significantly greater magnitude than the negative peak, and that the power supply draws current only once per cycle – on the higher amplitude voltage portion of the waveform. Note that the current draw of 1.31 amps has a similar “area under the curve” as the previous current; the power draw by the device does not change. For this Lenovo monitor, power draw during the ‘normal’ 120 V sinusoidal signal was calculated at 14.4 watts; during the distorted voltage waveform, power draw was calculated at 14.6 watts.

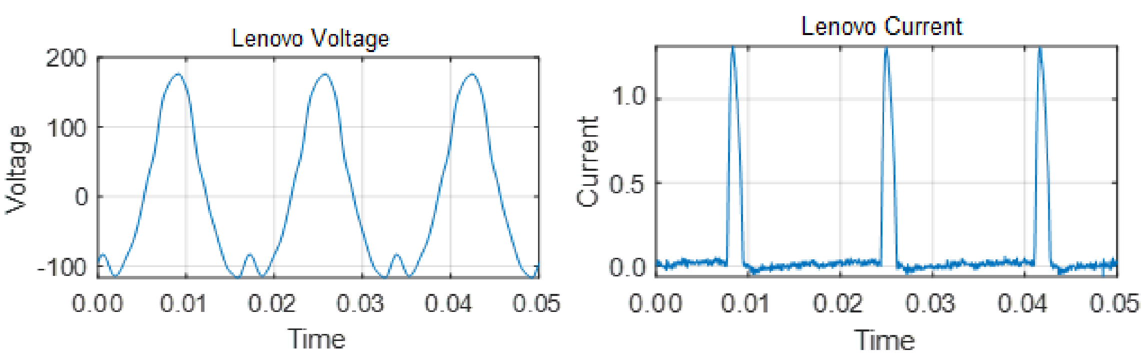

Figure 7.5. Harmonic Voltage and Current Waveforms, Lenovo 15” Monitor

iMac and MacBook Testing

Additional analysis was performed on the MacBook laptop and the iMac desktop computer. The MacBook power supply performed like most other switched-mode power supplies with its current draw. The iMac desktop draws current for a longer duration during the cycle and thus has a different waveform characteristic - a more sinusoidal waveform than most switched mode supplies. Examples of this with clean input 120V and 240V voltage waveforms are shown in Figure 7.6.

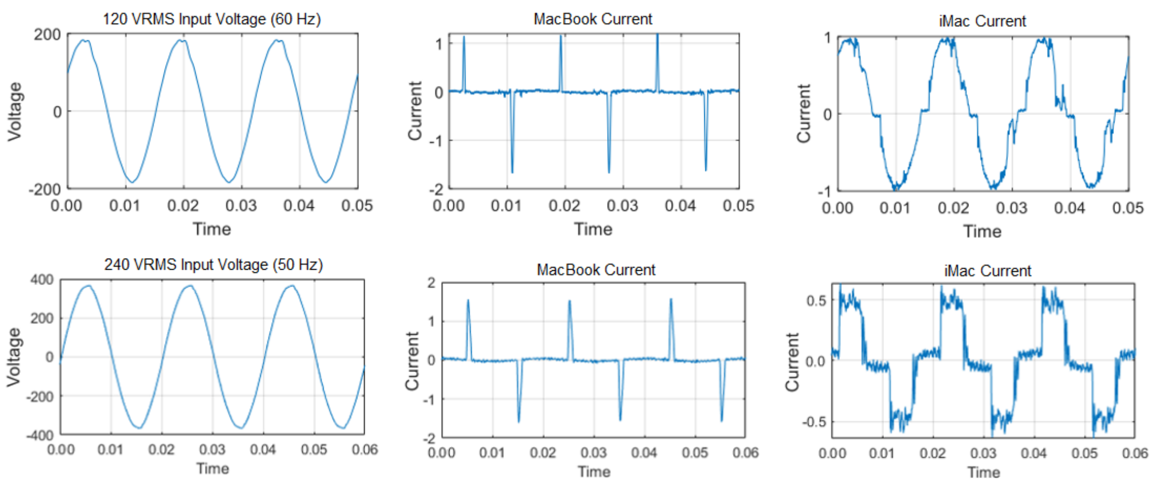

Figure 7.6. Normal Operation at 120V/60Hz and 240V/50Hz, iMac and MacBook Voltage and Current

The upper graphs in Figure 7.6 are 120V/60Hz, while the lower graphs are 240V/50Hz. The left column is the voltage waveform, the middle column is the MacBook power supply current draw, and the right column is the iMac desktop current draw.

During maximum voltage harmonics (S024 WEST test) shown in Figure 7.7, the asymmetry of the voltage waveform is mirrored by the current draw of the devices. For the MacBook, the current draw is unipolar and corresponds to the peak magnitude of the voltage waveform. For the iMac, the current draw resembles the voltage waveform, but the higher voltage (lower set of graphs) has significantly more distortion.

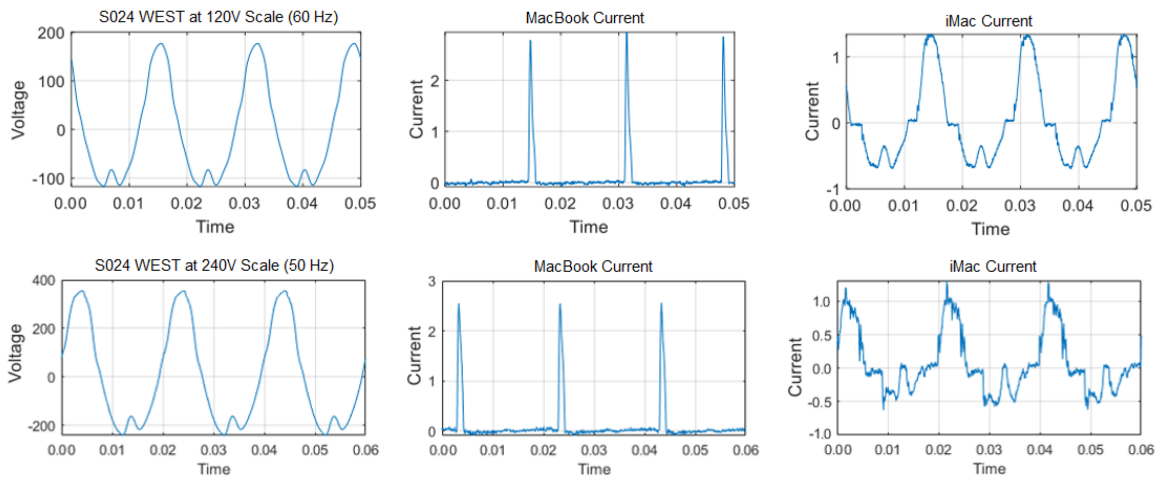

Figure 7.7. Voltage Distortion at 120V/60Hz and 240V/50Hz, iMac and MacBook Voltage and Current

250V/50Hz Monitor Testing

Modern electronic equipment with switched-mode power supplies is typically rated for 100-240V at 50/60 Hz. It is possible that the E3 phenomenon may cause a slight increase in voltage, so a series of stepped tests were developed to test a device at the 250V/50Hz RMS level. A Hewlett Packard 22 inch monitor was selected as the test device and was connected to a computer for display during the test.

The theory was that the overvoltage combined with the unipolar current draw could be damaging. No damage occurred during testing. No observable performance degradation was observed. For this test, the pre-test waveform is shown in Figure 7.8, while the S024 WEST-based test waveform is shown in 7.9.

There is still a possibility of damage from overvoltage, but the peak testing voltage would need to be higher.

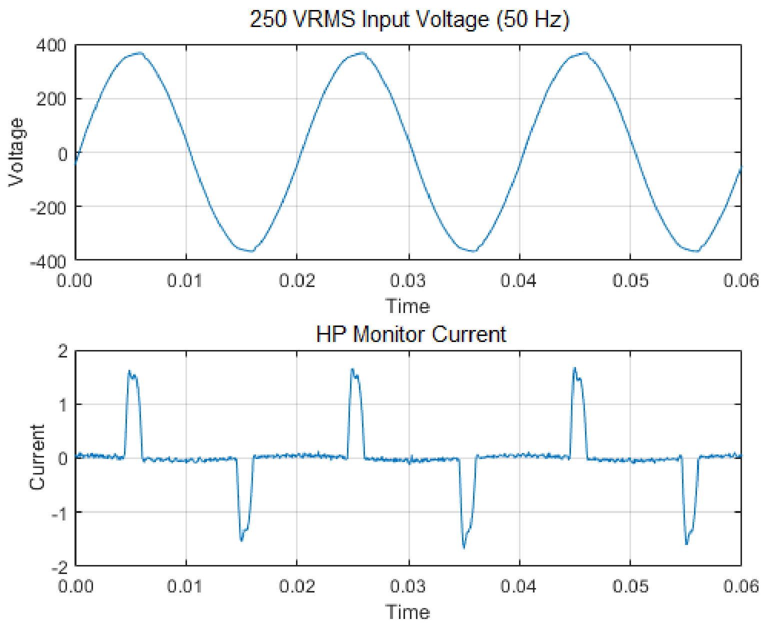

Figure 7.8. Normal Operation at 250V/50Hz, HP Monitor

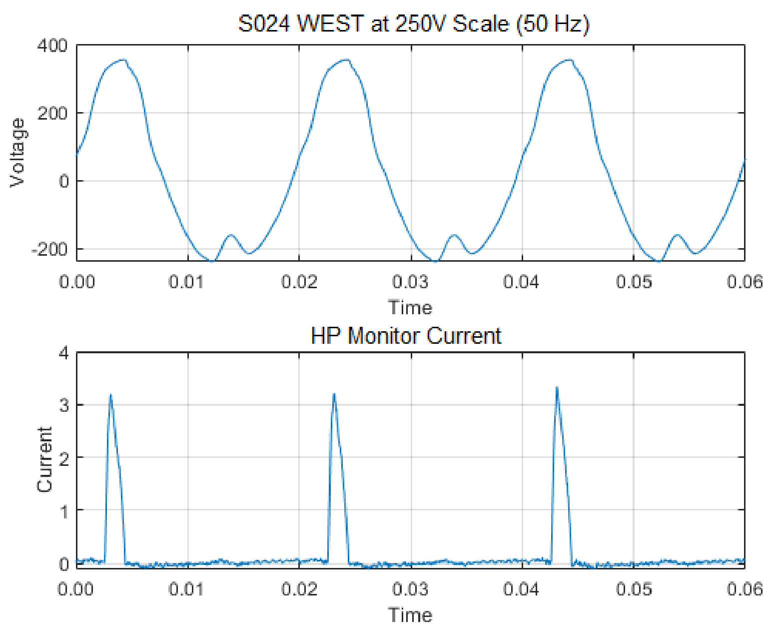

Figure 7.9. Harmonic Voltage Operation at 250V/50Hz, HP Monitor

Discussion of Primary COTS-IT Testing

For a power supply that is operating within its design specifications, it is not anticipated that this 'near-doubling' of input current on one side of the input rectifier is a problem. There exists the possibility that a power supply operating near its output limit under normal voltage conditions could fail when exposed to the asymmetric waveform, but this has not yet been tested.

By collecting the voltage and current data for each device during each test, the data was available for an average power calculation. The results of the average power calculation show that for all of the SMPS-based devices, power draw was consistent – within a few watts. The incandescent lamp's power requirements dropped significantly, but this was due to the reduced RMS voltage of the harmonic waveform. The other devices that showed a significant reduction in power were the transformer-rectifier-capacitor based power supplies of the handheld radios. The reduced voltage on the negative polarity side of the input waveform caused the charger to stop working. The radio itself was unaffected, only the output of the charger was impacted. Regarding the power consumption and COTS-IT electronics, no significant changes in power consumption were observed during testing.

The final stage of testing was a set of voltage reduction tests. The S024 2400V and Dirtyfeed waveforms were used for these tests. The first piece of equipment (HP Desktop Computer) failed at 71% of the harmonic waveform nominal voltage for both tests (72 volts RMS). This is well below the power grid's operational range. Based on this testing, it is plausible to consider that the majority of COTS-IT equipment will ride-through a 20% undervoltage event.

At the upper end of the voltage range, no problems were experienced. Device design should be capable of riding through a 5%-10% overvoltage. In power system distribution grid simulations, this level of overvoltage may be experienced by loads towards the ends of distribution feeders. It is anticipated that the components impacted by overvoltage would be the metal oxide varistors (MOV's) and the main power capacitors.

Preliminary Power Supply Testing

Prior to the formal COTS-IT testing, a small sample of surplus power supplies were tested using the waveforms and procedure outlines in Savage, Radasky, and Madrid [11] and then using some of the waveforms sampled during the INL testing. The testing by Savage et.al. [11] applied a percentage of specific harmonic (i.e., 30% second harmonic at 90 degree phase shift) to a fundamental waveform and then tested the device until either failure or thermal equilibrium was reached. The duration of this testing could reach beyond an hour in length. An observation that was not performed during this testing was monitoring the output voltage and current from the power supply using a high-speed acquisition device. This detail was listed as part of possible "future work" in Savage et.al. [11] and was accomplished during the Baylor preliminary tests.

While the formal testing was of relatively short duration (100 seconds because of the anticipated duration of an MHD-E3 event), the intent of the preliminary testing was to observe thermal rise and possible failure of the equipment during longer tests. The equipment tested was selected from a surplus electronics bin and consisted of switched-mode power supplies and small "wall warts" that used a transformer, rectifier, and capacitor circuit to create a DC output. These devices are listed in Table 7.3.

Thermal monitoring during testing was performed by attaching a K-style thermocouple to the case of the device under test, with the exception of the Unknown Brand power supply. For this power supply, the plastic shell was removed and the thermocouple was attached directly to the core of the transformer. During early 5-minute duration testing, all power supplies were allowed to run for 30 minutes to come "up to temperature" using regular line 120 VAC as input. Temperature was recorded

Table 7.3. Devices Tested During Preliminary Investigations

Device	Technology	V Output	I Output (Max)
Dell 65W Laptop Power Supply	SMPS	19.5	3.33A
HP 120W Laptop Power Supply	SMPS	18.5	6.5A
OMRON 5V DIN Rail Power Supply	SMPS	5	3A
Uniden Phone base Power Supply	Rectifier	9	210mA
Unknown Brand “Wall Wart”	Rectifier	12	500mA

with the thermocouple and CompactDAQ during these early tests. After these tests, it was observed that temperature was not a problem with any device under test, so some tests were performed without temperature measurement for the sake of time.

Testing Comparisons with Savage et.al.

The testing in [11] used 115 volts RMS for all waveforms. Five waveforms were used:

(1) Pure sine wave
(2) Waveform A: Third harmonic with 0 degrees phase shift
(3) Waveform B: Second harmonic with 0 degrees phase shift
(4) Waveform C: Third harmonic with 180 degrees phase shift
(5) Waveform D: Second harmonic with 90 degrees phase shift

A recreation of these waveforms with 50% harmonic distortion is shown in Figure 7.10.

Of these five voltage waveforms, only one resulted in equipment failure during their testing: Waveform D, which features a second harmonic with a phase shift of 90 degrees. It should be noted that the peak magnitude of Waveform D for the 50% harmonic test is 218.4 volts, which is a 29% overvoltage when compared to the standard 120 volt RMS peak of 169.7 volts. The destructive testing result in [11] was confirmed during Baylor testing using the programmable AC source. The waveform

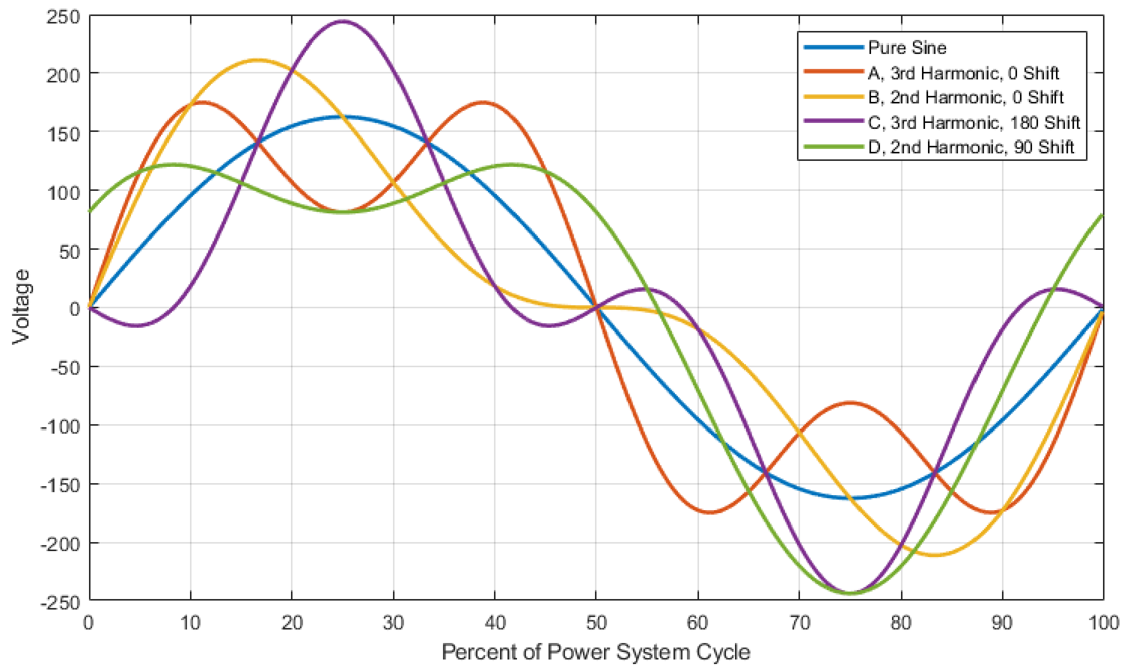

Figure 7.10. Waveforms from [11] at 50% Distortion, 115V RMS

caused transformer heating which eventually led to an open circuit failure on the primary winding of the transformer. Savage et.al. noted that the majority of the transformer failures in their tests occurred as the temperature approached 80°C.

Testing at Idaho National Labs has demonstrated that the shape of Waveform D is possible during an MHD-E3 event. The INL S024 WEST waveform closely resembles the characteristics of Waveform D. The inverted INL waveform is shown compared to Waveform D in Figure 7.11. Testing in the laboratory has demonstrated that the polarity of the transformer response depends on the polarity of the DC voltage and current entering the transformer. During an MHD-E3 or solar geomagnetic disturbance it is possible for a transformer to have this response depending upon the direction of the electric field.

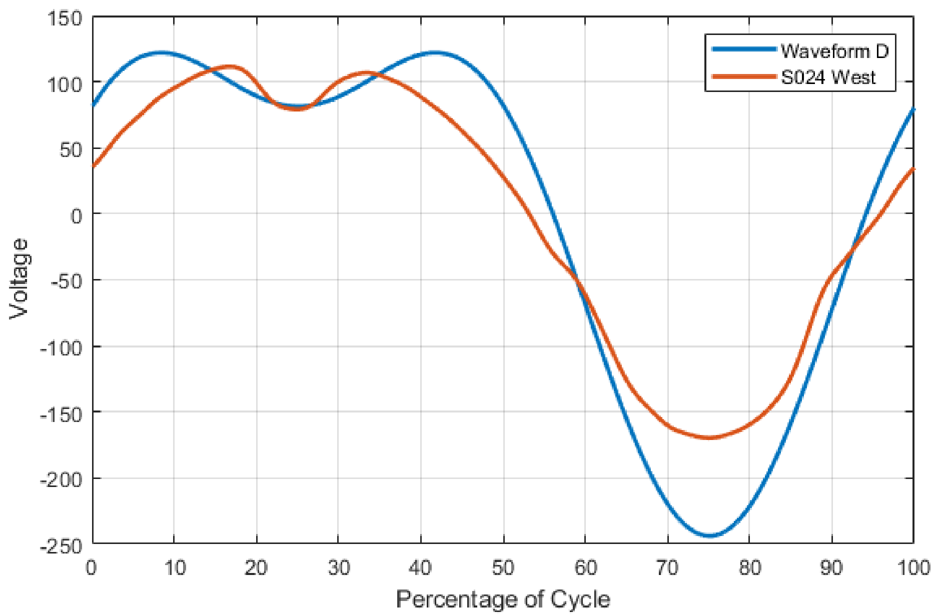

Figure 7.11. Waveform D Compared to S024 West INL Waveform

A long-duration 115 volt RMS rectifier wall wart test using the 30% distortion Waveform D, followed by an INL S024 WEST waveform insertion, was performed in the Baylor laboratory. This test more closely resembled a solar GIC event and had a duration far longer than the MHD-E3 event. The temperature of the wall wart rose quickly once the INL waveform was applied, and the wall wart failed after about 40 minutes. In Figure 7.12, the testing from 17:50 to 19:00 was based on Waveform D, while the testing from 19:00 to 19:53 was with the INL waveform. The transformer in the power supply failed at 19:53. The temperature shown pre-failure was based on the thermocouple attached to the plastic shell. The elevated temperature near 70°C was after the transformer had failed, the plastic shell was opened, and the thermocouple placed directly on the transformer core. There were some adjustments made during the tests leading to the output voltage drop-outs. The noise in the output voltage is an artifact of the sampling; 3 cycles of samples at 25kHz were taken every 30 seconds. Noise in the temperature log was determined to be a grounding issue at the thermocouple transducer.

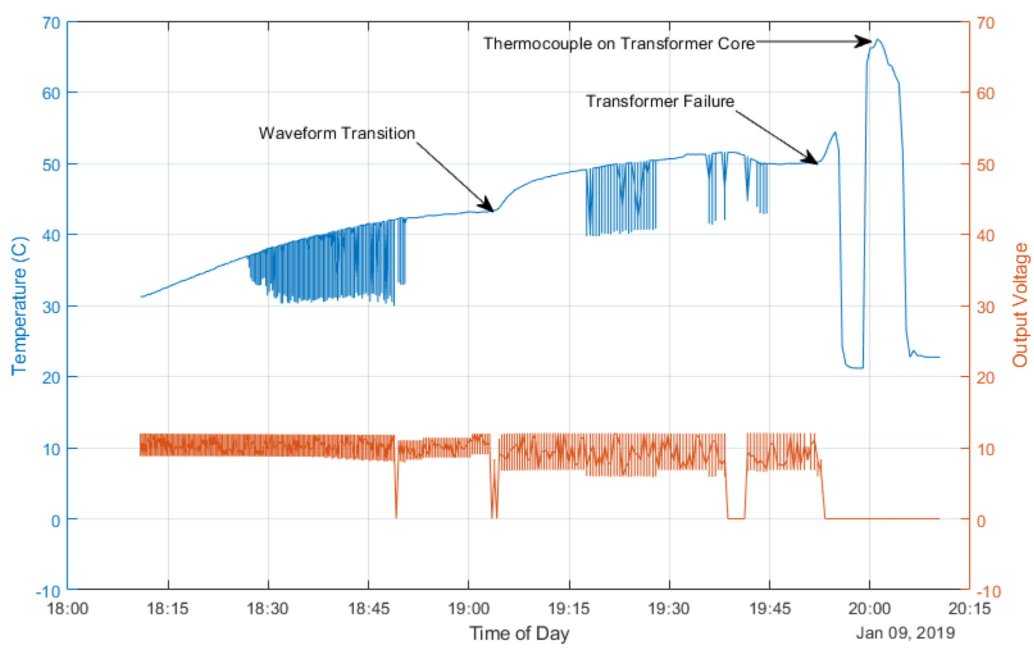

Figure 7.12. Thermal Response of Wall Wart to Waveform D and INL S024 WEST

Observations and Discussion

During the “clean sine wave” pre-injection period, all power supplies performed as expected. The switched-mode power supplies held much tighter voltage and current regulation than the rectifier-based power supplies. This may be due to the age of the capacitor in the rectifier-based supply, but generally, the DC output of this design is not as clean as a switched-mode supply. Rectifier supplies consist of a simple transformer, diode bridge, and capacitor circuit with no active regulation. One typically expects poor voltage regulation with the simple rectifier supplies. For the rectifier-type supplies, charging of the capacitor for the DC source typically occurs during both the positive and negative half-cycles. Examples of a rectifier-based power supply input and output voltages and currents are shown in Figure 7.13. Note that the voltages are scaled for the purpose of waveform comparison.

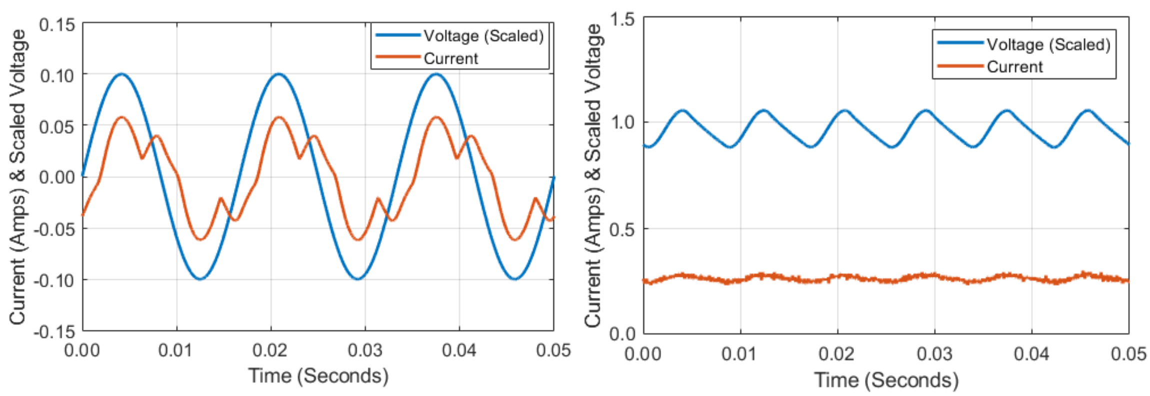

(a) Input Voltage & Current Waveforms (b) Output Voltage & Current Waveforms

Figure 7.13. Clean Sine Wave Input and Output for Rectifier-based Power Supply

When subjected to distorted voltage waveforms such as the S024 WEST, the reduced half-cycle voltage proves insufficient for continued charging of the capacitor. This results in a low voltage output. There is a possibility that equipment powered by this technology may become inoperative when exposed to an asymmetrically reduced peak waveform. If the purpose of the supply is to charge a battery, it may cease charging. Fortunately, on newer equipment this style of power supply has been replaced by smaller, more efficient switched mode power supplies, though the threat exists with older equipment. The response of a rectifier based power supply to S024 WEST is shown in Figure 7.14.

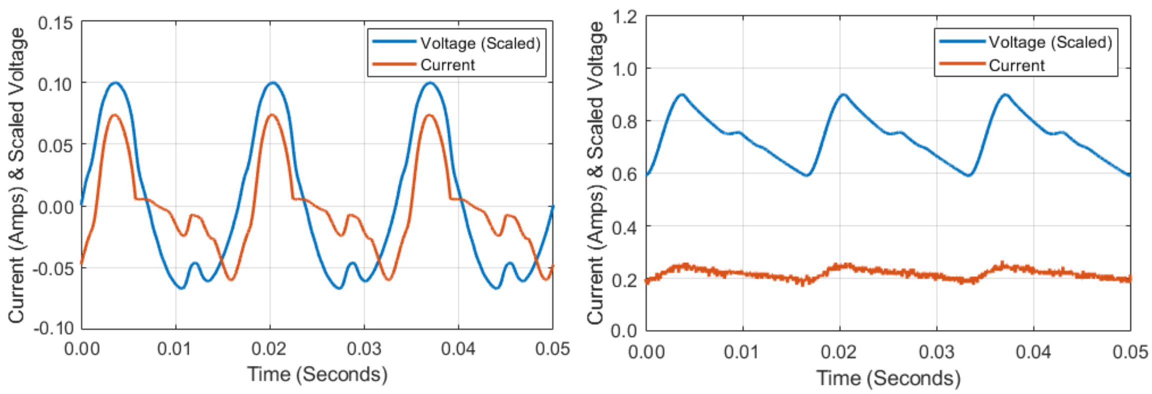

(a) Input Voltage & Current Waveforms

(b) Output Voltage & Current Waveforms

Figure 7.14. Response to S024 WEST Input and Output for Rectifier-based Power Supply

When examining the output of the power supply, the 'normal' 9 volt average DC output with +/- 1V DC ripple exhibits a 7.5 volt average with a +/- 1.5V DC ripple when subjected to the asymmetrically reduced peak waveform. At slightly higher RMS magnitudes than these tests, this waveform is also capable of thermally damaging the transformer in this power supply.

Lessons Learned from COTS-IT Testing

During the formal test period of a 100 second duration, 19 harmonic waveforms were tested against COTS-IT equipment. The results of these tests include:

- No device upsets occurred during testing. All equipment remained intact: networked equipment communications continued to function, computers continued to respond to user input while playing a video and communicating over the network, and chargers continued to charge battery-operated devices, though the possibility exists for rectifier-based battery chargers to cease charging during the distorted voltage waveform interval.
- No significant thermal change was observed during testing. While thermal rise is evident during long duration tests, the MHD-E3 period is of insufficient length to cause noticeable temperature rise in rectifier-based power supplies.
- Switched-mode power supply current draw will move to once per cycle instead of twice per cycle, essentially doubling the current on one half of the input rectifier circuit. In general, this should not be considered a problem, but there may be some poorly designed devices that could fail because of the excessive current.
- No significant change in the magnitude of power draw was observed. Power calculations were performed for all tests, and the before and after values were virtually identical for switched mode power supply-based electronics, but power requirements were reduced for resistive devices (light bulb) because the RMS voltage decreased during the test.
- COTS-IT equipment that utilize a switched mode power supply can ride through a 20% undervoltage during harmonic distortion event without upset.

During the early testing, extended duration testing of a set of five waveforms proved that rectifier based power supplies can fail with slight overvoltage concurrent with a high second harmonic characteristic.

It is the author's opinion that if failure of a switched-mode power supply is to occur, it would be at the higher international (230-240V) voltage levels rather than at lower (120 V) voltage levels that are common in the United States. Most of the small electronic load power supplies available today operate over a wide range of input voltage and are frequency-tolerant. Tests have shown that even at double the normal US 120V wall outlet level, this type of power supply continues to operate normally. In 230V-240V regions, a significant increase in voltage could be beyond the rating of the design of the power supply.

CHAPTER EIGHT

Conclusion

This research set out to explore power grid related impacts as a response to MHD-E3, which may also apply to phenomenon associated with strong solar geomagnetically induced currents. These phenomena cause quasi-direct currents to flow in the power grid, and these currents will result in voltage and current distortion that have characteristics that are atypical of normal power system operation. The areas explored include the response of transformers to induced quasi-direct currents, the impact of harmonic currents on the response of power system protective relays, and the impact of voltage harmonics on information technology equipment

A benchtop transformer testing system was designed and constructed to compare the DC response of smaller, commonly available single phase, three phase three limb wye-wye, and three phase three limb autotransformers with test results from experiments performed by the Defense Threat Reduction Agency at Idaho National Laboratories on large grid-scale 138kV transformers. Transformer analysis techniques under DC influence included current waveform harmonic spectrum comparisons, a definition and calculation of the transformer loss hysteresis loop and its enclosed area, and per unit comparisons of real and reactive power absorption.

The results of the comparison between benchtop transformer testing and the testing by the Defense Threat Reduction Agency at Idaho National Laboratories proved to be mixed. An increase in primary winding second harmonics, an increase in watt and VAR absorption, and a strong third harmonic instantaneous power oscillation are all common characteristics between the benchtop and the grid scale transformers. The high levels of transformer secondary winding voltage and current harmonic distortion observed during the INL testing was not replicated on the benchtop testbed. The transformer secondary voltage distortion observed on the benchtop testbed was only evident at the highest levels of DC injection and did not approach the distortion characteristics of the INL testing. The high accuracy of the laboratory test bench data acquisition system assisted in offering valuable visualization insight into the magnitude of power absorption of transformers during both low and high levels of magnetic saturation through the transformer loss hysteresis loop analysis technique. Low levels of saturation produced a small tail on the saturation loop, while high levels of saturation produced a much larger secondary loop.

The benchtop test data provided a set of distorted current waveforms that were used for protective relay testing. Distorted current waveform data from the 1989 geomagnetic disturbance and from the DTRA INL testing were also used. These waveforms were converted to COMTRADE (Common Format for Transient Data Exchange) files and applied to protective relays via a secondary current injection relay test set. Three types of relays were tested: electromechanical, solid state, and microprocessor. These protective relays are traditionally installed and tested such that they operate at a specific time interval using a clean sinusoidal waveform of fixed frequency. The electromechanical overcurrent relays that were tested operate on the RMS characteristics of the current, so distorted current waveforms that were created using the three test waveforms provided unpredictable operation because of the harmonics present within the RMS current. Solid state and microprocessor-based relays commonly utilize filtering techniques so that they operate more predictably on the fundamental frequency, but in the extreme harmonic case some filtering relays may allow damaging levels of harmonics to exist on the system. Electromechanical transformer differential relays that have built-in second harmonic blocking or restraint may delay operating on an internal fault because of the strong second harmonic characteristic of a transformer that is being influenced by DC.

The benchtop testbed also served as a template for a software model that was created in the transients program ATP/EMTP. Because of the transformer's importance in the power grid and its susceptibility to DC, a matrix of relay tests were created using the ATP model to evaluate a pair of modern microprocessor based transformer differential relays. The goal of this testing was to evaluate the reliability, dependability, and security of these relays to properly operate for an internal fault and not operate for an external fault while under the influence of DC based harmonics. It was found that, at a minimum, both harmonic blocking and harmonic restraint should be used together. Harmonic blocking alone significantly reduced the sensitivity of the relay to proper operation during internal faults, while the combination of blocking and restraint proved more sensitive, yet some faults were still undetected. The addition of a second harmonic waveshape recognition algorithm resulted in the greatest sensitivity to internal faults without compromising security against mis-operation during a time of high second harmonic currents being present.

While benchtop testing did not result in secondary voltage distortion of significant levels, the Idaho National Laboratories testing data contained voltage waveforms that could prove problematic to electronic loads. A programmable power source coupled with a high performance data acquisition system was used as the foundation for a common, off-the-shelf information technology (COTS-IT) harmonic voltage response testbed. Even though the duration of testing was much longer than the hypothetical MHD-E3 event, a slight overvoltage combined with strong second harmonic waveform from the highly distorted INL S024 test was capable of permanently damaging small transformer-rectifier-capacitor based power supplies. During the 100-second structured testing resembling the MHD-E3 period, no additional types of devices had any negative response to the waveforms, though many of the switched-mode power supplies exhibited current draw changing to a once-per-cycle draw instead of the normal every-half-cycle current draw. Apart from this change in current draw timing, modern switched-mode power supplies are capable of operating across a wide voltage and frequency range and did not experience any device upset reactions. Tests were performed in the 120V to 250V ranges and at 50 and 60 Hz. No device upsets were experienced.

Future Work

For the transformer test bench, alternate winding configurations should be tested. The tests at Idaho National Laboratories were performed on wye-delta transformers, so for a more accurate comparison, benchtop testing should be performed based on this winding and loading configuration. Existing transformers were tested as wye-delta, but the voltage range of the secondary winding was outside of a normal, usable range. Additional testing and modeling of the autotransformers should also be performed to determine any cases in which there may be secondary voltage or current distortion. Additional work to further the analysis of power absorption visualization via the hysteresis loop technique is ongoing, particularly for transformers equipped with a delta winding.

For protective relay testing, the next step is to use the Real Time Digital Simulator (RTDS) to create a more realistic grid test model using a three phase transformer instead of the three single phase transformers used in the ATP model. It is anticipated that RTDS Technologies has improved their transformer modeling in recent releases of software compared with ATP/EMTP, and that there are saturation characteristics available for simulation. The use of this software in conjunction with real-time use of protective relays would allow for a large number of tests to be run automatically and provide greater granularity of results.

For COTS-IT testing, more and larger power electronics based devices are slated for testing, including uninterruptible power supplies, a refrigerator, variable frequency drives, and three phase motors. Additional harmonic voltage waveforms based on distribution feeder simulations are also in progress.

BIBLIOGRAPHY

[1] A. K. Mattei and W. M. Grady, "Response of power system protective relays to solar and hemp mhd-e3 gic," in *2019 72nd Conference for Protective Relay Engineers (CPRE)*, 2019, pp. 1–7.

[2] A. Mattei, D. Haas, J. Candeleria, and W. M. Grady, "The response of a transformer differential relay to internal faults while influenced by geomagnetically induced currents," Schweitzer Engineering Laboratories, Technical Paper, 2020. [Online]. Available: https://selinc.com/api/download/132014/

[3] J. R. Labadie, "Electric power emergency handbook," U.S. Department of Energy, Report, 1980. [Online]. Available: https://www.osti.gov/servlets/purl/7041053

[4] V. D. Albertson, J. M. Thorson, R. E. Clayton, and S. C. Tripathy, "Solar-induced-currents in power systems: Cause and effects," *IEEE Transactions on Power Apparatus and Systems*, vol. PAS-92, no. 2, pp. 471–477, 1973.

[5] W. A. Radasky, "Geomagnetic storm impacts on the high-voltage power grid: Current understanding and mitigation concepts," in *2014 International Symposium on Electromagnetic Compatibility, Tokyo*, 2014, Conference Proceedings, pp. 597–600.

[6] D. H. Boteler, R. M. Shier, T. Watanabe, and R. E. Horita, "Effects of geomagnetically induced currents in the bc hydro 500 kv system," *IEEE Transactions on Power Delivery*, vol. 4, no. 1, pp. 818–823, 1989.

[7] J. Gilbert, J. Kappenman, W. Radasky, and E. Savage, "The late-time (e3) high-altitude electromagnetic pulse (hemp) and its impact on the u.s. power grid," Report, 2010. [Online]. Available: https://www.ferc.gov/industries/electric/indus-act/reliability/cybersecurity/ferc_meta-r-321.pdf

[8] MIL-STD-188-125-1, "High-altitude electromagnetic pulse (hemp) protection for ground-based c4i facilities performing critical time-urgent missions."

[9] S. Dahman, T. Overbye, R. Walling, and R. Horton, "Magnetohydrodynamic electromagnetic pulse assessment of the continental u.s. electric grid: Geomagnetically induced current and transformer thermal analysis," Electric Power Research Institute (EPRI),, Report, 2017. [Online]. Available: https://www.epri.com/#/pages/product/3002009001/

[10] B. Bozoki, S. R. Chano, L. L. Dvorak, W. E. Feero, G. Fenner, E. A. Guro, C. F. Henville, J. W. Ingleson, S. Mazumdar, P. G. McLaren, K. K. Mustaphi, F. M. Phillips, R. V. Rebbapragada, and G. D. Rockefeller, "The effects of gic on protective relaying," *IEEE Transactions on Power Delivery*, vol. 11, no. 2, pp. 725–739, 1996.

[11] E. Savage, W. Radasky, and M. Madrid, "Ac harmonics effects on small external power supplies (wall warts)," in *2014 IEEE International Symposium on Electromagnetic Compatibility (EMC)*, Conference Proceedings, pp. 538–543.

[12] S. Glasstone and D. J. Philips, *The Effects of Nuclear Weapons*. Washington: Dept. of Defense, 1977. [Online]. Available: http://hdl.handle.net/2027/uc1.31822004829784

[13] E. Savage, J. Gilbert, and W. Radasky, "The early-time (e1) high-altitude electromagnetic pulse (hemp) and its impact on the u.s. power grid," Report, 2010. [Online]. Available: https://www.ferc.gov/industries/electric/indus-act/reliability/cybersecurity/ferc_meta-r-320.pdf

[14] L. Andivahis, J. Morrow-Jones, and S. Swanekamp, "Dtra j9's electromagnetic pulse modeling and simulation project," *The Dispatch*, vol. 5, no. 3, p. 8, June 2016. [Online]. Available: http://www.dtra.mil/Portals/61/Documents/DTRIAC/Dispatch%20June%202016.pdf

[15] V. J. Kruse, D. L. Nickel, J. J. Bonk, and J. Taylor, E. R., "Impacts of a nominal nuclear electromagnetic pulse on electric power systems," Oak Ridge National Laboratory,, Report AD-A237 104, 1991. [Online]. Available: https://www.osti.gov/servlets/purl/5804860

[16] J. Morrow-Jones, "Nominal high-altitude electromagnetic pulse (hemp) waveforms," Defense Threat Reduction Agency, Report DTRA-TR-19-22, 2019. [Online]. Available: https://apps.dtic.mil/dtic/tr/fulltext/u2/1067769.pdf

[17] J. Marable, J. Baird, and D. Nelson, "Effects of electromagnetic pulse (emp) on a power system," Oak Ridge National Laboratory,, Report ORNL-4836, 1972. [Online]. Available: https://www.osti.gov/servlets/purl/4477360

[18] J. H. Marable, P. R. Barnes, and D. B. Nelson, "Power system emp protection. final report," Oak Ridge National Laboratory,, Report ORNL-4958, 1975. [Online]. Available: https://www.osti.gov/servlets/purl/4198431

[19] S. Chavin, W. F. Crevier, R. W. Kilb, and C. L. Longmire, "Mhdemp code simulation of starfish," Defense Nuclear Agency,, Report DNA 5055F, 1979. [Online]. Available: http://www.dtic.mil/dtic/tr/fulltext/u2/a106089.pdf

[20] C. Longmire, "On the electromagnetic pulse produced by nuclear explosions," *IEEE Transactions on Antennas and Propagation*, vol. 26, no. 1, pp. 3–13, 1978.

[21] T. Minteer, T. Mooney, S. Artz, and D. E. Whitehead, "Understanding design, installation, and testing methods that promote substation ied resiliency for high-altitude electromagnetic pulse events," in *2017 70th Annual Conference for Protective Relay Engineers (CPRE)*, Conference Proceedings, pp. 1–18.

[22] V. Gurevich and K. Bridge, "Protection of substation critical equipment against intentional electromagnetic threats," 2017. [Online]. Available: https://app.knovel.com/hotlink/toc/id:kpPSCEIET1/protection-substation/protection-substation

[23] G. B. Rackliffe, J. C. Crouse, J. R. Legro, and V. J. Kruse, "Simulation of geomagnetic currents induced in a power system by magnetohydrodynamic electromagnetic pulses," *IEEE Transactions on Power Delivery*, vol. 3, no. 1, pp. 392–397, 1988.

[24] J. Morrow-Jones, "Unclassified emrep e3 (late-time) over joint base san antonio," Applied Research Associates, Screenshot, 2021.

[25] "Recommended e3 hemp heave electric field waveform for the critical infrastructures," Commission to Assess the Threat to the United States from Electromagnetic Pulse (EMP) Attack, Report, 2017. [Online]. Available: http://www.firstempcommission.org/uploads/1/1/9/5/119571849/recommended_e3_waveform_for_critical_infrastructures_-_final_april2018.pdf

[26] NERC, "Tpl-007-1 - transmission system planned performance for geomagnetic disturbance events," North American Electric Reliability Corporation,, Report, 2017. [Online]. Available: https://www.nerc.com/_layouts/15/PrintStandard.aspx?standardnumber=TPL-007-1&title=Transmission%20System%20Planned%20Performance%20for%20Geomagnetic%20Disturbance%20Events&jurisdiction=United%20States

[27] B. McConnell, P. Barnes, F. Tesche, and D. Schafer, "Impact of quasi-dc currents on three-phase distribution transformer installation," Oak Ridge National Laboratory,, Report AD-A254 187, 1992. [Online]. Available: http://www.dtic.mil/dtic/tr/fulltext/u2/a254187.pdf

[28] "High-altitude electromagnetic pulse and the bulk power system: Potential impacts and mitigation strategies," Electric Power Research Institute, Report 3002014979, 2019. [Online]. Available: https://www.epri.com/research/products/000000003002014979

[29] W. Graham, J. Foster, E. Gjelde, R. Hermann, H. Kluepfel, R. Lawson, G. Soper, L. Wood, and J. Woodard, "Report of the commission to assess the threat to the united states from electromagnetic pulse (emp) attack," Critical National Infrastructures,, Report, 2008. [Online]. Available: http://www.empcommission.org/docs/A2473-EMP_Commission-7MB.pdf

[30] NERC, "March 13, 1989 geomagnetic disturbance," North American Electric Reliability Corporation, Report. [Online]. Available: https://www.nerc.com/pa/CI/CIPOutreach/Documents/1989-Quebec-Disturbance.pdf

[31] P. Kundur, N. Balu, and M. Lauby, *Power System Stability and Control*. New York: McGraw-Hill, 1994.

[32] R. Girgis, K. Vedante, and G. Burden, "A process for evaluating the degree of susceptibility of a fleet of power transformers to the effects of gic," ABB Power Transformers,, Report, 2013. [Online]. Available: https://library.e.abb.com/public/469d792afc65c8fd85257d80004169c0/Evaluating%20Susceptibility%20of%20Transformers%20to%20effects%20of%20GIC%20IEEE%2004%202014.pdf

[33] M. Nazir, K. Burkes, and J. Enslin, "Converter-based solutions: Opening new avenues of power system protection against solar and hemp mhd-e3 gic," *IEEE Transactions on Power Delivery*, pp. 1–1, 2020.

[34] "Mhd-e3 transmission level power grid test report part iii - phase ivb emprimus solidground evaluation," Defense Threat Reduction Agency, Report DTRA-TR-13-40-VIII, 2013.

[35] E. E. Bernabeu, "Single-phase transformer harmonics produced during geomagnetic disturbances: Theory, modeling, and monitoring," *IEEE Transactions on Power Delivery*, vol. 30, no. 3, pp. 1323–1330, 2015.

[36] I. Nisja, M. H. Idris, M. Syafrudin, S. Hardi, and M. Isa, "The effect of harmonic distortion on the performance of differential relay for distribution transformer protection," *Applied Mechanics and Materials*, vol. 793, pp. 182–186, 2015.

[37] T. Hutchins, "Modeling, simulation, and mitigation of the impacts of the late time (e3) high-altitude electromagnetic pulse on power systems," Dissertation, 2016. [Online]. Available: http://hdl.handle.net/2142/90451

[38] T. R. Hutchins and T. J. Overbye, "Power system dynamic performance during the late-time (e3) high-altitude electromagnetic pulse," in *2016 Power Systems Computation Conference (PSCC)*, Conference Proceedings, pp. 1–6.

[39] A. R. v. C. Warrington, *Protective Relays: their Theory and Practice*. New York, New York: John Wiley and Sons, Inc., 1962, vol. 1.

[40] "Geomagnetic disturbance effects on power systems," *IEEE Transactions on Power Delivery*, vol. 8, no. 3, pp. 1206–1216, July 1993.

[41] B. Kasztenny, N. Fischer, D. Taylor, T. Prakash, and J. Jalli, "Do cts like dc? performance of current transformers with geomagnetically induced currents," in *2016 69th Annual Conference for Protective Relay Engineers (CPRE)*, Conference Proceedings, pp. 1–17.

[42] "Mhd-e3 transmission level power grid test report part ii - phase iv test results," Defense Threat Reduction Agency, Report DTRA-TR-15-47, 2013.

[43] M. Rooney, D. Fromme, G. Edmiston, A. Walker, S. West, and S. McBride, "Dtra mhd-e3 phase ivb measured harmonic response of power grid transformers subjected to severe e3/gic currents, august 2013," Report. [Online]. Available: https://www.swpc.noaa.gov/sites/default/files/images/u33/INL_GMD_Measured_Harmonic_Response-Public_Release_NOAA.pdf

[44] "Mhd-e3 transmission level power grid test report part i - phase iv test description," Defense Threat Reduction Agency, Report DTRA-TR-15-46, 2013.

[45] S. V. Kulkarni and S. A. Khaparde, *Transformer engineering: design and practice*. Marcel Dekker, Inc., 2004.

[46] "Finite element method magnetics (femm)," *D. Meeker*, 2020. [Online]. Available: https://www.femm.info

[47] J. G. Kappenman, V. D. Albertson, and N. Mohan, "Current transformer and relay performance in the presence of geomagnetically-induced currents," *IEEE Transactions on Power Apparatus and Systems*, vol. PAS-100, no. 3, pp. 1078–1088, 1981.

[48] J. F. Fuller, E. F. Fuchs, and D. J. Roesler, "Influence of harmonics on power distribution system protection," *IEEE Transactions on Power Delivery*, vol. 3, no. 2, pp. 549–557, 1988.

[49] "Ieee guide for establishing power transformer capability while under geomagnetic disturbances," *IEEE Std C57.163-2015*, pp. 1–50, 2015.

[50] G. Zweigle, J. Pope, and D. Whitehead, "Geomagnetically induced currents – detection, protection, and mitigation," Report, 2011. [Online]. Available: https://www.selinc.com

[51] A. Pulkkinen, S. Lindahl, A. Viljanen, and R. Pirjola, "Geomagnetic storm of 29–31 october 2003: Geomagnetically induced currents and their relation to problems in the swedish high-voltage power transmission system," *Space Weather*, vol. 3, no. 8, 2005. [Online]. Available: https://agupubs.onlinelibrary.wiley.com/doi/abs/10.1029/2004SW000123

[52] B. Kasztenny, N. Fischer, and H. J. Altuve, "Negative-sequence differential protection - principles, sensitivity, and security," in *2015 68th Annual Conference for Protective Relay Engineers*, 2015, pp. 364–378.

[53] H. J. Altuve-Ferrer and E. O. Schweitzer III (eds), *Modern Solutions for Protection, Control, and Monitoring of Electric Power Systems*. Pullman, WA: Schweitzer Engineering Laboratories, Inc., 2010.

[54] M. J. Thompson, "Percentage restrained differential, percentage of what?" in *2011 64th Annual Conference for Protective Relay Engineers*, 2011, pp. 278–289.

[55] B. Kasztenny, M. J. Thompson, and D. Taylor, "Time-domain elements optimize the security and performance of transformer protection," in *2018 71st Annual Conference for Protective Relay Engineers (CPRE)*, 2018, pp. 1–15.

[56] "2012 special reliability assessment interim report: Effects of geomagnetic disturbances on the bulk power system," pp. 48–52, 2012. [Online]. Available: https://www.nerc.com/files/2012GMD.pdf

[57] K. Behrendt, N. Fischer, and C. Labuschagne, "Considerations for using harmonic blocking and harmonic restraint techniques on transformer differential relays," Schweitzer Engineering Laboratories, Technical Paper, 2006. [Online]. Available: https://selinc.com/api/download/3470/?lang=en